Task #1:

BLIND PREDICTION OF THE STATIC CYCLIC RESPONSE OF A RECTANGULAR RC CANTILEVER COLUMN

The cyclic tests of RC cantilever column were performed. The main task is to simulate the response using the appropriate model in OpenSees platform.

The height of the column is H=1.8 m. The width and height of the column cross-section is equal to 30 and 40 cm, respectively. The diameter of longitudinal reinforcement is d_{bl}=16 mm. The type of detailing and level of the lateral reinforcement that should be considered is for each group presented in Figure 1.

Consider the loading protocol shown in Figure 2 for the cyclic analysis of the column. Analysis should be performed until the estimated failure. The mean material properties of the lateral and longitudinal reinforcement with respect to the group number are presented in Table 1 and 2, respectively.

The mean properties of the compressive cylindrical strength f_{cm} and level of axial force for each group number is presented in Table 3. Consider the lumped plasticity numerical model using Takeda hysteretic rules with the unloading stiffness degradation parameter α=0.5 at the location of the plastic hinge. The substandard details should be properly addressed.

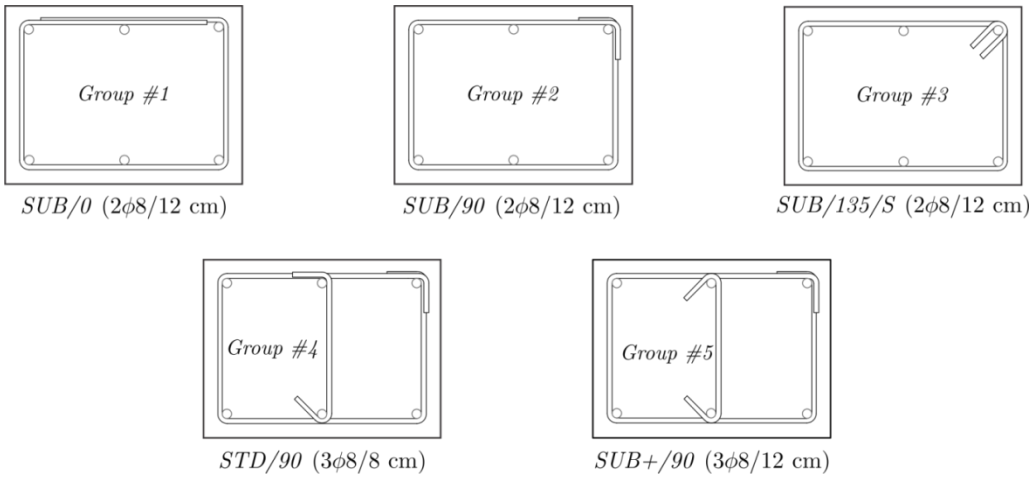

Figure 1: Different levels and type of detailing of lateral reinforcement with respect to the number of group

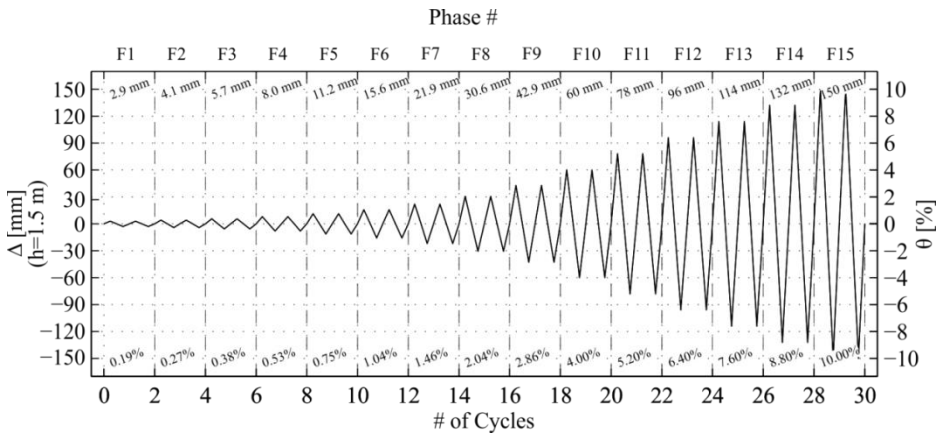

Figure 2: Loading protocol used for cyclic test of the columns

Table 1: The mean material properties of lateral reinforcement for each number of group

Group #	f_y [MPa]	f_t [MPa]	ε_y [%]	ε_u [%]	E [GPa]
1-3	495	577	0.25	7.48	198
4-5	554	668	0.30	10.12	186

Table 2: The mean material properties of longitudinal reinforcement for each number of group

Group #	f_y [MPa]	f_t [MPa]	ε_y [%]	ε_u [%]	E [GPa]
1-3	541	691	0.29	8.96	189
4-5	600	709	0.30	7.56	198

Table 3: The mean material properties of the compressive cylindrical strength f_{cm} and level of axial force for each group number

Group #	1	2	3	4	5
f_{cm} [MPa]	46.5	43.9	44.5	36.3	35.8
N [kN]	577	542	539	577	577

The project report in written form should be submitted at the second part of the course in September. It should include:

- Calculation of the moment-rotation envelope (crack, yield and near collapse),
- The full non-linear cyclic response of the column (force-displacement curve)
- Detailed report about the cyclic analysis of the column
- Comparison of the results with the results of a column STD/135 (see Exercise Lectures) and the comments of the differences.
- The analysis of the influence of the different parameters to the ductility of the analysed column (level of axial force, concrete compressive strength, amount of lateral reinforcement, amount of longitudinal reinforcement)

Task #2:

PUSHOVER ANALYSIS OF A MULTI-SPAN BRIDGE IN THE TRANSVERSE DIRECTION

Perform a pushover analysis of a six-span bridge (26+4x32+26=180 m) supported by five I-shaped bridge columns (see Figure 3). Take into account Eurocode 8 elastic acceleration spectrum corresponding to soil C.

The cross-section of the columns with the dimensions and the position of longitudinal reinforcement are presented in Figure 4. Two different configurations of lateral reinforcement are presented in Figure 4, i.e. the substandard (the as-built) and standard (according to EC8/2) design. The non-linear numerical model of a multi-span bridge with non-linear springs located at the bottom of each pier as shown in Figure 4. The displacemenets of the superstructure above the abutment are enabled in the longitudinal and prevented in the transverse direction.

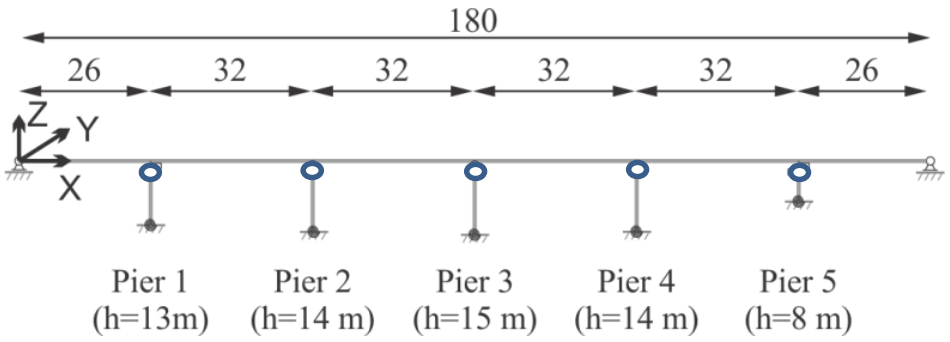

Figure 3: The scheme of the six span bridge

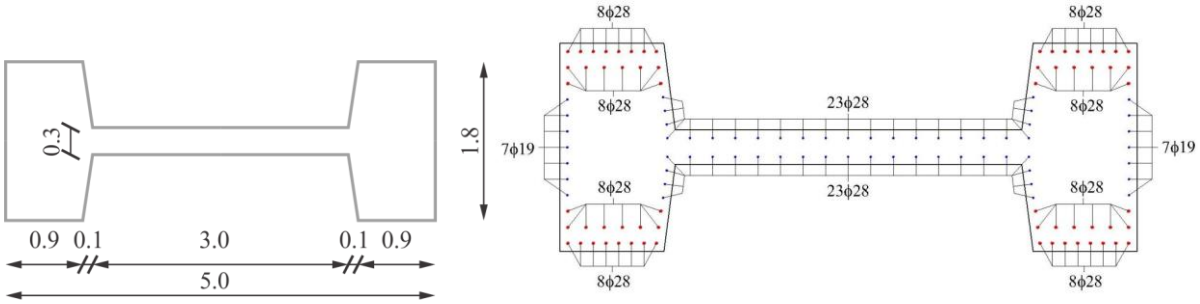

Figure 4: The cross-section of an I-shape column and the flexural reinforcement

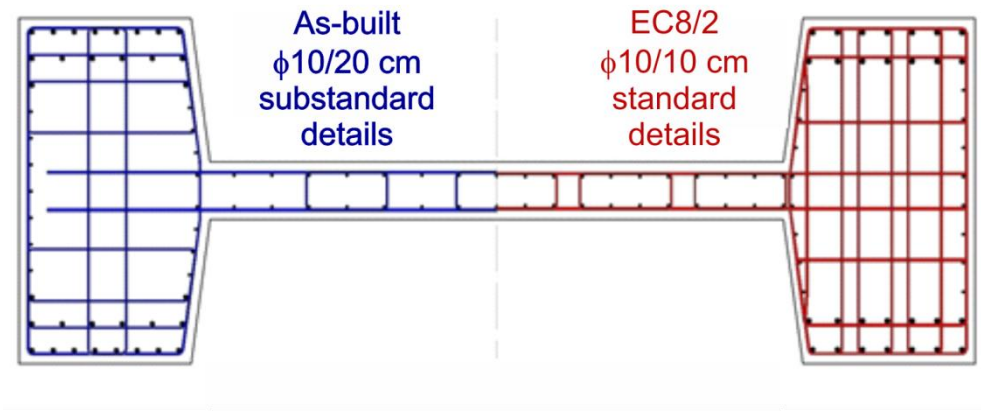

Figure 5: The detailing of the lateral reinforcement in the case of the substandard – as-built (left) and standard - Eurocode 8/2 design (right)

Analysis should be performed using lumped plasticity model with Takeda hysteretic rules (consider unloading stiffness degradation parameter α=0.5). For each group the method that should be used for the assessment of the moment-rotation envelope is defined in Table 4 for each working group. The definition of the standard and substandard details is defined in Figure 5.

Group #	1	2	3	4	5
Method	EC8/2	EC8/3	EC8/3	EC8/2	EC8/2
Details	Standard	Standard	Substandard	Standard considering improper hooks	Standard considering s/dbl = 8

Consider the same material properties, bridge deck dimensions nad masses as in the case study presented at the course.

The detailed written report about the pushover analysis should be submitted at the second part of the course in September. It should also include:

- Define the peak ground acceleration (PGA) corresponding to the failure of the first pier for longitudinal and transverse direction separately.
- How would the doubled mass of a bridge deck (double deck bridge) impact on the seismic behaviour of a structure?

University of Ljubljana
Faculty of Civil and Geodetic Engineer
Institute of Structural and Earthquake Engineering
Lecturer: Prof. Dr. Tatjana Isaković
Dr. Andrej Anžlin

NONLINEAR ANALYSIS OF STRUCTURES: SEISMIC RESPONSE OF RC BRIDGES – BLIND PREDICTION

GROUP 3

- Ana Pavičić, anapavacic96@gmail.com
- Antonio Janevski, antiniojanevski@hotmail.com
- Lajos Gerse, gerselajos@gmail.com
- Mostafa Gad, mostafa.gad@uni-weimar.de
- Rafael Amorim, ramorim@ua.pt

1. TASK 1: BLIND PREDICTION OF THE STATIC CYCLIC RESPONSE OF A RECTANGULAR RC CANTILEVER COLUMN

1.1. Introduction

Target of the Task 1 is to study the cyclic behaviour of R.C. columns, and each group was assigned a specific case to study, with a certain detailing level and concrete properties.

Starting from material properties, the effects of confinement on concrete is a critical point in our study, and in the beginning we will discuss the section properties and states considering the different between confined and unconfined cases so it is numerically noticeable how can a good confinement affect the overall behaviour, and specifically on cyclic behaviour.

By performing the cyclic analysis, we will be much closer to the seismic behaviour of the column; by monitoring the reaction values for each induced displacement we can estimate the column response to seismic motion considering stiffness degradation after cracking up to column failure. Hence we can investigate the influential factors and the extent of their effects on the cyclic response of the column, helping to reach an optimum design for column according to the required case.

1.2. Case Definition

1.2.1. Study Case

The cyclic test of RC cantilever column is to be performed using OpenSees platform.

The height of the column is H=1.8 m. The width and height of the column cross-section is equal to 30 and 40 cm, respectively. The diameter of longitudinal reinforcement is dbl=16 mm. The type of detailing and level of the lateral reinforcement that should be considered is presented in Figure 1.

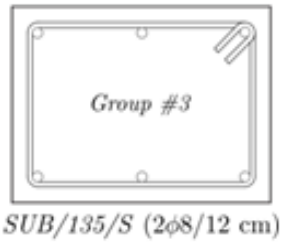

Figure 1: Levels and type of detailing of lateral reinforcement

Table 1. The mean material properties of lateral reinforcement

Group	F_y [MPa]	F_t [MPa]	ε_y [%]	ε_u [%]	E [GPa]
3	495	577	0.25	7.48	198

Table 2: The mean material properties of longitudinal reinforcement

Group	F_y [MPa]	F_t [MPa]	ε_y [%]	ε_u [%]	E [GPa]
3	541	691	0.29	8.96	189

Table 3: The mean material properties of the compressive cylindrical strength fcm and level of axial force

Group	F_{cm} [MPa]	N [kN]
3	44.5	539

1.2.2. Material Properties

Using the mean compressive strength of the concrete we were able to define the loading behaviour of the material under different cases of loading, for both Unconfined and Confined concrete cases are shown in the tables below using Mander and Popovic's Model:

Table 4: Unconfined Concrete Properties

Unconfined Concrete Properties		
Fc	**44.5**	MPa
ε_1	**2.27**	‰
Ec	**34.43**	GPa
Esec	**19.60**	GPa
r	**2.32**	-
$\varepsilon_{sp.}$	**9.97**	‰

Table 5: Confined Concrete Properties

Confined Concrete Properties		
F_c	**44.5**	MPa
h'	**31.6**	cm
b'	**21.6**	cm
h_o	**34**	cm
b_o	**24**	cm
S	**12**	cm
α_s	**0.40**	-
α_n	**0.62**	-
α	**0.25**	-
φ stirr.	**0.8**	cm
$A_{stirr.}$	**0.50**	cm^2
ρ_x	**0.003**	-
ρ_y	**0.002**	-
ρ_w	**0.006**	-
f_{yw}	**495**	MPa
ε_{su}	**7.48**	%
fl'	**0.36**	MPa
λ	**1.06**	-
$F_{cm,c}$	**46.99**	MPa
$\varepsilon_{c1,c.}$	**2.56**	‰
$\varepsilon_{cu,c.}$	**10.57**	‰

1.3. Moment-Curvature Relation

Firstly we calculated mentioned damage states for unconfined concrete using material models according to EC2/1. Because we observe different levels and type of detailing of lateral reinforcement we included material models for confined concrete according to the Mander's model (EC8/2) and EC2/1. Moment-rotation envelope was also estimated using the appropriate models in OpenSees platform. The results are shown below.

Unconfined concrete

Crack moment and curvature

Crack moment and associated curvature where estimated using following equations:

$$\sigma_{cr} = \frac{N}{A} - \frac{M_{cr}}{W} = -f_{ctm}\,(EC2)$$

$$\Phi_{cr} = \frac{M_{cr}}{EI_{gross}}$$

$$W = \frac{bh^2}{6} = \frac{40 \cdot 30^2}{6} = 6000\ cm^3$$

$$A = bh = 40 \cdot 30 = 1200\ cm^2$$

$$I_{gross} = \frac{bh^3}{12} = \frac{40 \cdot 30^3}{12} = 90000\ cm^4$$

Using the material characteristis we get:

Mcr =46,15 kNm

$\Phi_{cr} = 0{,}00149\ 1/m$

Yield moment and curvature (first yield)

We define deformation in longitudinal reinforcement ε_y and by fulfilling the equilibrium of cross-section we calculated the M_y and corresponding Φ_y.

Results are shown below:

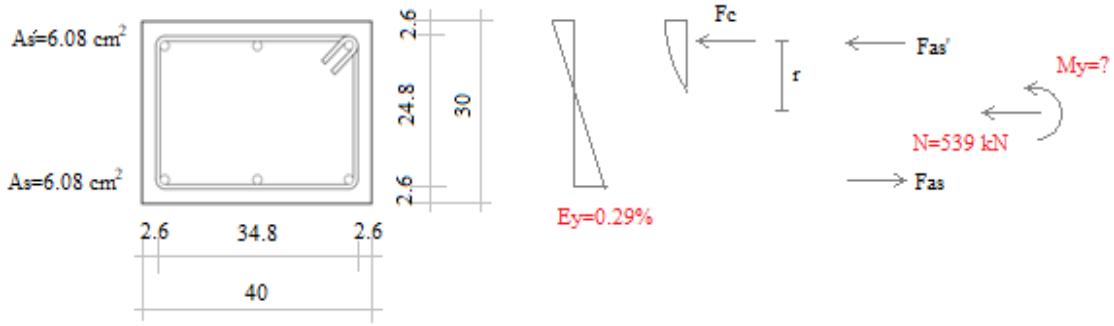

$$N = F_c + -F_{as} + F'_{as} = 782 - 326 + 83 = 539\ kN$$

$$M_y = Mc + F_{as}\left(\frac{h}{2} - a\right) + F'_{as}\left(\frac{h}{2} - a\right) = 93{,}4 + \frac{326\left(\frac{30}{2} - 4{,}2\right)}{100} + \frac{83\left(\frac{30}{2} - 4{,}2\right)}{100} = 137{,}65\ kNm$$

Ultimate moment and curvature

We define the limit deformation in concrete ε_c and same as before calculate M_u and corresponding Φ_u. Results are shown below:

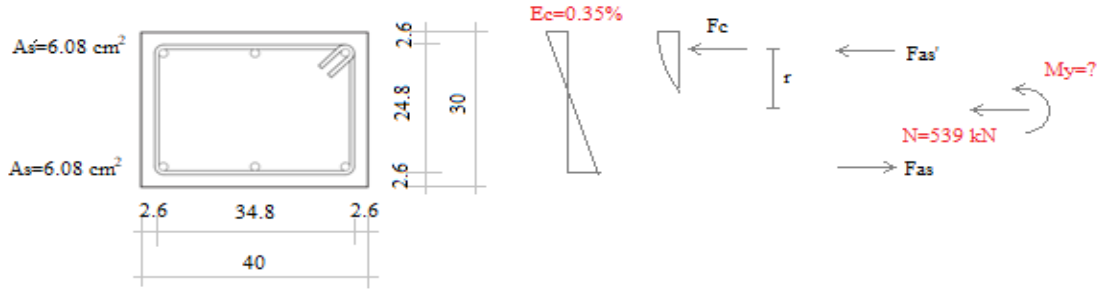

$$N = F_c + -F_{as} + F'_{as} = 758 - 338 + 119 = 539\ kN$$

$$M_y = Mc + F_{as}\left(\frac{h}{2} - a\right) + F'_{as}\left(\frac{h}{2} - a\right) = 93{,}6 + \frac{338(\frac{30}{2} - 4{,}2)}{100} + \frac{119\left(\frac{30}{2} - 4{,}2\right)}{100} = 142{,}85\ kNm$$

Graphic representation of damage states shown in figure 2

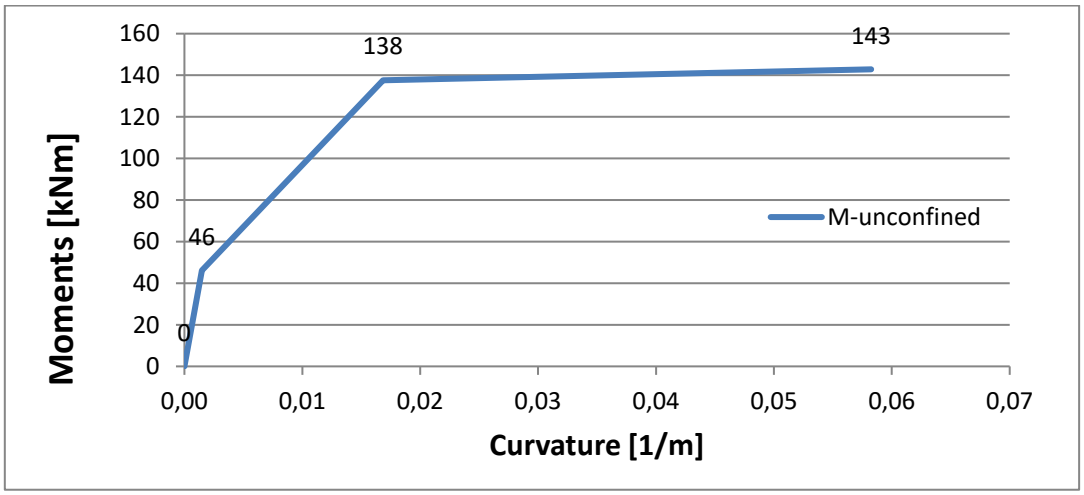

Figure 2: Unconfined Concrete Moment-Curvature Relation

Confined concrete

According to confined concrete properties menstioned in 1.2.2, it is now possible to evaluate curvature properties of the cantilever compared to unconfined ones, where we can observe the effect of concrete confinement on ductility of the system.

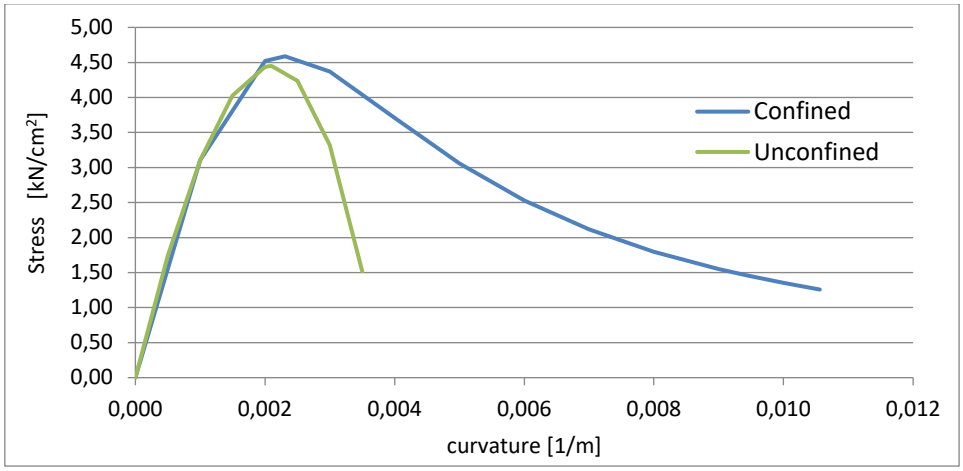

Figure 3: Stress-Curvature Relation for Confined and Unconfined Concrete

After calculations of material characteristics, we calculate crack, yield and ultimate state of damage for confined concrete at the same manner as for confined concrete. Table 5 shows results:

Table 6: Moment-Curvature values

	M_{cr}	M_y	M_u
Moment [kNm]	48,0	138	123
Curvature [1/m]	0.001567	0.01692	0.1883

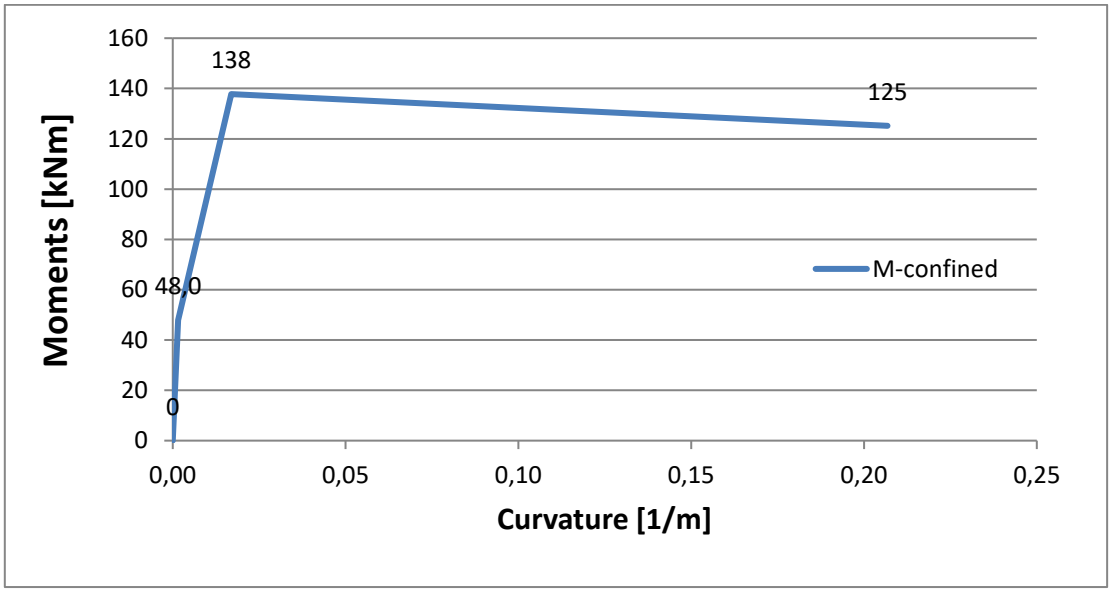

Figure 4: Confined Concrete Moment-Curvature Relation

By plotting the two curves on the same scale, the confinement effect on results is more obvious in terms of column ductility, as shown in figure 5.

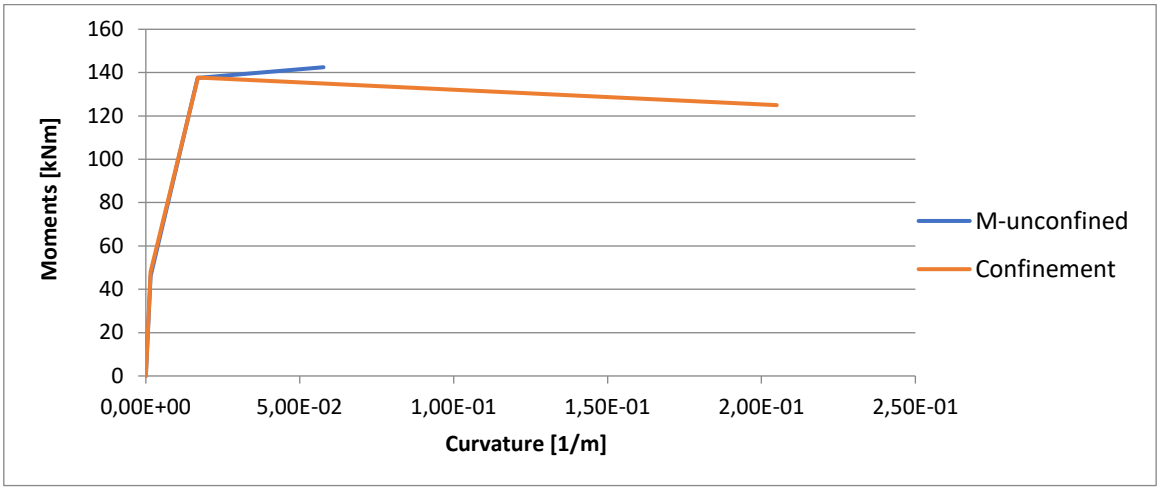

Figure 5: Confined and Unconfined concrete Moment-Curvature Values

Moment-rotation envelope was also estimated using the appropriate models in OpenSees platform. Firstly we prepare material and cross section filed and then using the code from mphi analysis calculates moment-curvature correlation.

The results of both hand calculation and FE model of OpenSees are shown in figure 6, and it came almost matching with relatively close values, and also the linear behaviour of section up to cracking moment which is expected due to elastic properties of the full section.

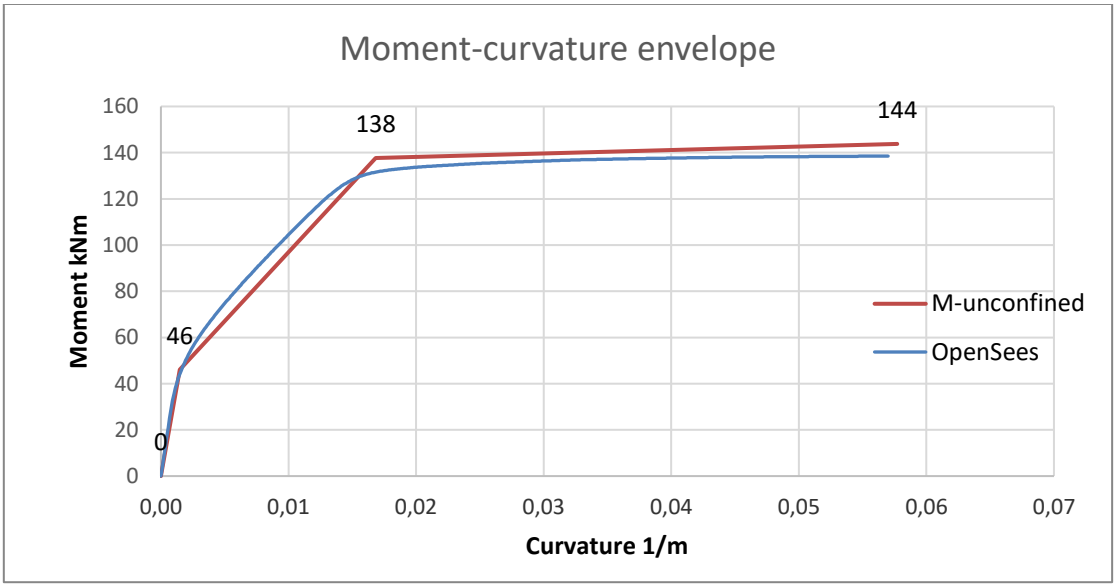

Figure 6: Unconfined Concrete OpenSees Results

Same for confined section, the behaviour of both results was the same, taking into consideration that the linear results are only calculated at specific points, and that is why the results between control points will differ, as shown in figure 7.

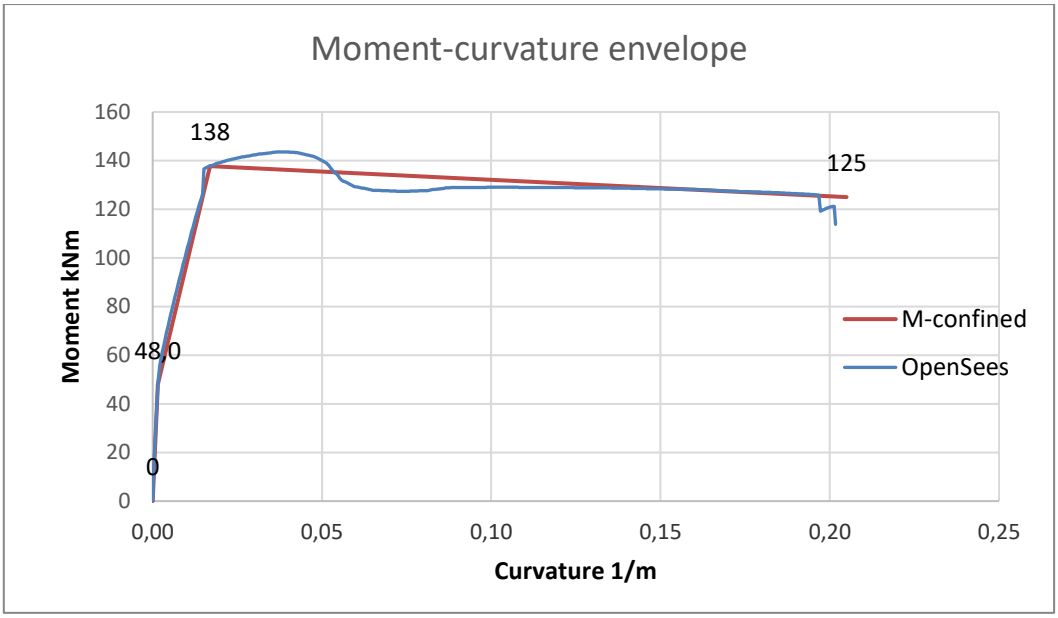

Figure 7: Confined Concrete OpenSees Results

It was clear here that there is a sudden degradation of strength took place before 0,05 [1/m] curvature value, and mostly the reason is assumed to be due to the failure of concrete cover, which decreased the whole cross-sectional area of the column.

1.4. Moment-Rotation Relation

Using EC8/2, the envelope of moment-rotation relation was estimated to evaluate the limiting value of the column rotation.

$$\theta_{cr} = \varphi_{cr} \cdot \frac{l}{3}$$

$$\theta_y = \varphi_y \cdot \frac{l}{3}$$

$$\theta_{p,u} = (\varphi_u - \varphi_y).l_p \,.(1 - l_p/12)$$

$$\theta_u = \theta_y + \theta_{p,u}$$

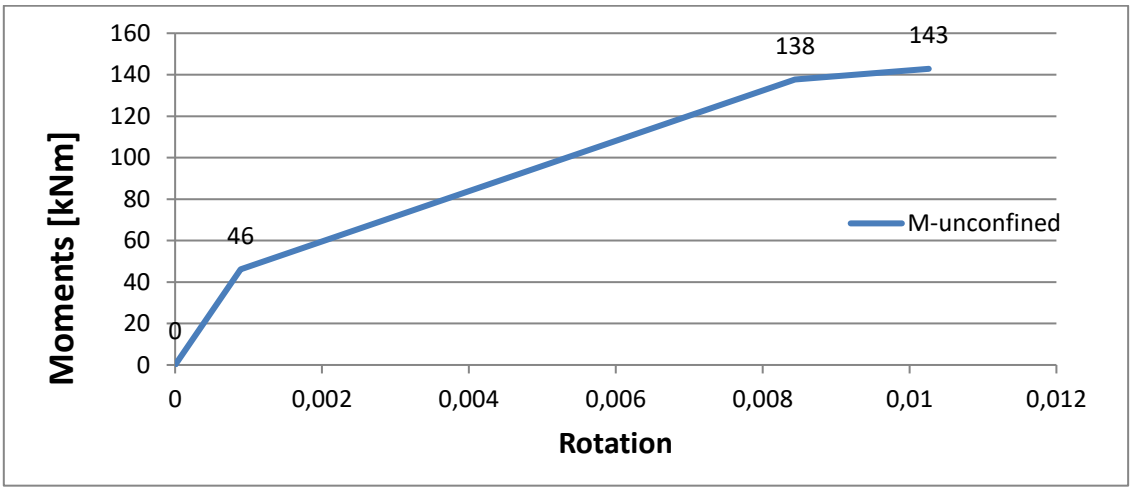

Figure 8: Unconfined Concrete Moment-Rotation Envelope

And for the confined concrete the envelope was calculated using EC8/3 equations.

$$\theta_y = \Phi_y \frac{L_v + \alpha \cdot z}{3} + 0{,}0013\left(1 + 1{,}5\frac{h}{L_v}\right) + 0{,}13\frac{d_{bl} \cdot f_y}{\sqrt{f_c}}$$

$$\theta_{um} = \frac{1}{\gamma_{el}} 0{,}016(0{,}3^{\nu}) \left[\frac{\max(0{,}01;\omega')}{\max(0{,}01;\omega)} fc\right]^{0{,}225} \left(\min\left(9;\frac{Lv}{h}\right)\right)^{0{,}35} 25^{\left(\alpha \cdot \rho_{sx}\frac{f_{yw}}{f_c}\right)} (1{,}25^{100\rho_d})$$

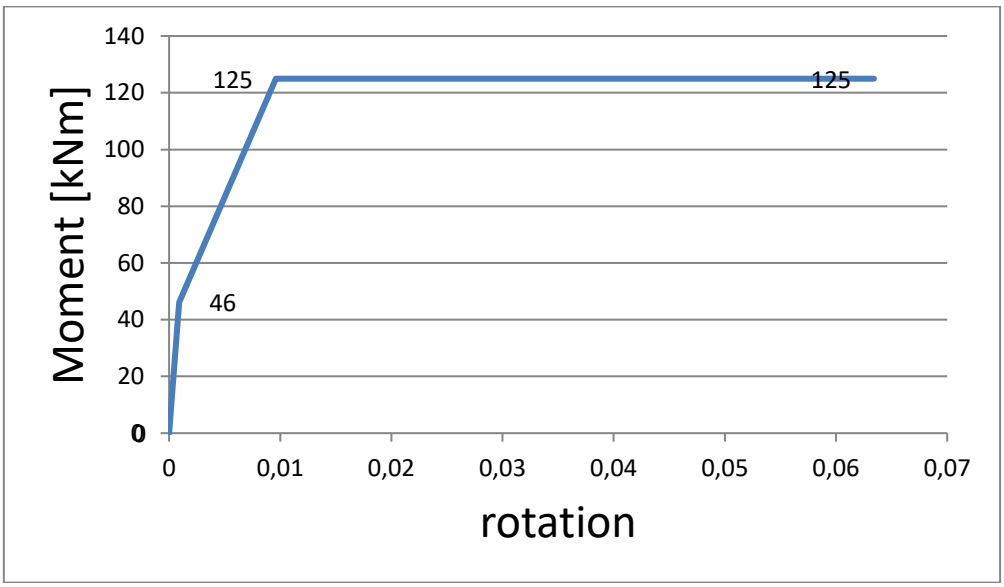

Figure 9: Confined Concrete Moment-Rotation Envelope

1.5. Cyclic Analysis

1.5.1. Section Analysis

Using the new material properties, via OpenSees we are able to run cyclic analysis for our section using the following protocol, taking into consideration multiplying all the values by the ratio of 1.8/1.5 to take into account the difference in height for our system.

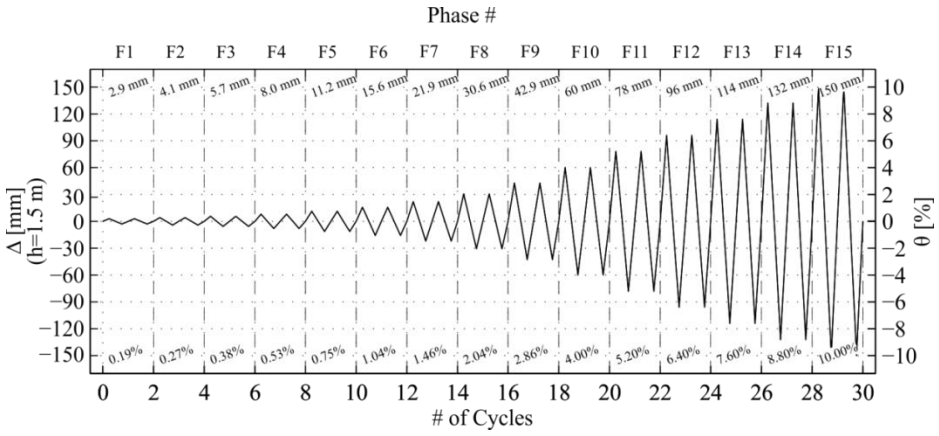

Figure 10: Cyclic Loading Protocol for 1.5m Height Column

Instead of Lumped-Plasticity model, as problems with converging took place, it was advisable to use fibre model which gave a reasonable results, with less problems in our case study.

The results of the cyclic analysis is shown in figure 11, where we can observe the highest reaction of 80.5 kN and after that the stiffness degradation takes place and giving the chance for higher deformation values to reach a maximum at 7.6% rotation .

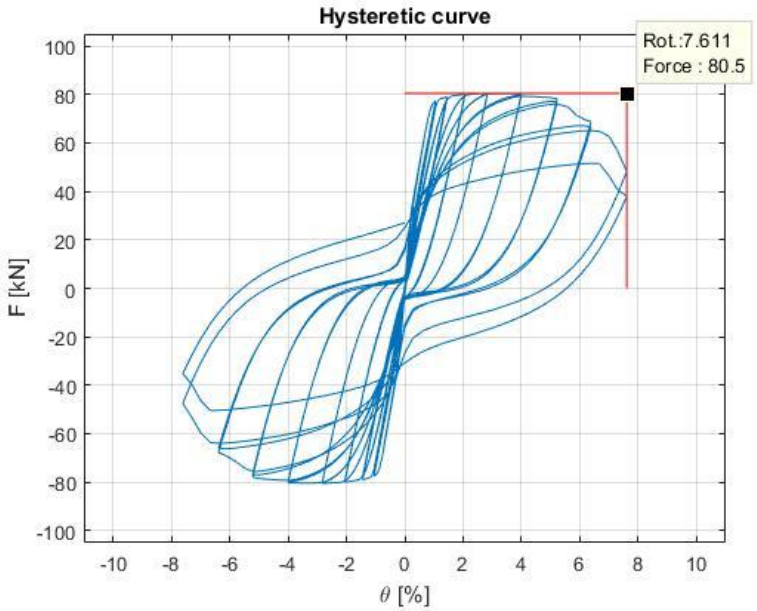

Figure 11: Cyclic Loading Force-Rotation Relation for the Column

1.5.2. Comparison with Experimental Results

An Important step to validate our numerical model is to compare with the experimental results, so we can decide – according to the required degree of accuracy – wither the numerical results show an acceptable simulation for our model or not, which will allow us to have a better judgment on the affecting parameters.

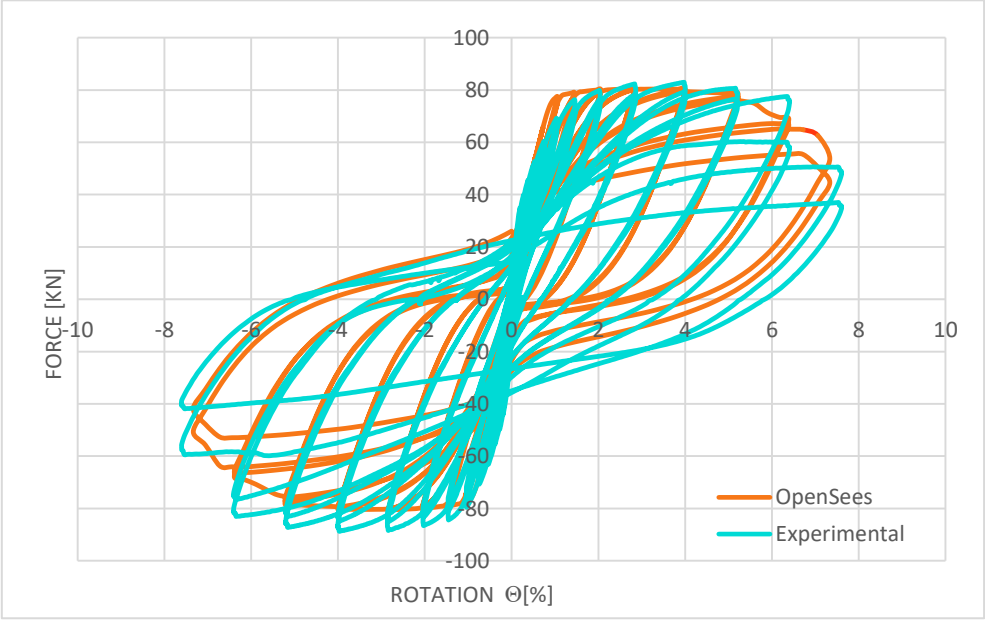

Figure 12: Comparison of Force-Rotation with Experimental Results

OpenSees results shows a very acceptable simulation for the cyclic behaviour of the column, compared to the experimental results.

For one side the maximum force reaction for both round about the value of 80kN, while the maximum reached displacements are also close enough for the model to be validated.

Also, for the experimental results was not very symmetric, as it is noticeable that the force limit at the positive side is around 80kN while on the negative side it exceeded that value in an obvious way, the reason here for this problem was mostly due to the hook location, which forces a side to behave differently with a less strength, as for high compressive stresses.

1.5.3. Comparison with STD-135

To estimate the effect of code requirements we compared our results with the standard section STD-135 so we can evaluate the difference that the code provisions can add through proper detailing.

Figure 13 shows the comparison between our case (Sec-3) and STD-135, it is easy to see higher reaction forces and also higher ductility, utilising the same dimensions and longitudinal reinforcement.

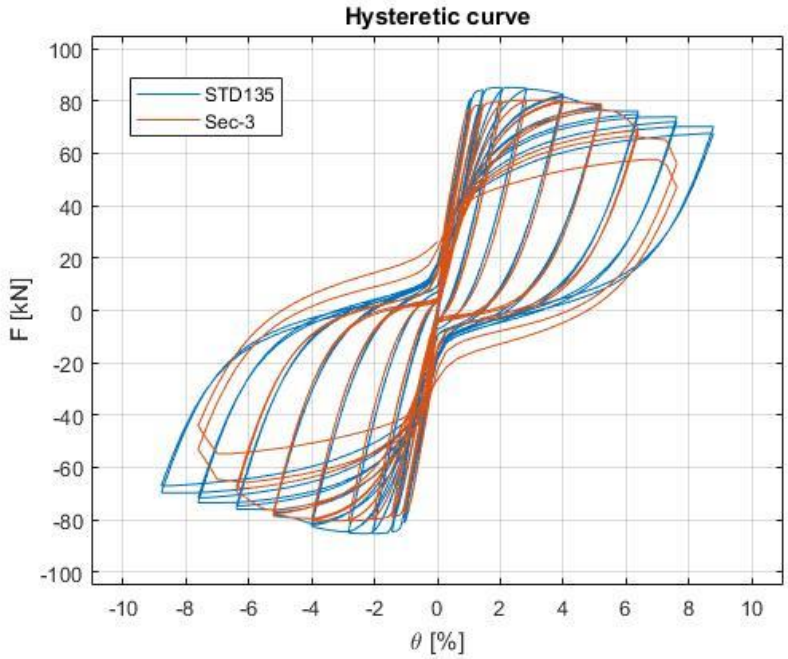

Figure 13: Comparison of Force-Rotation with STD-135

1.6. Influential Factors

1.6.1. Axial Force

To fully understand the behaviour of our system it is useful to start changing certain parameters and monitor the effect of each parameter individually.

Starting with the axial force, we can observe that decreasing the axial force from our case (N=539kN) to (N=450kN) decreases the reaction of the column but does not affect the ductility so much, as shown in figure 14.

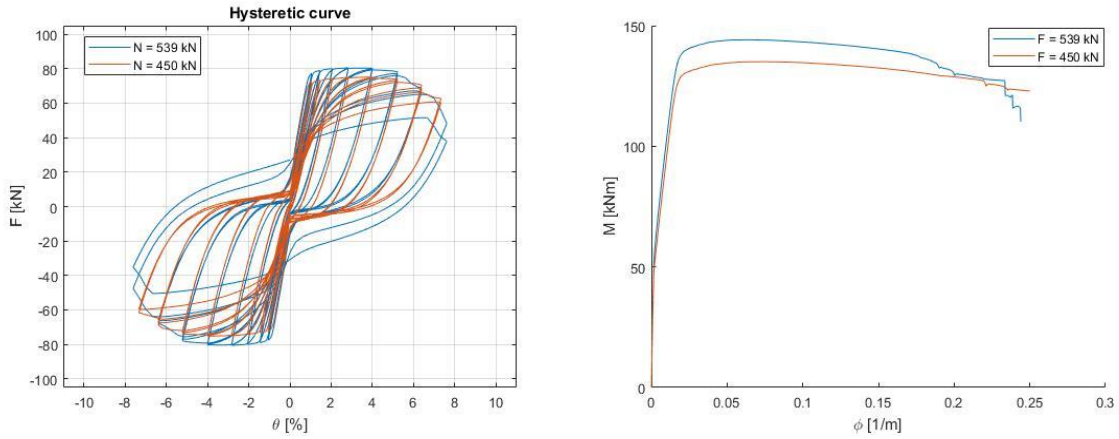

Figure 14: Comparison For Different Normal Force Values (450 kN)

In figure 15, the comparison with even lower normal force values with 300kN, where it is noticeable the effect of normal force decreasing in the capacity of section also the behaviour during cyclic loading.

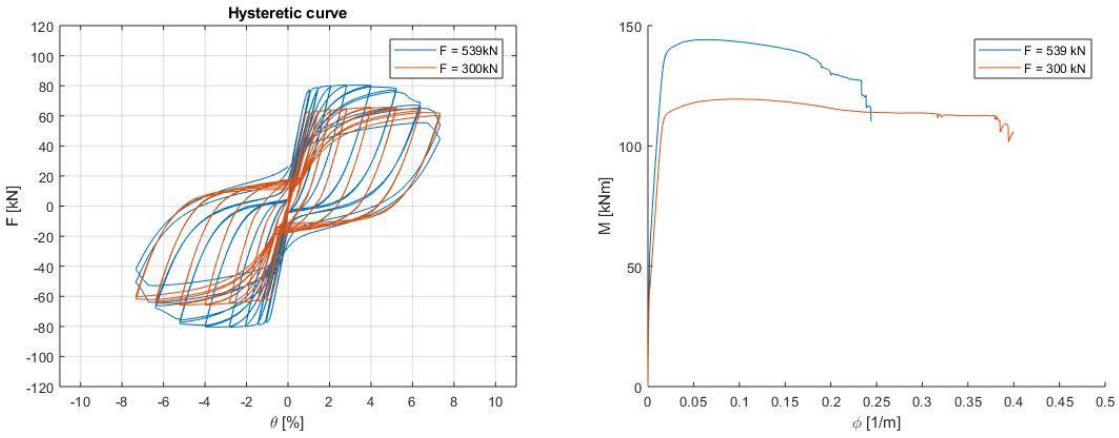

Figure 15:Comparison For Different Normal Force Values (300 kN)

While when the force increased to 600kN for small deformation values we can see a slight change in reaction up to 84kN, but it also limited the ductility of the column and caused earlier failure for the system.

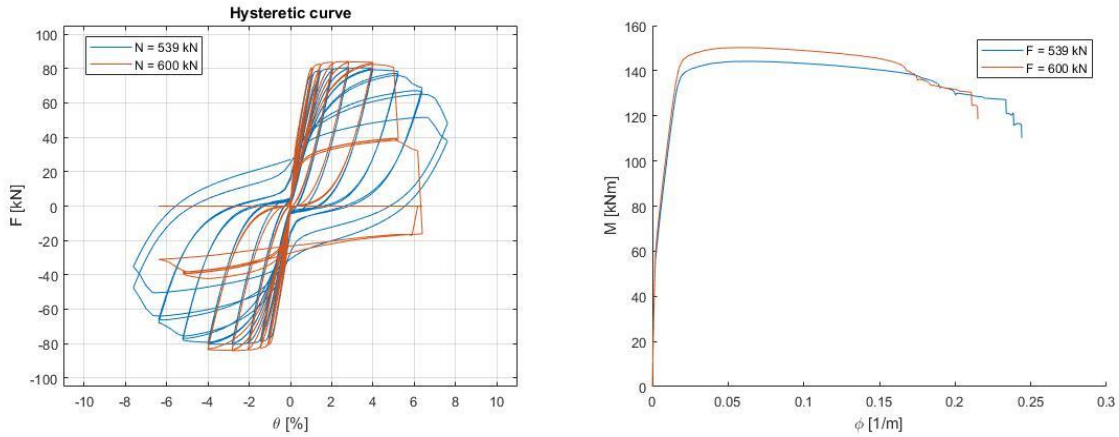

Figure 16: Comparison For Different Normal Force Values (600 kN)

1.6.2. Compressive Strength

Decreasing the compressive strength to 35MPa caused a small decrease in strength and almost no change in the ductility of the column, as shown in figure 17.

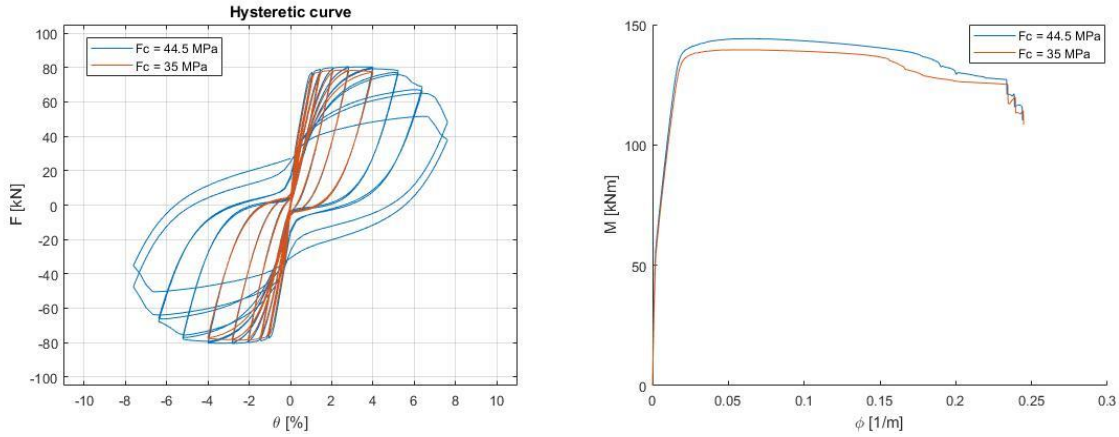

Figure 17: Comparison For Different Compressive Strength Values (35 MPa)

For even lower values of compressive strength, the same comparison was set using 30MPa in figure 18

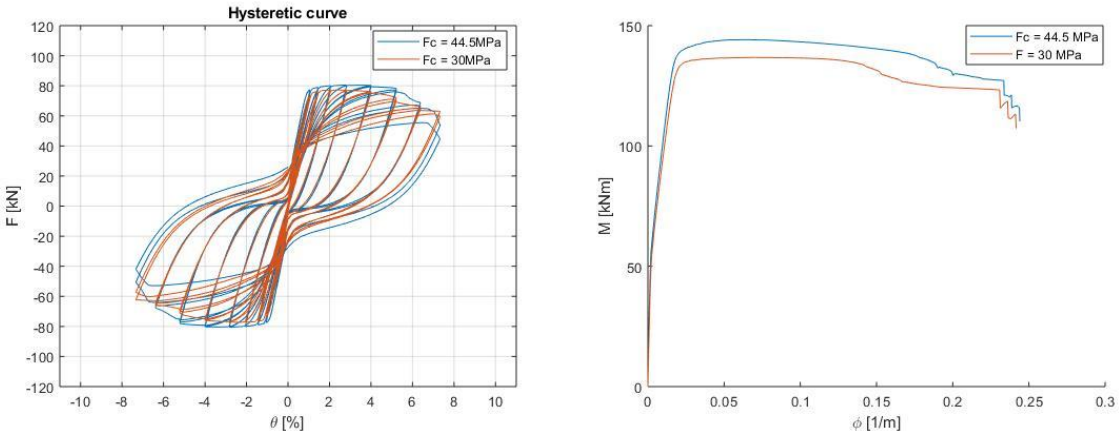

Figure 18: Comparison For Different Compressive Strength Values (30 MPa)

Same as increasing the normal force, increasing compressive strength caused an increase in the strength of the column but also earlier failure took place due to lower ductility of concrete.

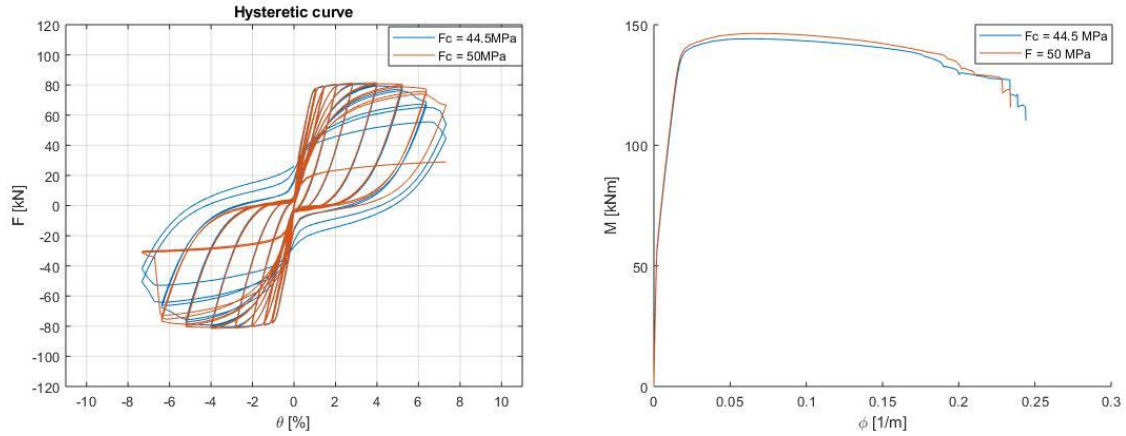

Figure 19: Comparison For Different Compressive Strength Values (50 MPa)

Along the same line the effect is more obvious using Fc = 55MPa, as shown in figure 20.

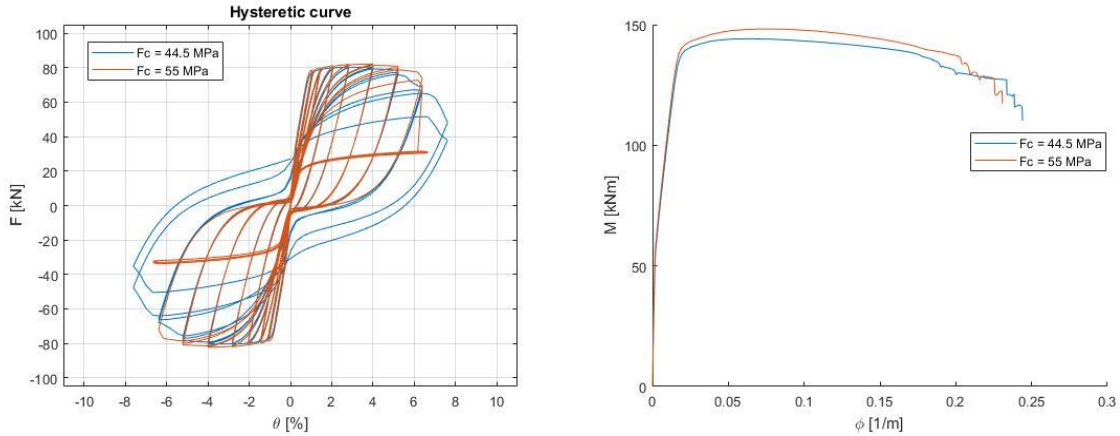

Figure 20:Comparison For Different Compressive Strength Values (55 MPa)

1.6.3. Lateral Reinforcement

Increasing the lateral reinforcement from 8mm to 10mm (same shape), got a remarkable effect on the section ductility which shows how effective is the lateral reinforcement can be for both capacity curve and cyclic analysis behaviour.

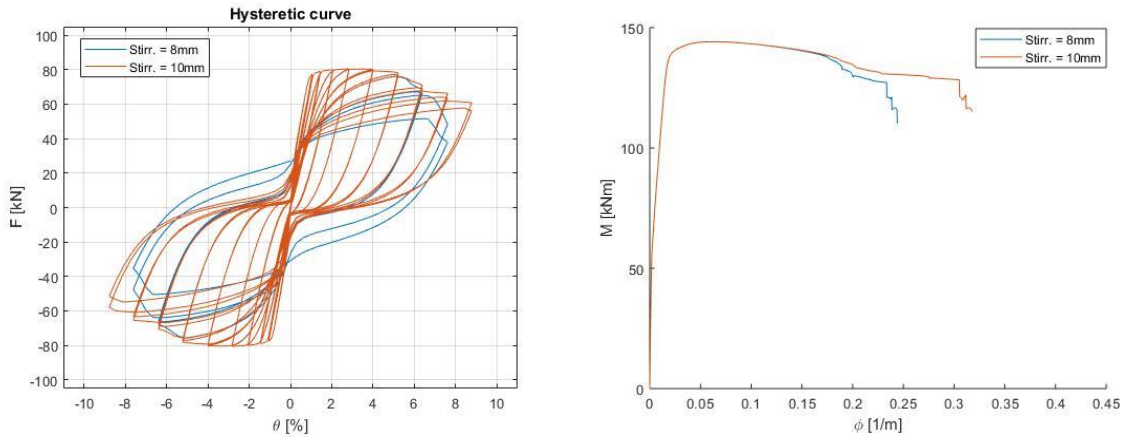

Figure 21: Comparison For Different Lateral Reinforcement Values (10mm)

And still for higher values of lateral reinforcement, the section shows a higher values of ductility which ensures the same concept.

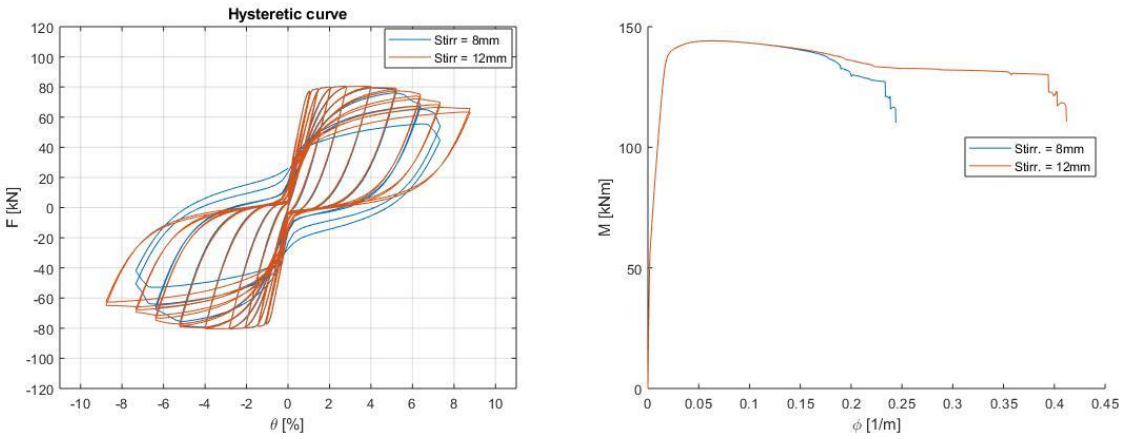

Figure 22: Comparison For Different Lateral Reinforcement Values (12mm)

1.6.4. Longitudinal Reinforcement

On the other, changing the longitudinal reinforcement only affects the strength of the section; it can be observed by changing the diameter of longitudinal bars from 16mm to 12mm and then 20mm we can see the shifting of the curves that indicates only an increase in force reaction of the column without any change in the column ductility.

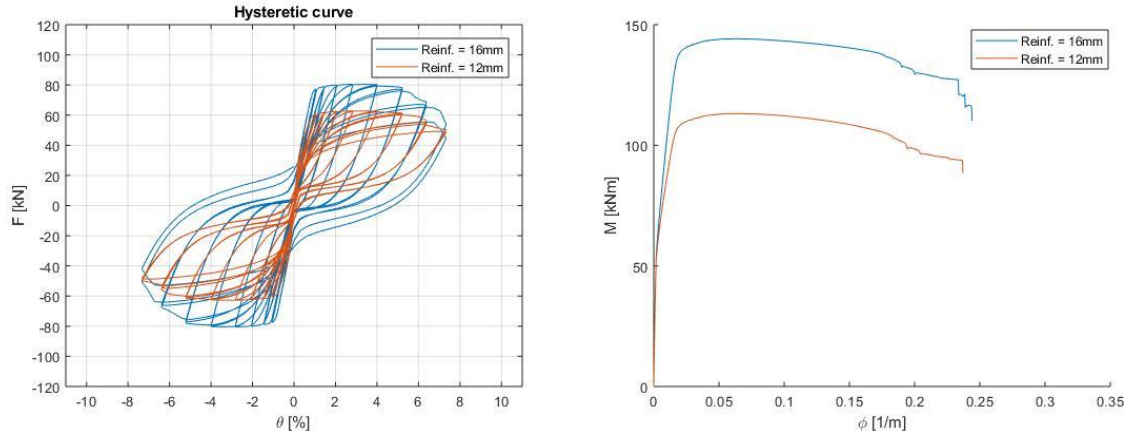

Figure 23: Comparison For Different Longitudinal Reinforcement Values (12mm)

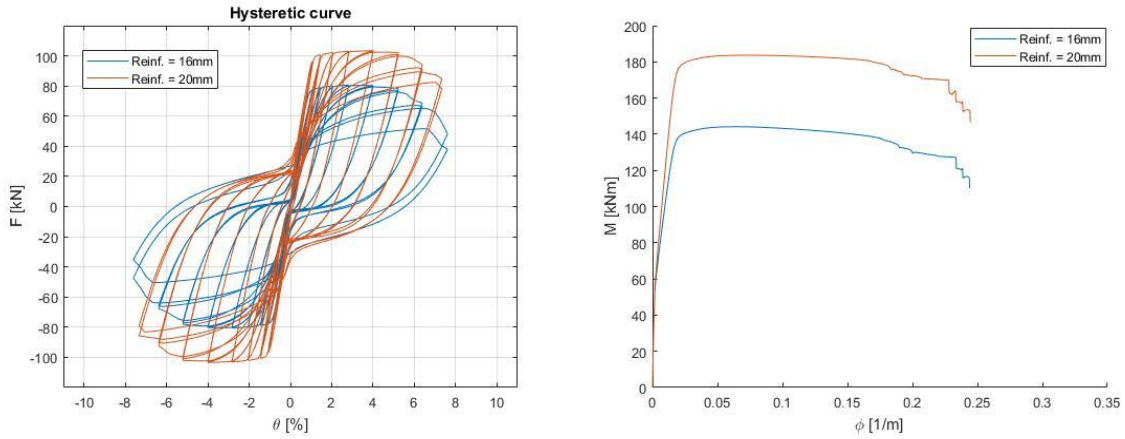

Figure 24: Comparison For Different Longitudinal Reinforcement Values (20mm)

And for higher values of reinforcement, we can still see the same behaviour of increasing capacity with almost the same ductility of the section.

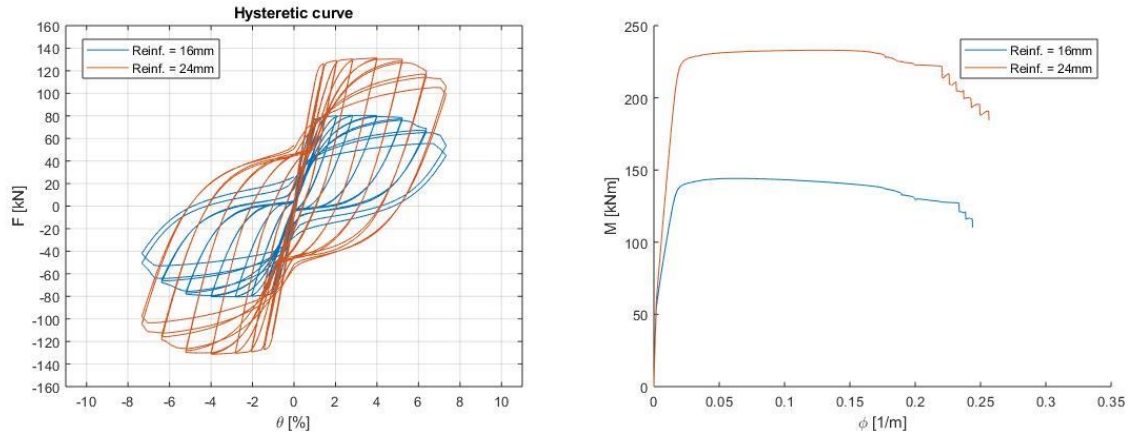

Figure 25: Comparison For Different Longitudinal Reinforcement Values (24mm)

CONCLUSIONS

- Proper confinement is a considerable issue in seismic design, it provides a remarkable increase in section ductility which is the most useful parameter for seismic resistance in columns.
- Confinement of concrete is mostly only effective for non-linear analysis (after yielding), as the true effect is for ductility and the ultimate strength ingrease is not the real benefit for the section charecteristics.
- OpenSees Model provided close enough results for us to assume that the model is validated, and hence we can proceed to change parameters to evaluate each parameter's effect on the overall behaviour.
- In comparing with STD-135, a noticeable increase in both strength and ductility was seen, leading to confirm the fact the the standard methods of detailing provides a better ductility and higher strength values.
- The most effective parameter to increase the strength of the section, is changing the longitudinal reinforcement of the section (bars diameter), knowing that there are other effective factors such as axial load and concrete compressive strength, but longitudinal reinforcement showed the most obvious results.
- The most effective parameter to increase the ductility of the section, is changing the diameter of the lateral reinforcement (knowing that all other factors remains the same), as the normal force also can be effective, but not as much.
- The fibre model that was used does not give accurate information regarding the energy dissipated and the permenant damage, where a better results can be introduced with lumped-plasticity model.

REFERENCES

[1] **ANŽLIN, A. (2017).** "*Influence of Buckling of Longitudinal Reinforcement in Columns on Seismic Response of Existing Reinforced Concrete Bridges"*, PhD. Thesis, University of Ljubljana.

[2] **ISAKOCIĆ, T. And ANŽLIN, A. (2018)**. "*Non-Linear Analysis of Structures: Seismic Response of RC Bridges – Blind Prediction"*, Lecture Notes, University of Ljubljana.

[3] **"OPENSEES"** *The Open System for Earthquake Engineering Simulation* (2000), IKPIR Version 2.0.0, http://opensees.berkeley.edu.

University of Ljubljana
Faculty of Civil and Geodetic Engineer
Institute of Structural and Earthquake Engineering
Lecturer: Prof. Dr. Tatjana Isaković
Dr. Andrej Anžlin

NONLINEAR ANALYSIS OF STRUCTURES: SEISMIC RESPONSE OF RC BRIDGES – BLIND PREDICTION

GROUP 3

- Ana Pavičić, anapavicic96@gmail.com
- Antonio Janevski, antiniojanevski@hotmail.com
- Lajos Gerse, gerselajos@gmail.com
- Mostafa Gad, mostafa.gad@uni-weimar.de
- Rafael Amorim, ramorim@ua.pt

1. TASK 2: PUSHOVER ANALYSIS OF A MULTI-SPAN BRIDGE IN THE TRANSVERSE DIRECTION

1.1. Introduction

The objective of the task 2 of the course "Nonlinear Analysis of Structures: Seismic Response of RC Bridges - Blind Prediction", is to analyse an existing bridge with five piers (Fig. 1) situated in Slovenia, define the peak ground acceleration corresponding to the failure of the first pier and to know How would the doubled mass of a bridge deck (double deck bridge) impact on the seismic behaviour of a structure. The bridge is composed by 5 piers and has 180 metres, the pier sections are using substandard details (Fig. 2) compared to what the Eurocode dictates.

The analysis is made by calculation with the program OpenSees in cooperation with MatLab, calculating the moment-curvature, mphi idealization, pushover analysis and N2 method.

1.2. Case Definition

1.2.1. Study Case

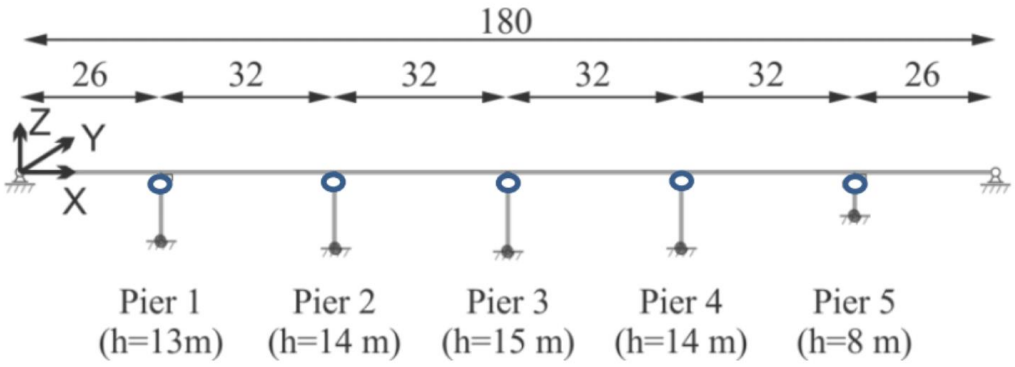

Figure 1: Bridge Layout

The Required case was to study the As-Built case for the bridge pier, which is also on substandard details with 20cm longitudinal spacing between Stirrups.

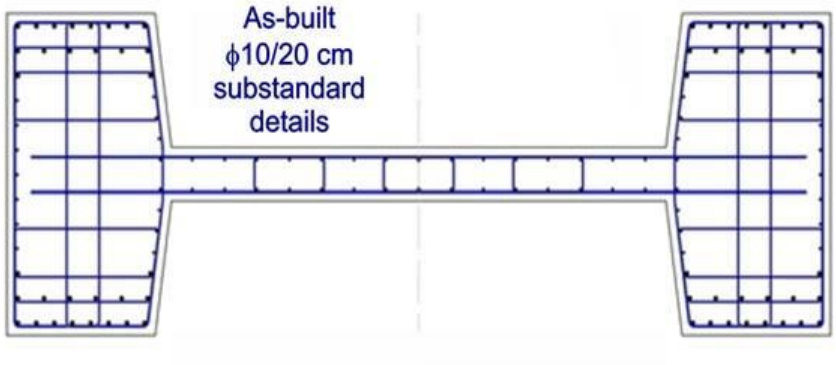

Figure 2: Study Case Section Details

1.2.2. Material Properties

Using The EC material properties and the provided specifics for material grade we have the main material properties for the unconfined concrete, shown in table 1.

Table 1: Unconfined Concrete Properties

Unconfined concrete	
f_{cm} [Mpa]	38
ε_{c1} [‰]	2,2
ε_{cu} [‰]	3,5
E_{cm} [Gpa]	33
$\varepsilon_{spaling}$ [‰]	10,88

Using Mander´s Model the confined concrete properties were calculated, but with the assumption of only the confinement of the section flanges and neglecting the web confinemnt.

Also by assuming the flange shape to be rectangular as the difference is not that much, and the trapizoidal section calculation will be much more complicated.

Table 2: Confined Concrete Properties

Confined concrete	
α	0,74
ρw	0,004
se [Mpa]	1,480
λ	1,25
fcm,c [Mpa]	47,380
εc1,c [‰]	4,47
εcu,c [‰]	12,89

As given, the steel properties of longitudinal reinforcement are listed in table 3.

Table 3: Reinforcement Steel Properties

Reinforcement S500	
fy [Mpa]	500
fu [Mpa]	575
E [Mpa]	200000
εsu [‰]	7,5

1.2.3. Cross Section Properties

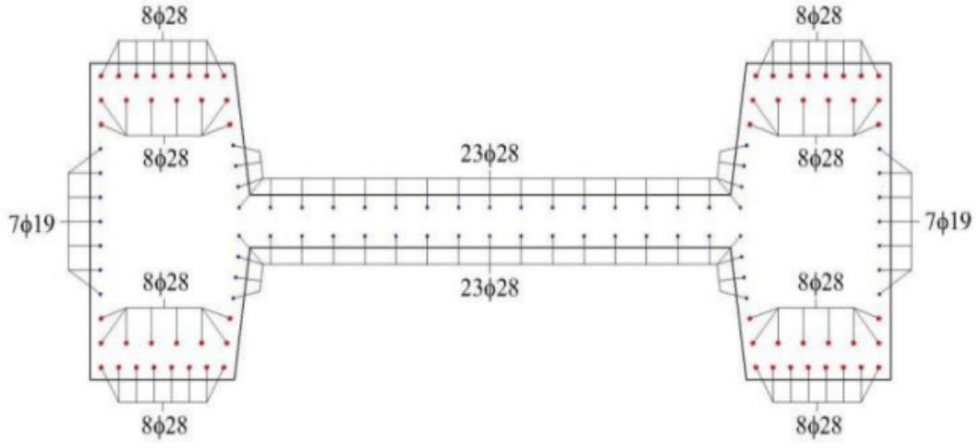

Figure 3: Section Longitudinal Reinforcement

Geometric properties of the section was calculated, in order to later estimate the columns axial and flexural stiffness, which plays an important rule in pushover results of the column.

Table 4: Section Properties

E	33000000	kN/m^2
G	13200000	kN/m^2
A	4,35	m^2
I_z	0,91	m^4
I_y	15,02	m^4
A_{sy}	3	m^2
A_{sz}	0,9	m^2
Mass-piers	9,6	t/m

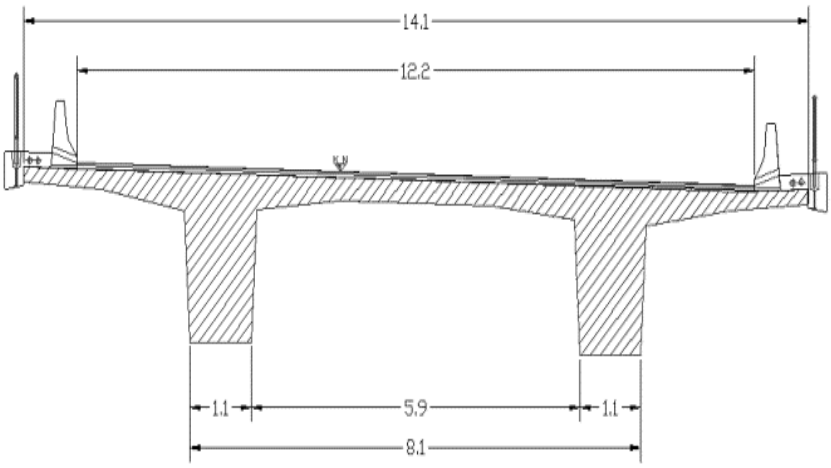

Figure 4: Bridge Deck Cross Section

Mainly for weight and connecting considerations, the properties of the super structure were calculated, not that they will fall under any analysis type.

Table 5: Bridge Deck Section

E	33000000	kN/m^2
G	13200000	kN/m^2
A	4,35	m^2
I_z	0,91	m^4
I_y	15,02	m^4
A_{sy}	3	m^2
A_{sz}	0,9	m^2
Mass-piers	9,6	t/m

1.3. Axial Force

For each pier the axial loads were calculated, depending on the span and the weight of the bridge deck, also taking into account the self weight of the piers, the results are listed in table 12.

Table 6: Single Deck Axial Force

Single Deck

	Height [m]	Axial force [kN]
Pier 1	13	9948
Pier 2	14	10940
Pier 3	15	11049
Pier 4	14	10940
Pier 5	8	9405

Table 7: Double Deck Axial Force

Double Deck

	Height [m]	Axial force [kN]
Pier 1	13	18483
Pier 2	14	20358
Pier 3	15	20466
Pier 4	14	20358
Pier 5	8	17939

1.4. Moment-Curvature relation

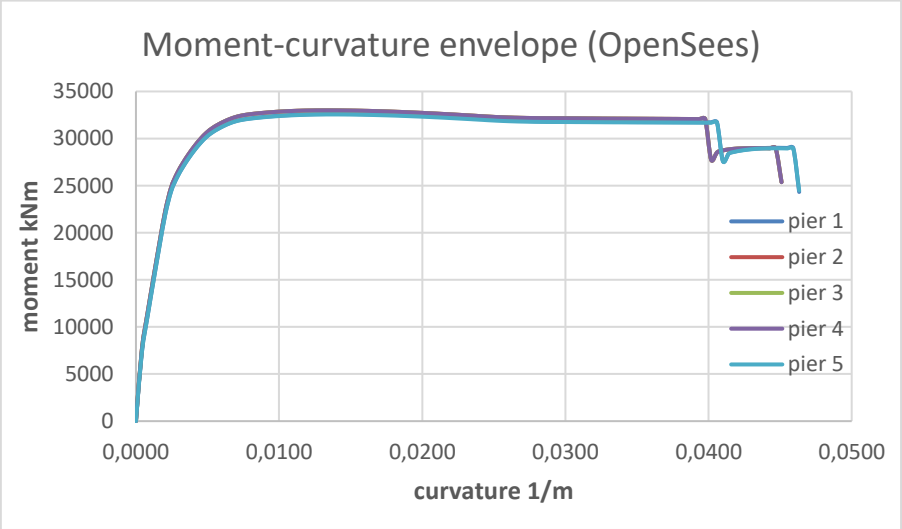

Figure 5: Moment-Curvature Relation for Five Piers

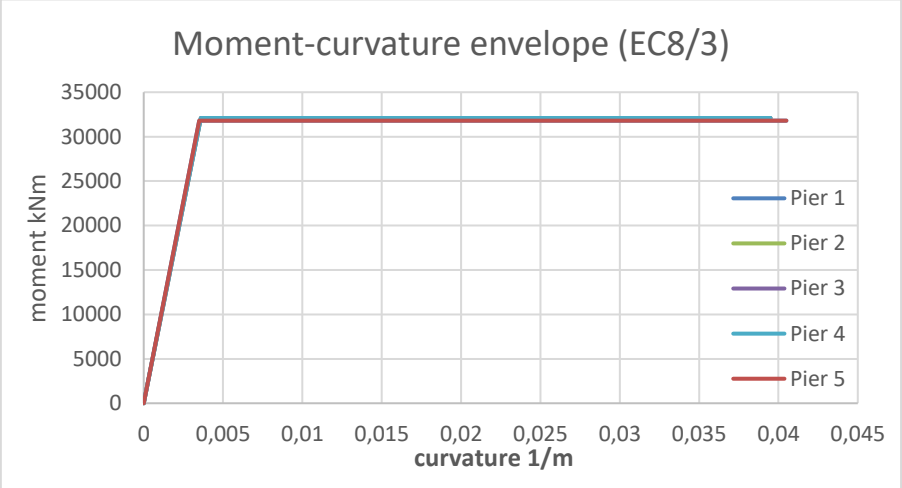

Figure 6: Moment-Curvature Relation for Five Piers - Idealized

Table 8: Moment curvature Results

EC8/3	Moment [kNm]		Curvature [1/m]	
	Yield	Ultimate	Yield	Ultimate
Pier 1	31800	31800	0,0035	0,0405
Pier 2	32100	32100	0,0036	0,0395
Pier 3	32100	32100	0,0036	0,0395
Pier 4	32100	32100	0,0036	0,0395
Pier 5	31800	31800	0,0035	0,0405

1.5. Moment-Rotation Envelope

1.5.1. Single Deck

Using EC8/3 yield and ultimat Rotation equations, the moment rotation envelope of the five piers was calculated, as shown in figure 7.

$$\theta_y = \Phi_y \frac{L_v + \alpha \cdot z}{3} + 0{,}0013\left(1 + 1{,}5\frac{h}{L_v}\right) + 0{,}13\frac{d_{bl} \cdot f_y}{\sqrt{f_c}}$$

$$\theta_{um} = \frac{1}{\gamma_{el}} 0{,}016(0{,}3^{\nu}) \left[\frac{\max(0{,}01;\omega')}{\max(0{,}01;\omega)} fc\right]^{0{,}225} \left(\min\left(9;\frac{Lv}{h}\right)\right)^{0{,}35} 25^{\left(\alpha \cdot \rho_{sx} \frac{f_{yw}}{f_c}\right)} (1{,}25^{100\rho_d})$$

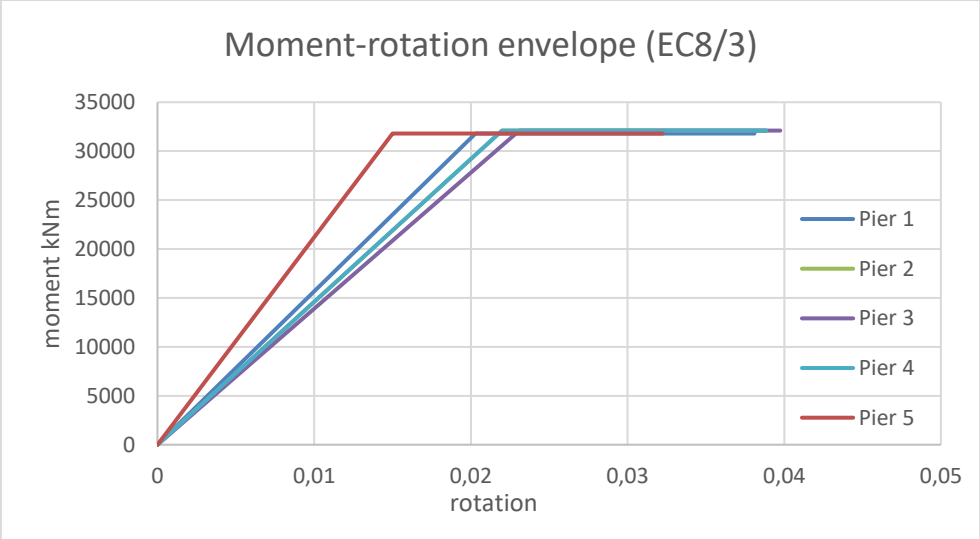

Figure 7: Moment Rotation Envelopes for Five Piers – Single Deck

Table 9: Moment Rotation Results – Single Deck

	Moment [kNm]		Curvature [1/m]		Rotation	
EC8/3	Yield	Ultimate	Yield	Ultimate	Yield	Ultimate
Pier 1	31800	31800	0,0035	0,0405	0,0203	0,0381
Pier 2	32100	32100	0,0036	0,0395	0,022	0,03885
Pier 3	32100	32100	0,0036	0,0395	0,0231	0,03975
Pier 4	32100	32100	0,0036	0,0395	0,022	0,03885
Pier 5	31800	31800	0,0035	0,0405	0,015	0,03225

1.5.2. Double Deck

Same procedures took place for the calculations of the double mass deck,

Aggregated results for five piers shown in figure 8, and numerical results are shown in table 10

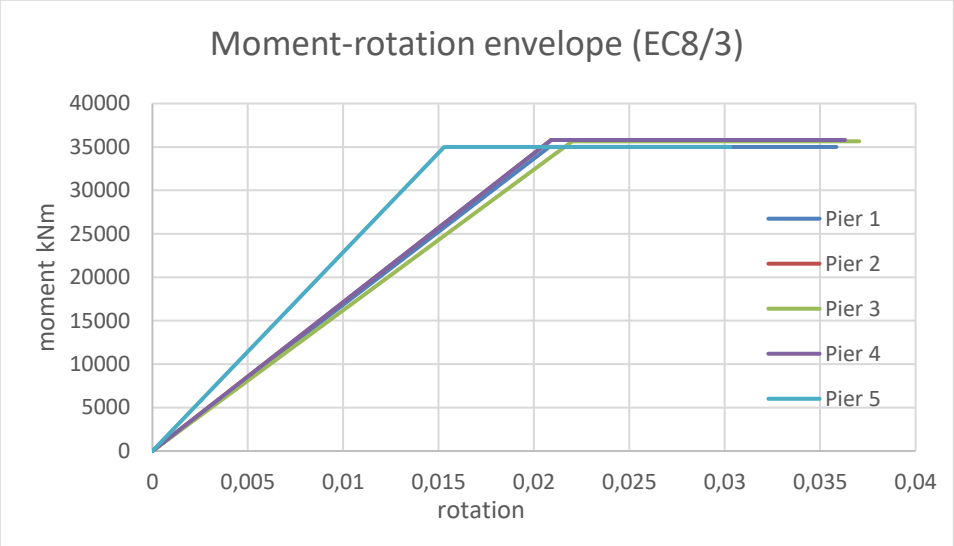

Figure 8: Moment Rotation Envelopes for Five Piers – Double Deck

Table 10: Moment Rotation Results – Double Deck

	Moment [kNm]		Curvature [1/m]		Rotation	
EC8/3	Yield	Ultimate	Yield	Ultimate	Yield	Ultimate
Pier 1	35000	35000	0,0036	0,0308	0,0208	0,03585
Pier 2	35800	35800	0,0034	0,03	0,0209	0,0363
Pier 3	35650	35650	0,0034	0,03	0,022	0,03705
Pier 4	35800	35800	0,0034	0,03	0,0209	0,0363
Pier 5	35000	35000	0,0036	0,0308	0,0153	0,0303

1.6. Pushover Analysis

The next step in our procedures, was to perform the pushover test for all the five piers, and it obvious from the initial observation that the fifth pier (8m), is associated with the lowest rotation possibility, which will lead to earlier failure than the other piers.

1.6.1. Single Deck

The value of the ultimate force was obtained using the ultimate displacement (calculated from the lowest ultimate rotation), which indicates the earlier failure (pier 5).

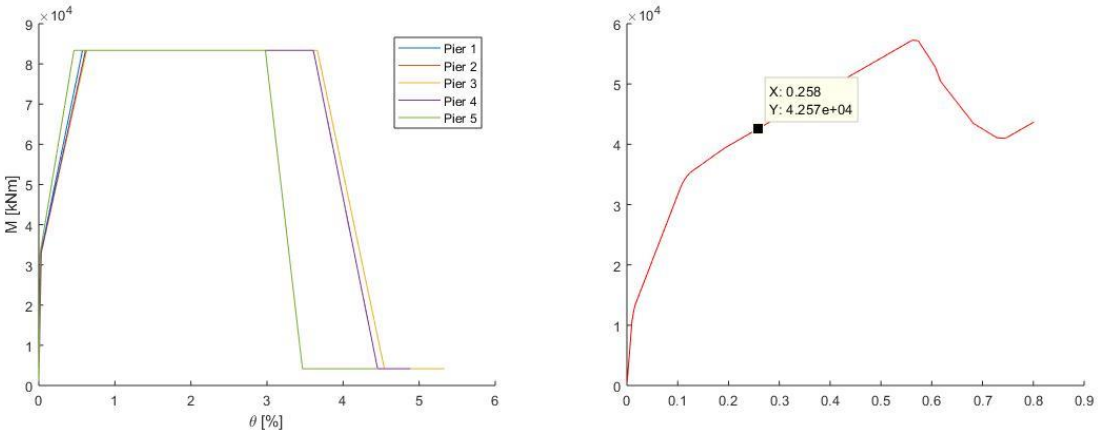

Figure 9: Pushover analysis for single deck load

Table 11: Displacement Results - Single Deck

	Yield displacement [m]	Ultimate displacement [m]
Pier 1	0,264	0,495
Pier 2	0,308	0,544
Pier 3	0,347	0,596
Pier 4	0,308	0,544
Pier 5	0,120	0,258

1.6.2. Double Deck

Same test was performed for double deck load

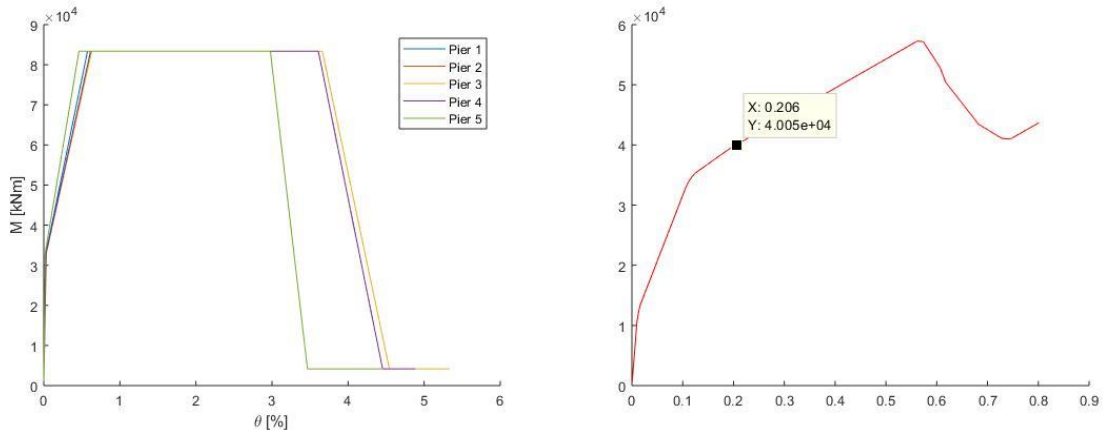

Figure 10: Pushover analysis for double deck load

Table 12: Displacement Results - Double Deck

	Yield displacement [m]	Ultimate displacement [m]
Pier 1	0,270	0,466
Pier 2	0,293	0,508
Pier 3	0,330	0,556
Pier 4	0,293	0,508
Pier 5	0,122	0,242

1.7. N2 Method

As the last step of our procedures, we used the N2 method to calculate the PGA corresponding to the earliest failure for the piers, for both single and double deck cases.

Table 13: N2 Method Calcation – Single and Double Deck

EC8/3 Single deck	
∑mΦi [t]	3576
∑mΦi²[t]	2861
Γ	1,25
F* [kN]	34062
D* [m]	0,206
k* [kN/m]	165000
T* [s]	0,925
ω² [1/s2]	46,139
Sa [m/s2]	9,525
Sd [m]	0,206
PGA	0,651

EC8/3 Double deck	
∑mΦi [t]	7152
∑mΦi²[t]	5723
Γ	1,25
F* [kN]	33438
D* [m]	0,194
k* [kN/m]	172401
T* [s]	1,28
ω² [1/s2]	24,104
Sa [m/s2]	4,675
Sd [m]	0,194
PGA	0,442

The summarized results for N2 methods are gathered in table 14 that shows the ultimate force, displacement and the corresponding PGA calculated using N2 method.

Table 14: N2 Method Calculation Results

	EC8/3	
Compare	Single_deck	Double_deck
Ultimate Displacement [m]	0,258	0,242
Ultimate Force [kN]	42570	41790
Period [s]	0,925	1,280
PGA	0,65	0,44

1.8. EC8/2 and EC8/3 Rotation Envelopes

Just numerically and Using the factor of safety of 1, the envelopes of moment rotation results was calculated using both EC8/3 (mentioned earlier) and EC8/2 to compare both results, giving the fact that EC8/2 is used for design and EC8/3 is only used for assessment.

1.8.1. Single Deck

Table 15: EC8/2 - EC8/3 Results Comparison – Single Deck

Ultimate rotation	EC8/3	EC8/2	Ratio
Pier 1	0,0381	0,053	1,38
Pier 2	0,03885	0,054	1,40
Pier 3	0,03975	0,058	1,46
Pier 4	0,03885	0,054	1,40
Pier 5	0,03225	0,035	1,09

1.8.2. Double Deck

Table 16: EC8/2 - EC8/3 Results Comparison – Double Deck

Ultimate rotation	EC8/3	EC8/2	Ratio
Pier 1	0,03585	0,039	1,08
Pier 2	0,0363	0,040	1,11
Pier 3	0,03705	0,043	1,16
Pier 4	0,0363	0,040	1,11
Pier 5	0,0303	0,026	0,85

1.9. Results

At the end all the results including the EC8/2 and 3 methods comparison are shown in table 17, to have a final overview for all the available resutls for this task.

Table 17: Aggregated Final Results

	EC8/3		EC8/2	
Compare	Single_deck	Double_deck	Single_deck	Double_deck
Ultimate Displacement [m]	0,258	0,242	0,868	0,643
Ultimate Force [kN]	42570	41790	43540	40000
Period [s]	0,925	1,280	0,953	1,206
PGA	0,65	0,44	0,69	0,40

CONCLUSIONS

- Ultimate displacement are not very different (after modifying the factor of safety) according to EC8/2 against to EC8/3, this gave us close values of peak groud acceleration.
- Double mass of deck gave us lower value of peak groung acceleration.
- Double mass of deck has small influence to horizontal forces.
- Period is in the correlation with the horizontal force and mass of the construction.
- Characteristics of the ground have also influence to peak ground acceleration.

REFERENCES

[1] **ANŽLIN, A. (2017).** "*Influence of Buckling of Longitudinal Reinforcement in Columns on Seismic Response of Existing Reinforced Concrete Bridges"*, PhD. Thesis, University of Ljubljana.

[2] **ISAKOCIĆ, T. And ANŽLIN, A. (2018)**. "*Non-Linear Analysis of Structures: Seismic Response of RC Bridges – Blind Prediction"*, Lecture Notes, University of Ljubljana.

[3] **"OPENSEES"** *The Open System for Earthquake Engineering Simulation* (2000), IKPIR Version 2.0.0, http://opensees.berkeley.edu.

Project report

‘Task-1’

BLIND PREDICTION OF THE STATIC CYCLIC RESPONSE OF A RECTANGULAR RC CANTILEVER COLUMN

Submitted by

‘Nooshin Hadidian Moghaddam’
‘Denis Berbić’
‘Gregor Udovč’
‘Zsombor Illés’

Group-5

M.Sc. Erasmus course

University of Ljubljana, faculty of Civil and Geodetic Engineering

Prof. Dr.Tatjana Isakovic´
Prof. Dr.Marjeta Kramar
Dr. Andrej Anžlin

Table of Contents

Declaration

Hereby, we declare that, we worked on this Report independently and using only the specified sources and programs which are referred.

Ljubljana, 03.09.2018 Nooshin Hadidian.M

Denis Berbić

Gregor Udovč

Zsombor Illés

1 Abstract

Performance based design (PBD), can be defined as a procedure that can provide reliable design and construction process to attain desired seismic performance of structure. This performance can be provided by effective ductile behaviour and increased the level of inelastic deformation of structure. This process can be expressed as capacity design approach which avoids from brittle failure mechanism (shear failure/compression failure of concrete) and causes the formation of plastic hinges in predetermined positions of the structure.

This work is a part of PhD project which had been performed in Ljubljana University, faculty for Civil and Geodetic Engineering, built environment. The report is mainly related to the consideration of RC cantilever column behaviour with pre-determined rectangular section type (Group-5, SUB+/90,3Φ8 @ 12 cm [1]) under specified cyclic loading protocol and the comparison of its response with STD/135 [2] section. The efficiency of stirrups is examined using Mander's model (EC8/2) in manual calculations and simulated procedure is performed by OpenSees tool and EC8/3 criteria are used for getting yield and ultimate (Near Collapse) rotation of RC column with substandard specifications.

2 Introduction

Capacity design of structures mainly deals with the concept of the level of ductility to get determined performance. Ductile components can be designed with sufficient capacity of deformation to satisfy the displacement-based demand capacity ratio. Contrarily, brittle components are designed to get sufficient strength level which satisfies the strength-based capacity ratio. So consideration of different parameters which can influence the ductility of structures is essential to get the more realistic picture about the response of structure. These parameters can be included as follows [1]:

- Axial force
- Tensile and Component reinforcement
- Compression zone
- Compression strength of concrete
- Amount of transverse reinforcement

***1. It is displayed in Table 1-1.** ***2.It is displayed in Table 1-7.**

Nonlinear analysis of structural components under cyclic loading can be modeled using Micro and Macro models. Fig 1-1, shows the several types of structural component models.

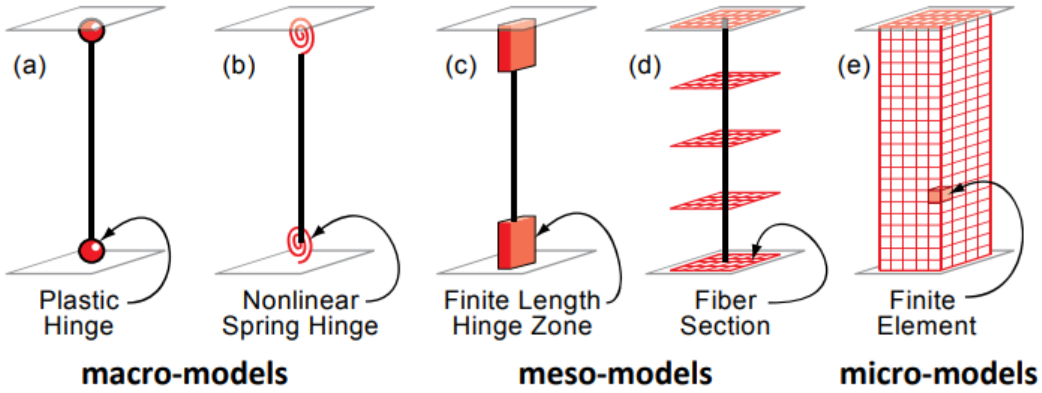

Fig 1-1. *Types of structural component models [2]*

3 Tasks

According to the specified tasks for this work as task-1, lumped plasticity numerical model using Takeda's hysteretic rules are used for calculation procedure. The sub-tasks are mentioned as follows:

- Calculation of the moment-rotation envelope (crack, yield and near collapse).
- The full non-linear cyclic response of the column (force-displacement curve)
- Detailed report about the cyclic analysis of the column
- Comparison of the results with the results of a column STD/135 (see Exercise Lectures) and the comments of the differences.
- The analysis of the influence of the different parameters to the ductility of the analysed column (level of axial force, concrete compressive strength, amount of lateral reinforcement, amount of longitudinal reinforcement)

The numerical lumped plasticity models are shown in Fig 1-2 for BWH and Giberson's model which is equal to Takeda's hysteretic rules.

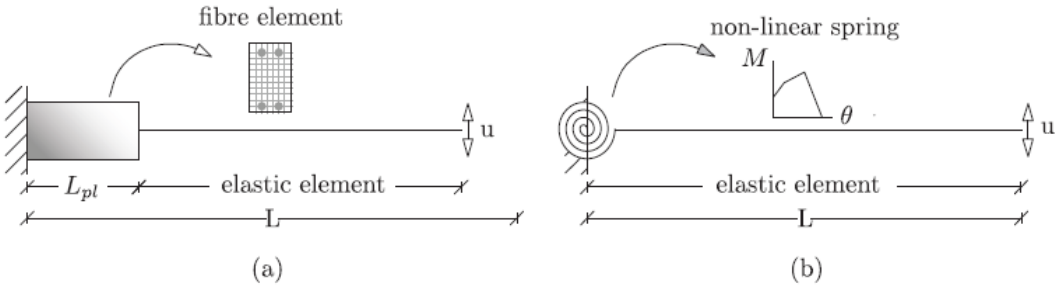

Fig 1-2. *The considered numerical lumped plasticity models:*

(a) The BWH fiber model and (b) Giberson's model. [3]

The behaviour of the non-linear spring for **Giberson's** numerical model was defined using **Takeda** hysteretic rules. Both types of approaches, micro and macro numerical modelling, have been used in this project. The properties of assigned frame for group-5 are described in Table 1-1.

Table 1-1. *The mean material properties of assigned section for group-5*

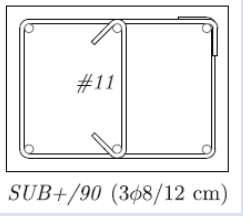

Calculations are around weak axis

Cross-section: b/h=30/40 cm
Concrete grade C30/37
Height=1.8 m

Lateral Reinforcement				
f_y [MPa]	**f_t [MPa]**	**ε_y [%]**	**ε_u [%]**	**E [GPa]**
554	668	0.30	10.12	186
Longitudinal reinforcement				
f_y [MPa]	**f_t [MPa]**	**ε_y [%]**	**ε_u [%]**	**E [GPa]**
600	709	0.30	7.56	198
Compressive cylindrical strength f_{cm} [MPa]			Axial force (N [kN])	
35.8			577	

Loading protocol and related setup are shown in Fig 1-3.

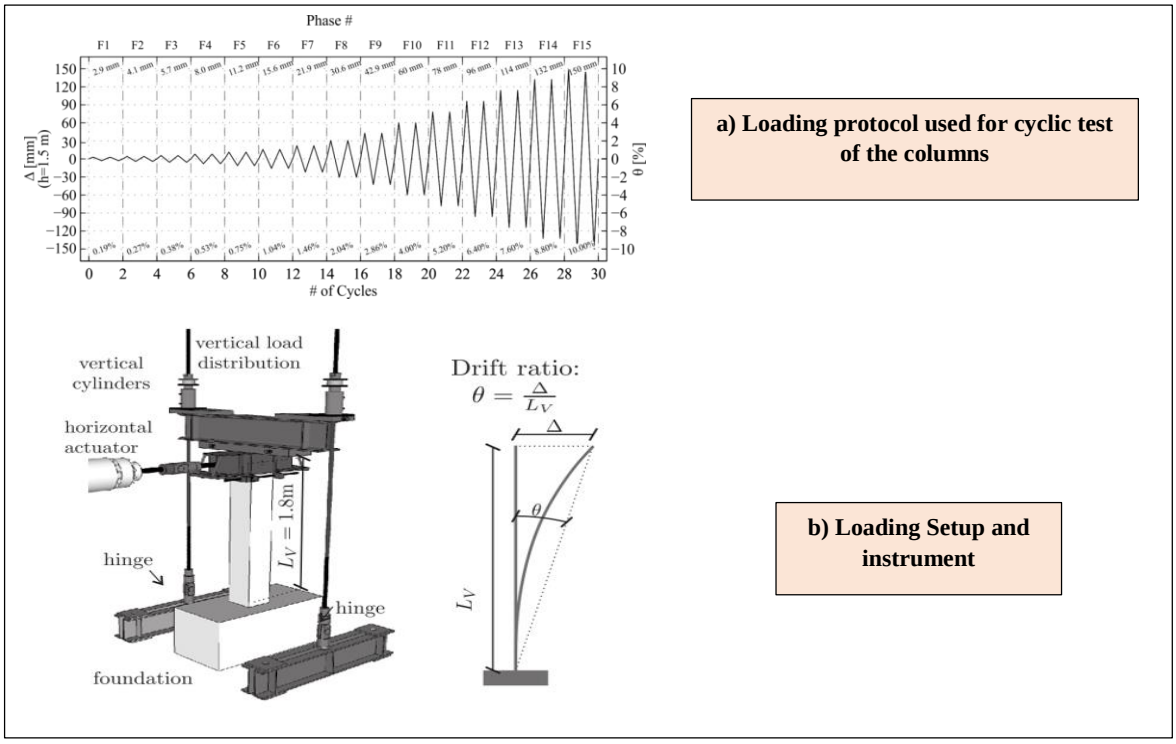

Fig 1-3. *Loading protocol and practical experiment setup*

As shown in Table 1-1, the assigned section for group-5 is **substandard** section which following conditions in Fig 1-4, should be observed.

s	d_{bl}	
12	1.6	SUB
s/d_{bl}	7.5	s/d_{bl} >6 √

S= distance between lateral reinforcement
$\mathbf{d_{bl}}$ = Diameter of longitudinal bar

1)

$2.5*(f_{su}/f_{sy})+2.25$	5.204	Ok, between 5 & 6. √

$$5 \leq \delta_s = 2.5\left(\frac{f_{su}}{f_{sy}}\right) + 2.25 \leq 6$$

$\mathbf{f_{su}}$ = Ultimate strength of longitudinal bars
$\mathbf{f_{sy}}$ = Yield strength of longitudinal bars

2)

Fig 1-4. *Anti-buckling limits for substandard section of column in bridge according to EC8/2*

3.1 Calculation of the moment-rotation envelope (crack, yield and near collapse).

The calculation of moment-curvature and moment-rotation envelops are performed both with **manual** approach and **OpenSees**. Following parts describe about the procedures in manual calculation.

1- Calculation of moment-curvature and moment-rotation envelope of RC section without consideration of efficiency of stirrups in confining RC section.

2- Calculation of efficiency of stirrups based on Mander's method (EC8/2).

3-Calculation of moment-curvature and moment-rotation envelope of RC section considering the efficiency of stirrups.

4- Comparison of results for moment curvature envelope between confined and unconfined sections and OpenSees results.

5- Comparison of efficiency of stirrups between Mander's method (EC8/2) and EC2.

The results of each part are shown in Fig 1-5, 1-6, 1-7, 1-8 and 1-9 respectively.

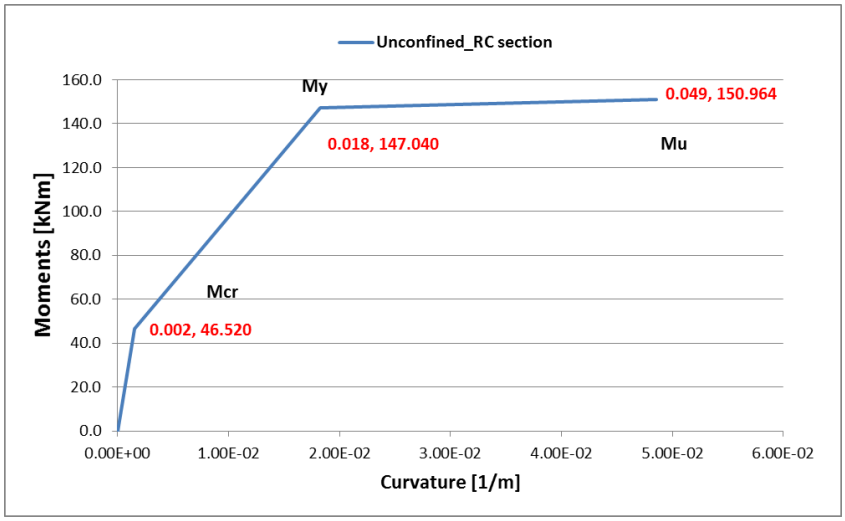

Fig 1-5. *Manual calculation of moment-curvature envelope for unconfined RC section*

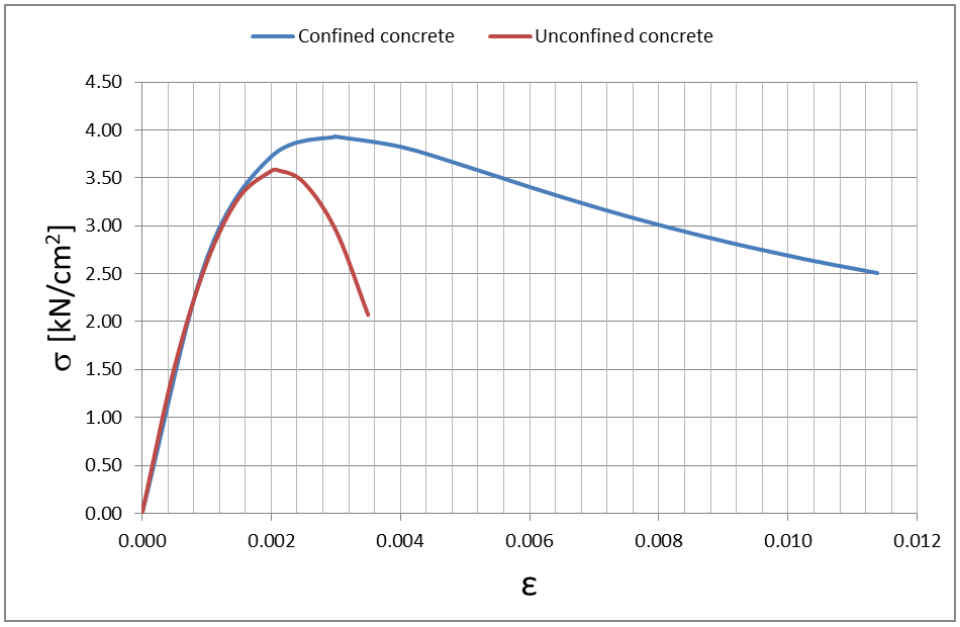

Fig 1-6. *Efficiency of stirrups based on Mander's method*

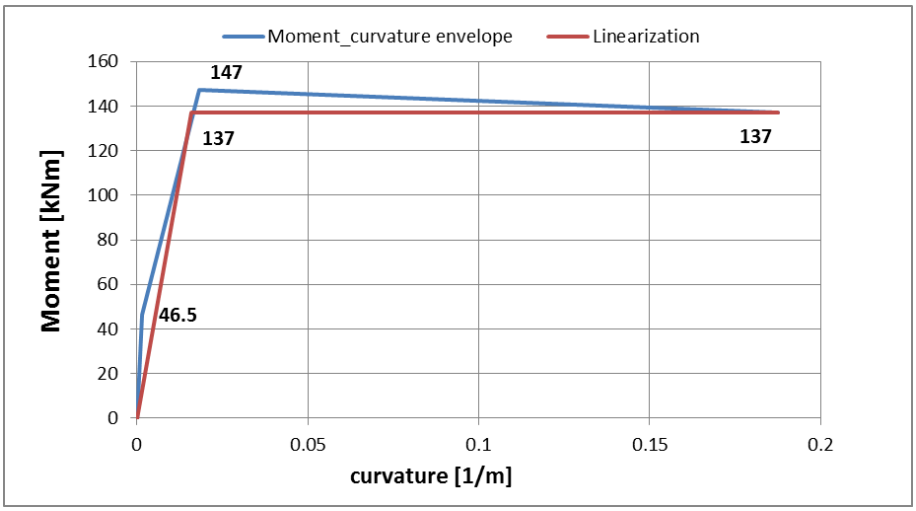

Fig 1-7. *Moment-curvature envelope of confined RC section and its linearization*

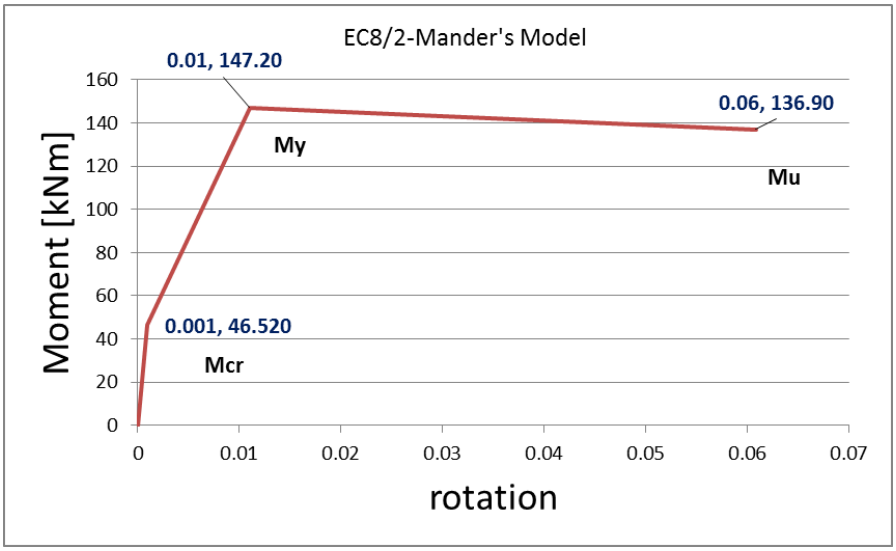

Fig 1-8. *Moment-rotation envelope of confined RC section based on Mander's model*

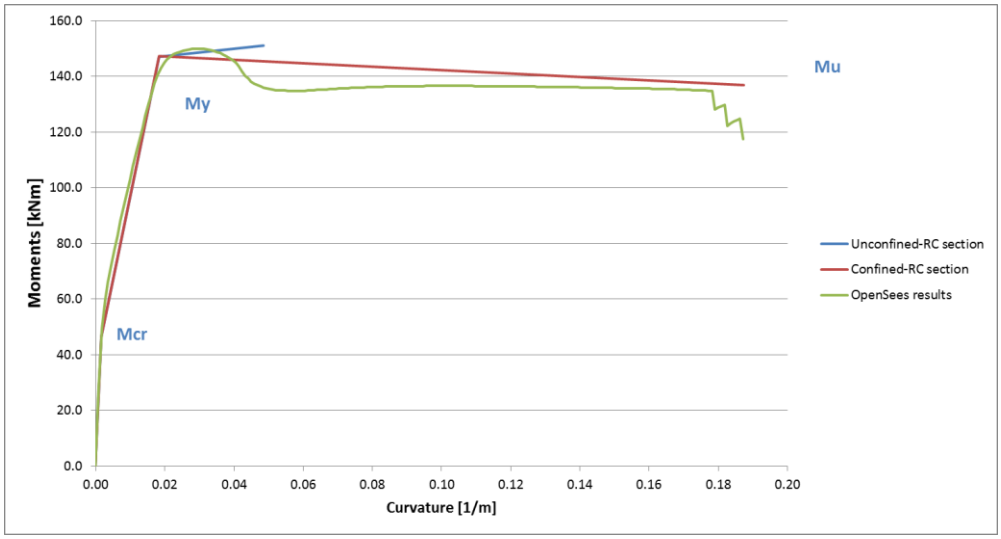

Fig 1-9. *Comparison of moment curvature envelopes between confined, unconfined sections and OpenSees*

Effectiveness of stirrups can be calculated according to defined equations in EC8/1 for rectangular section and Mander's model in EC8/2.These equations are shown as follows in Fig 1-10 and 1-11:

Confined concrete-Mander's model
(EC8/2)
Rectangular section

$$\sigma_e = \alpha\rho_w f_{ym}$$

$$\lambda_c = 2.254\sqrt{1 + 7.94\frac{\sigma_e}{f_{cm}} - \frac{2\sigma_e}{f_{cm}}} - 1.254$$

$$\varepsilon_{c1,c} = 0.002\left[1 + 5\left(\frac{f_{cm,c}}{f_{cm}} - 1\right)\right]$$

$$E_{sec} = \frac{f_{cm,c}}{\varepsilon_{c1,1}}$$

$$f_{cm,c} = f_{cm}\lambda_c$$

$$\varepsilon_{cu,c} = 0.004 + \frac{1.4\rho_s f_{ym}\varepsilon_{su}}{f_{cm,c}}$$

$$\frac{\sigma_c}{f_{cm,c}} = \frac{xr}{r-1+x^r}$$

$$x = \frac{\varepsilon_c}{\varepsilon_{c1,1}}$$

$$r = \frac{E_{cm}}{E_{cm}-E_{sec}}$$

Fig 1-10. *Defined equations in EC8/2 for confined concrete*

Effectiveness of the stirrups
(EC8/1)

$$\alpha = \alpha_n\alpha_s$$

$$\alpha_n = 1 - \sum_n \frac{b_i^2}{6b_o h_o}$$

$$\alpha_s = \left(1 - \frac{s}{2b_o}\right)\left(1 - \frac{s}{2h_o}\right)$$

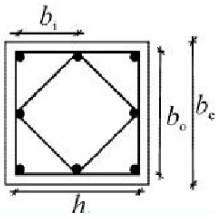

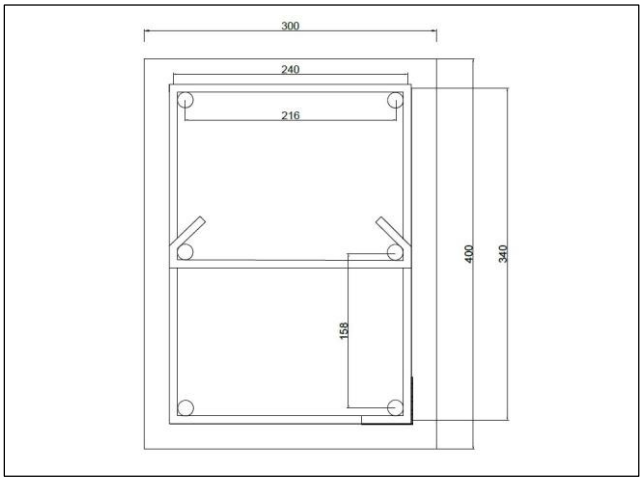

Details of RC column section for group-5

Fig 1-11. *Effectiveness of stirrups in EC8/1 for assigned RC column section for group-5*

Fig 1-12, demonstrates the defined equations in EC-2 for confined concrete.

$$f_{ck,c} = f_{ck}(1 + 5\left(\frac{\sigma_2}{f_{ck}}\right)) \qquad for \quad \sigma_2 \leq 0.05 f_{ck}$$

$$f_{ck,c} = f_{ck}\left(1.125 + 2.5\frac{\sigma_2}{f_{ck}}\right) \qquad for \quad \sigma_2 > 0.05\, f_{ck}$$

$$\varepsilon_{c2,c} = \varepsilon_{c2}(\frac{f_{ck,c}}{f_{ck}})^2$$

$$\varepsilon_{cu2,c} = \varepsilon_{cu2} + 0.2\,\frac{\sigma_2}{f_{ck}}$$

Fig 1-12. *Equations for confined RC section in EC-2*

Table 1-2 and 1-3, show the results of efficiency of stirrups and confined concrete without consideration of end hook angles based on related equations in EC8/2 (Mander's model) and EC-2.

Table 1-2. *Efficiency of stirrups in Mander's model and confined concrete results*

bo	24.00	cm			
ho	34.00	cm			
wi-1	15.8	cm			
wi-2	21.600				
s	12.000	cm			
alfan	0.605				
alfas	0.6176				
alfa	0.373959				
Asw	0.50	3.0		1.51	cm2
row	3.70E-03				

Table 1-3. *Confined concrete results in EC-2*

σe	0.052	
Ecm	3300	
fck	2.78	
ec2	0.002	
ecu2	0.0035	
σe/ fck	0.019	<0.05
fck,c	2.74	
ec2,c	0.00194	
ecu2,c	0.007	
k	2.45	

The effect of the end hook angle in the SUB+/90 confined column, is determined using the concept of effective confinement area according to the angle of utilized hooks which is shown in Fig 1-13.

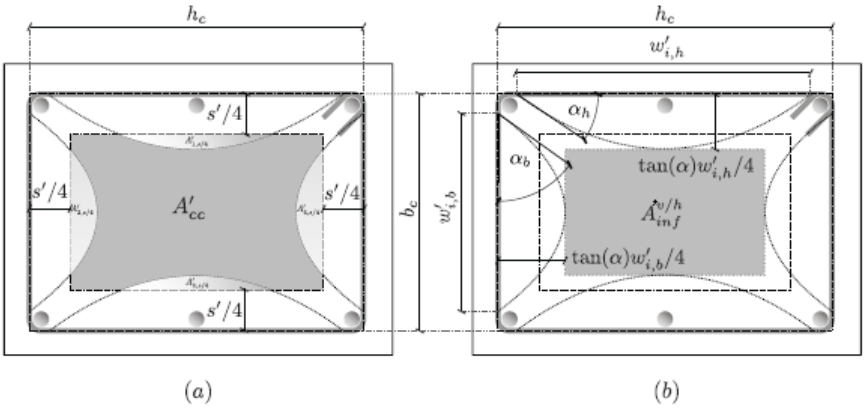

Fig 1-13. *(a) Definition of the confinement effectiveness area in a rectangular cross-section* A'_{cc} *and (b) the infimum area of confined concrete* $A'^{y=h}_{inf}$ *[3]*

According to the new definitions for effective confined core of concrete, Table 1-4, briefly shows the results of calculations to obtain modified values for confined section.

Table 1-4. *Calculation of related parameters for showing the effects of end hook angle in the SUB+/90* [3]

Parameter	Equation	Result
$\boldsymbol{K'_{eh,s/4}}$	$\sum_{1} \frac{\omega_i'^2}{6b_c h_c} \frac{(\tan(\alpha_i) - \frac{s'}{\omega_i'})^{3/2}}{tan\alpha_i^{1/2}}$	0.910
$\boldsymbol{K'_{e,inf}}$	$(1 - \frac{\max[s'; \tan(\alpha_h)\,\omega'_{i,h}]}{2b_c})(1 - \frac{\max[s'; \tan(\alpha_h)\,\omega'_{i,b}]}{2bh_c}$	0.44
$\boldsymbol{K'_{e,rect}}$	$\left(1 - \frac{s'}{2h_c}\right)\left(1 - \frac{s'}{2h_b}\right) - K'_{eh,s/4}$	0.640
$\boldsymbol{K'_{e,hooks}}$	$\left(1 - \frac{n_{imp}}{n_{imp} + n_{prop}}\right) k'_{e,rect} + (\frac{n_{imp}}{n_{imp} + n_{prop}}) k'_{e,inf}$	0.608
$\boldsymbol{K'_{hooks}}$	$\frac{k'_{e,hooks}}{k'_{e,rect}}$	0.95
$\sigma_{e,new}$	$\alpha \rho_w f_{ym} \frac{K'_{hooks}}{k_{eff,buck}}$	0.072

Parameter	Equation	Result
$\lambda_{c,new}$	$2.254\sqrt{1+7.94\frac{\sigma_{e,new}}{f_{cm}}-\frac{2\sigma_{e,new}}{f_{cm}}}-1.254$	1.1
$f_{cm,c,new}$	$f_{cm}\lambda_{c,new}$	3.93
$\varepsilon_{c1,c,new}$	$0.002\left[1+5\left(\frac{f_{cm,c,new}}{f_{cm}}-1\right)\right]$	0.0029
$\varepsilon_{cu,c,new}$	$0.004+\frac{1.4\rho_s f_{ym}\varepsilon_{su}}{f_{cm,c,new}}$	0.01

Fig 1-14, compares the behaviour of concrete in **σ-ε** diagram for both confined concrete in EC8/2 and EC-2 and unconfined concrete.

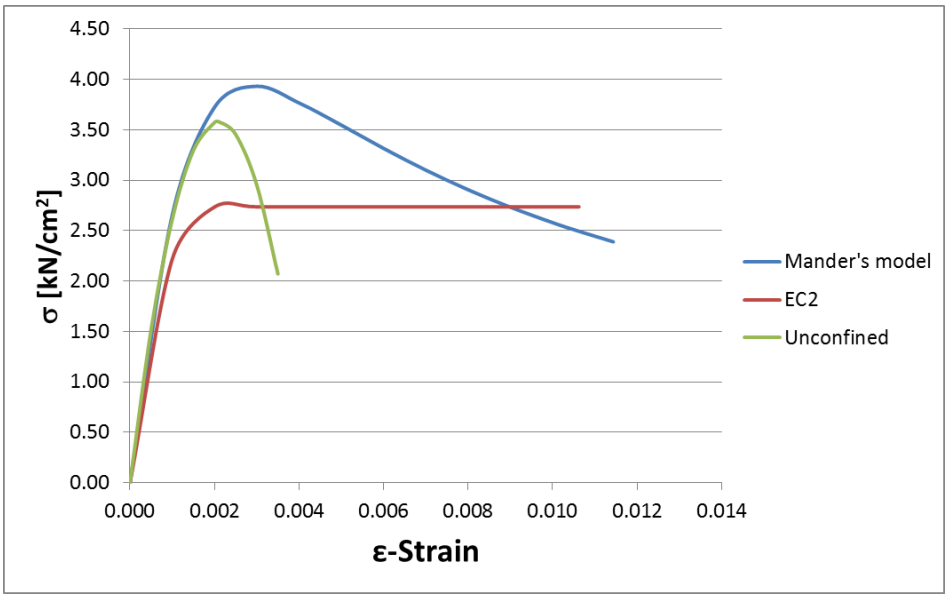

Fig 1-14. *Comparison of behaviour for confined concrete in EC8/2 and EC-2 and unconfined concrete*

Considering Takeda's rules, moment rotation relationships are calculated by affecting the plastic hinge length to get ultimate rotation. Table 1-5, describes in more detail about the utilized equations and related results.

Table 1-5. *EC8/2 equations for moment rotation relationships and related results for assigned section in group-5*

Parameter	Equation	Result
L_p	$0.10\ L + 0.015\ f_{yk}\ d_{bL}$	0.324
θ_y	$\frac{1}{3}\varphi_y L$	0.011
$\theta_{p,u}$	$(\varphi_u - \varphi_y)L_p(1 - \frac{L_p}{2L})$	0.0597
θ_u	$\theta_{y} + \theta_{p,u}$	0.0608

Beside mentioned equations in EC8/2 for moment-curvature and moment-rotation relationships, EC8/3 provides equations for calculating yield and ultimate (Near collapse) rotation which are more applicable for substandard RC sections like what is assigned for group-5. Table 1-6, shows these equations and related results for determined RC section.

Table 1-6. *EC8/3 equations for moment rotation relationships and related results for assigned section in group-5*

Parameter	Equation	Result
θ_y	$\varphi_y \frac{L_v + a_v z}{3} + 0.0013\left(1 + 1.5\frac{h}{L_v}\right) + 0.13\varphi_y \frac{d_b f_y}{\sqrt{f_c}}$	**0.0169**
θ_{um}	$\frac{1}{\gamma_{el}} 0.016(0.3^{\nu}) \left[\frac{\max(0.01;\omega')}{\max(0.01;\omega)} f_c\right]^{0.225} \left(\min\left(9;\frac{L_v}{h}\right)\right)^{0.35} 25^{\left(\alpha\rho_{sx}\frac{f_{yw}}{f_c}\right)} (1.25^{100\rho_d})$	**0.0615**

Fig 1-15, shows the comparison of results for moment-rotation calculation between EC8/2 and EC8/3 for specified RC section.

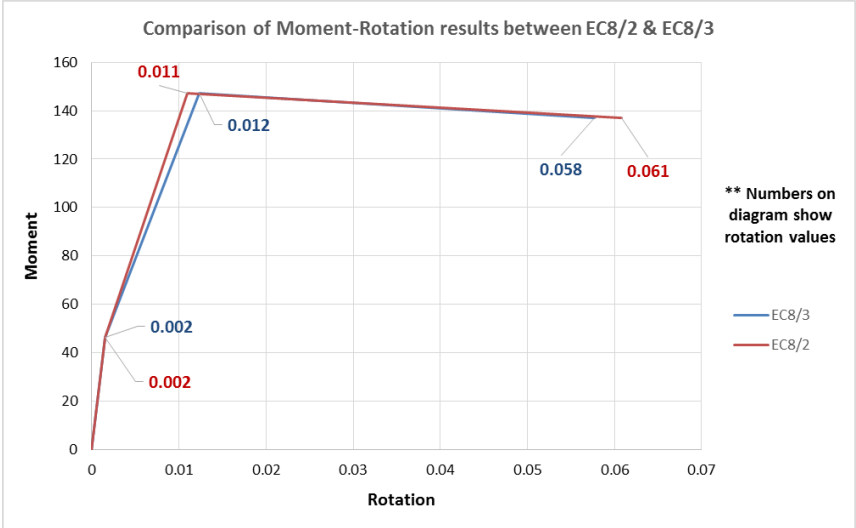

Fig 1-15. *Comparison of results for moment-rotation calculation between EC8/2 and EC8/3 for specified RC section*

3.2 The full non-linear cyclic response of the column (force-displacement curve)

This section which is mainly about the full nonlinear response of column with determined frame, analysed by OpenSees software and defined MATLAB codes according to the determined properties for SUB+/90 (3 ϕ 8 12 cm) such as material, cross section and essential protocols e.g. loading, moment-curvature and cyclic pushover. In part 2.3, the results of OpenSees process and their comparison with achieved results in part 2.1 as manual computations, are described in more details. Fig 1-16 and 1-17, show the moment-curvature and nonlinear cyclic response of RC section calculated by OpenSees.

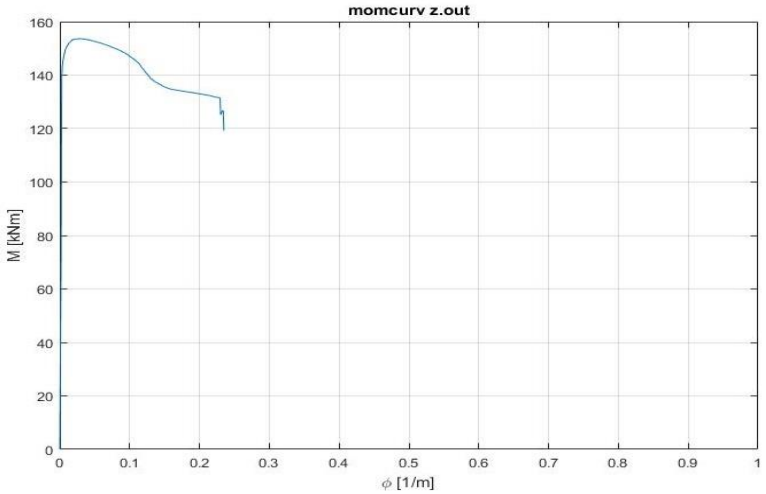

Fig 1-16. *Moment-curvature of assigned section for group-5 by OpenSees (Non-linear spring model)*

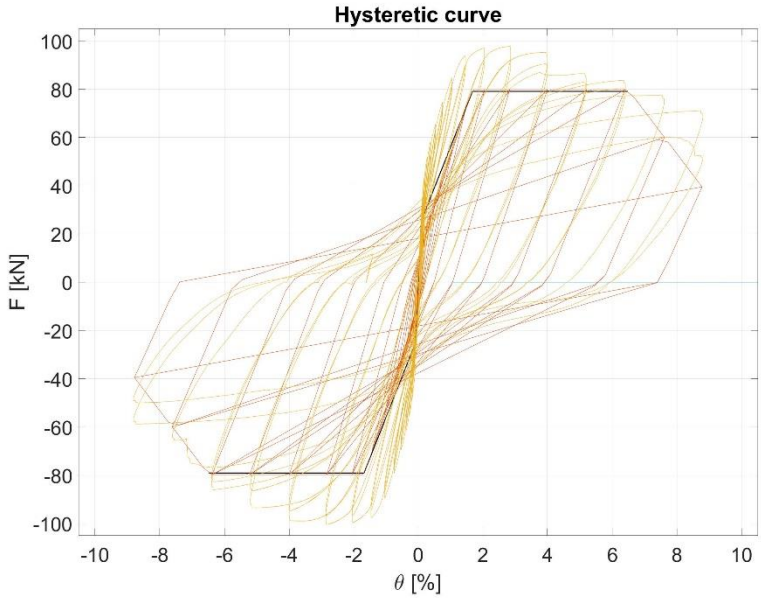

Fig 1-17. *Force-drift ratio curve of assigned section for group-5 by OpenSees (Non-linear spring model)*

3.3 Detailed report about the cyclic analysis of the column

In this part, the achieved results of moment-curvature, moment-rotation and cyclic behaviour of SUB+/90 (3 ϕ 8 12 cm) section - group 5 - by manual and OpenSees tools are more scrutinized and compared with together. Table 1-7 describes the computed results for SUB +/90(3 ϕ 8 12 cm) section both by manual calculations and OpenSees and the difference ratio between them.

Table 1-7. *Comparison of results between manual and OpenSees computations for SUB+/90*

Parameter	Manual Calculation/Linearization	OpenSees' Calculation/Linearization	Difference ratio (%)
(M_{cr},φ_{cr})	(46.5, 0.00153)	(45.6,0.00153)	(1.9, 0)
(M_y,φ_y)	(147,0.0183)	(142.3,0.0189)	(3.19, 3.17)
(M_u,φ_u)	(137,0.187)	(132.5.3,0.201)	(3.28 , 6.9)

As shown in Table 1-7, there are very small difference ratio between manual and software calculations for moment-curvature envelope of section. Although it should be mentioned that the effects of standard and substandard stirrups such as the angle of hooks cannot be clarified

via currently used properties in material and cross section in OpenSees. The most detailed information about moment-rotation and moment-curvature envelopes are described in part 2.1.

3.4 Comparison of the results with the results of a column STD/135

This part contains information about the material properties of column section STD/135 and its details and comparison of its related results with column section SUB+/90 which have been explained in part 2.1,2.2 and 2.3. Table 1-8, shows all detailed information about STD/135 properties as a standard detailed section.

Table 1-8. *The mean material properties of STD/135*

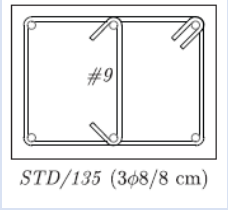

Cross-section: b/h=30/40 cm
Concrete grade C30/37
Height=1.8 m

Lateral Reinforcement				
f_y [MPa]	**f_t [MPa]**	**ε_y [%]**	**ε_u [%]**	**E [GPa]**
554	668	0.30	10.12	186
Longitudinal reinforcement				
f_y [MPa]	**f_t [MPa]**	**ε_y [%]**	**ε_u [%]**	**E [GPa]**
600	709	0.30	7.56	198
Compressive cylindrical strength f_{cm} [MPa]			Axial force (N [kN])	
36.5			577	

As shown in Table 1-1 and 1-8, both **SUB+/90** and **STD/135** have same type of longitudinal and lateral reinforcement, axial force and dimensions, but they are just different in $\mathbf{f_{cm}}$ parameter in concrete and the distance of stirrups. Table 1-9, shows the achieved results of moment-curvature and moment-rotation envelopes for STD/135 and its comparison with SUB+/90 section. This results are obtained from manual calculation.

Table 1-9. *Comparison of moment-curvature parameters*

between SUB+/90 & STD/135 –Manual computation/Linearization

Parameter	SUB+/90	STD/135
(M_{cr},φ_{cr})	(46.5, 0.00153)	(45.4, 0.00153)
(M_y,φ_y)	(137,0.0183)	(146,0.0185)
(M_u,φ_u)	(137,0.187)	(146,0.2)
L_p(Mander)	0.324	0.324
θ_y (Mander)	0.011	0.016
$\theta_{p,u}$(Mander)	0.0597	0.05425
θ_u(Mander)	0.0608	0.06213
θ_y (EC8/3)	0.0169	0.0169
θ_{um}(EC8/3)	0.0615	0.0619

The comparison of OpenSees results between SUB+/ 90 and STD/135 sections are shown in Table 1-10.

Table 1-10. *Comparison of moment-curvature parameters*

between SUB+/90 & STD/135 –OpenSees computation/Linearization

Parameter	SUB+/90	STD/135
(M_{cr},φ_{cr})	(45.62,0.00153)	(45.9, 0.001546)
(M_y,φ_y)	(142.3,0.0189)	(143.63,0.0189)
(M_u,φ_u)	(142.3,0.2043)	(143.63,[0.265/0.4146*])

* Two points are determined in linearized envelope by OpenSees as can be seen in Fig 1-18.

Fig 1-18 and 1-19, show the moment-curvature and force-drift ratio curves for STD/135.

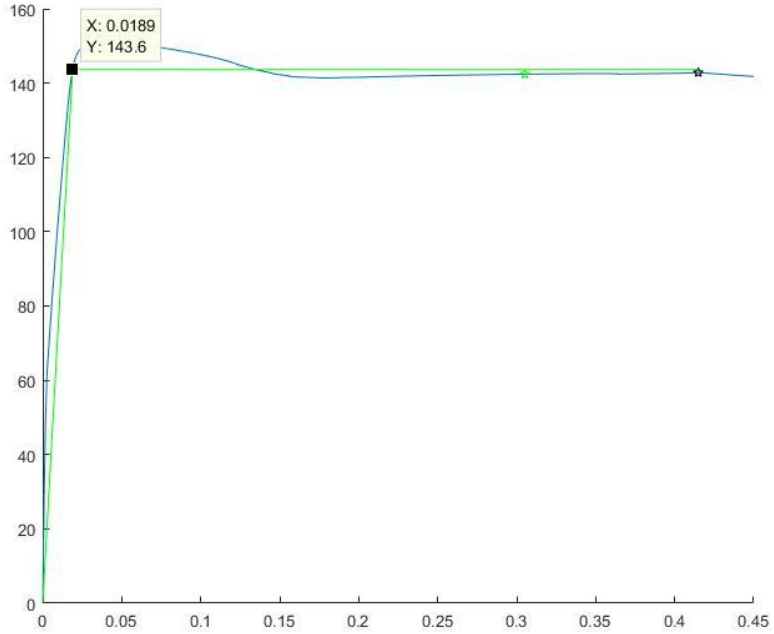

Fig 1-18. *Moment-curvature and its linearization curve for STD/135-OpenSees*

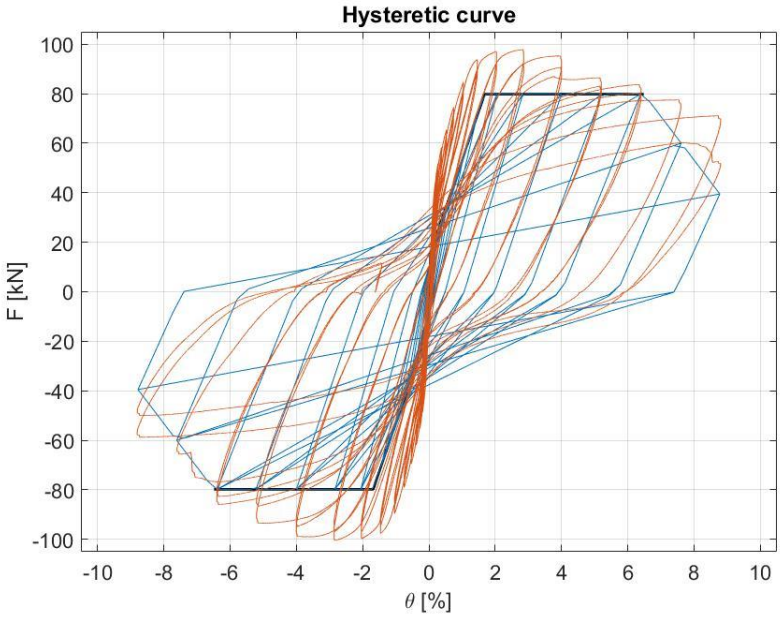

Fig 1-19. *Force-drift ratio curve for STD/135-OpenSees*

- **Comparison of moment-curvature results between SUB+/90 and STD/135**

As mentioned before, SUB+/90 and STD/135 sections just have differences in the compressive cylindrical strength (**f_{cm}**) and the distance between stirrups (**S**). The parameter of **f_{cm}** in STD/153 section is bigger than one in SUB+/90.So as it can be expected, the ductility level of STD/135 should be higher than one in SUB+/90, as shown in Table 1-11. Also the parameter of S, as distance between lateral reinforcements can show its effects in Mander's equations in parameter of **α**, which can affect the **$M_y - \varphi_y$** and **$M_u - \varphi_u$** in confined RC section. The results of this comparison are shown in Table 1-11.

Table 1-11. *Comparison of ductility level and near collapse rotation between SUB+/90 and STD/135*

Parameter	SUB+/90	STD/135	Comments	Ratio
Ductility (φ_u/φ_y)	4.68	4.96	$Du_{STD/135} > Du_{SUB+/90}$	1.06
$\alpha = \alpha_n \alpha_s$	0.256	0.305	$\alpha_{STD/135} > \alpha_{SUB+/90}$	1.19
σ_e	0.072	0.094	$\sigma_{e\ STD/135} > \sigma_{e\ SUB+/90}$	1.305
λ_c	1.10	1.17	$\lambda_{c\ STD/135} > \lambda_{c\ SUB+/90}$	1.06
$\varepsilon_{c1,1}$	0.0029	0.0037	$\varepsilon_{c1,1\ STD/135} > \varepsilon_{c1,1\ SUB+/90}$	1.23
$\varepsilon_{cu,c}$	0.01	0.01245	$\varepsilon_{cu,c\ STD/135} > \varepsilon_{cu,c\ SUB+/90}$	1.245
θ_{um}(EC8/3)	0.0615	0.0619	$\theta_{um\ ,\ STD/135} > \theta_{um\ ,\ SUB+/90}$	1.006

So as results, the ductility level of STD/135 is higher than SUB+/90, due to the higher amount of **f_{cm}** and shorter distance between lateral reinforcements, although these differences are not major.

- **Comparison of force-displacement results between SUB+/90 and STD/135**

Fig 1-20, compares the non-linear cyclic response curves between SUB+/90 and STD/135 sections and the values in threshold or important points. Table 1-12, describes about the slope differences in threshold lines for both mentioned sections.

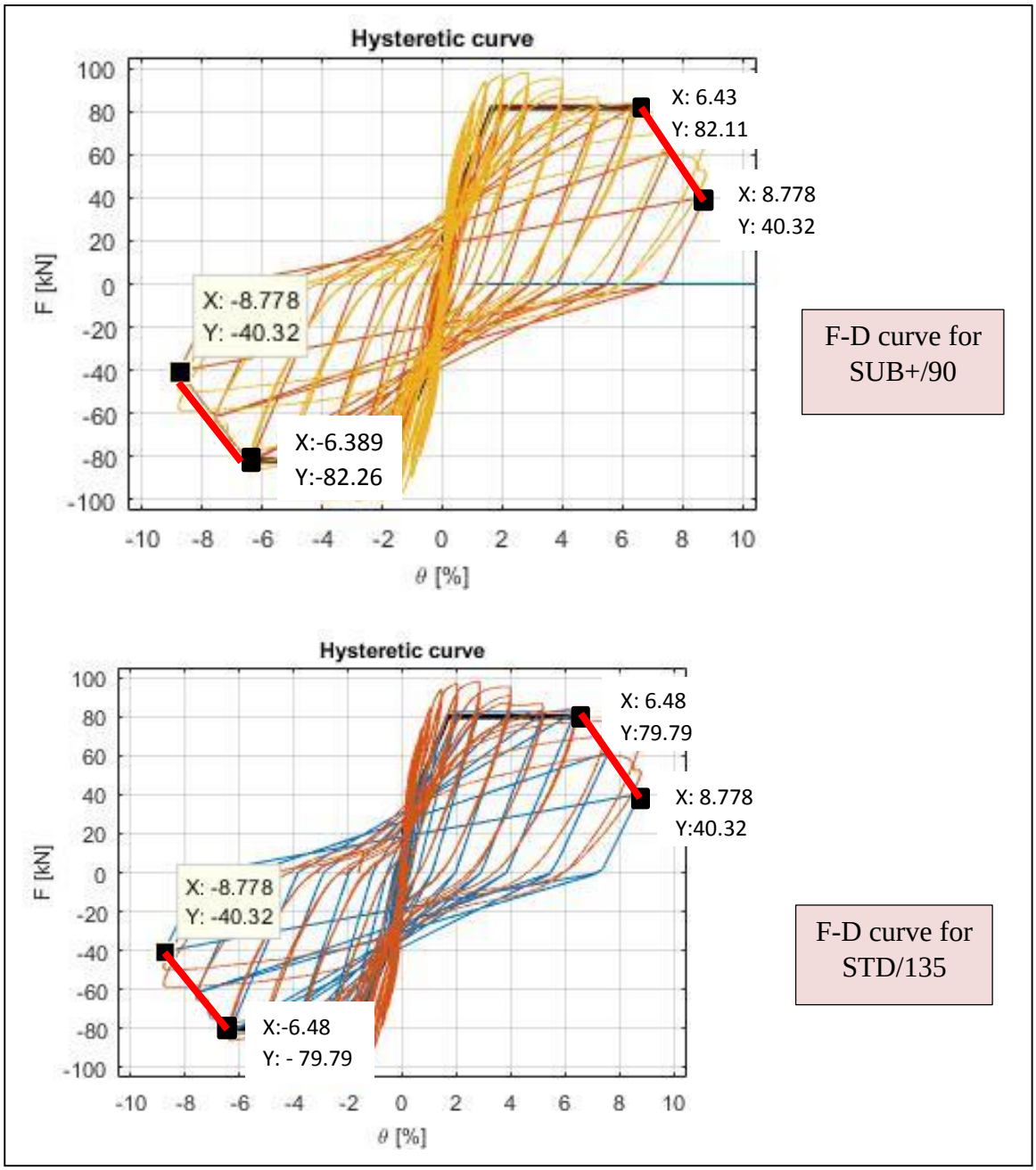

Fig 1-20. *Comparison of non-linear cyclic response curve between SUB+/90 and STD/135*

Table 1-12. *Comparison of threshold line slopes between SUB+/90 and STD/135*

Threshold line	|Slope|
SUB+/90 - Right	17.8
SUB+/90 - left	17.55
STD/135 -Right	17.17
STD/135 -left	17.17

As shown in Fig1-20, in numerical calculations by OpenSees, the drift ratio range of SUB+/90 section is less than one in STD/135 and both right and left threshold lines are steeper than ones in STD/135. This differences is related to the various distance of stirrups in both mentioned sections, which S=8cm in STD/135 cause more drift ratio range and smoother slope in threshold lines in comparison with S=12 cm in SUB+/90. As mentioned before the effect of different hook angles cannot be modeled via Mander's equations in OpenSees computations. So in the case of practical test, these differences between SUB+/90 and STD/135 are more clear and visible.

3.5 The analysis of the influence of the different parameters to the ductility of the analysed column

This part demonstrates the effects of several parameters on the ductility level of SUB+/90 section column such as level of axial force, concrete compressive strength, amount of lateral reinforcement, amount of longitudinal reinforcement. Table 1-13 explains about the application of different parameters and their influences on the level of ductility for assigned frame.

Table 1-13. *The effects of changing different parameters on ductility level of column*

Parameter	First value	Second value	First Ductility	Second Ductility
Axial force	557	659	4.68	4.50
f_{cm}	35.8	35.0	4.68	4.63
Long. Reinforcement	6 ϕ 16	4 ϕ 16	4.68	4.60
Lat. Reinforcement	3 ϕ 8	2 ϕ 8	4.68	4.56

As shown in Table 1-13, increasing the axial force causes the decrement of ductility level and the decreasing the concrete compressive strength, amount of lateral reinforcement, amount of longitudinal reinforcement afford the reduction of ductility, as expected.

Another interesting comparison might be between important parameters which related to standard and substandard stirrups and hook angles in RC SUB+/90 section, which is shown in Table 1-14.

Table 1-14. *Comparison between parameters in standard and substandard RC SUB+/90 section*

SUB+/90 section	Substandard	Standard
$f_{cm,c}(\frac{kN}{cm^2})$	3,83	4,09
$\varepsilon_{c1,c}$ (%)	0,27	0,341
$\varepsilon_{cu,c}$ (%)	0,962	1,11

4 Comparison of results between numerical and experimental analysis on RC section of SUB+/90

This chapter describes about the schematic comparison between numerical and experimental cyclic behaviour of assigned RC section for group -5 which is shown in Fig 1-21.

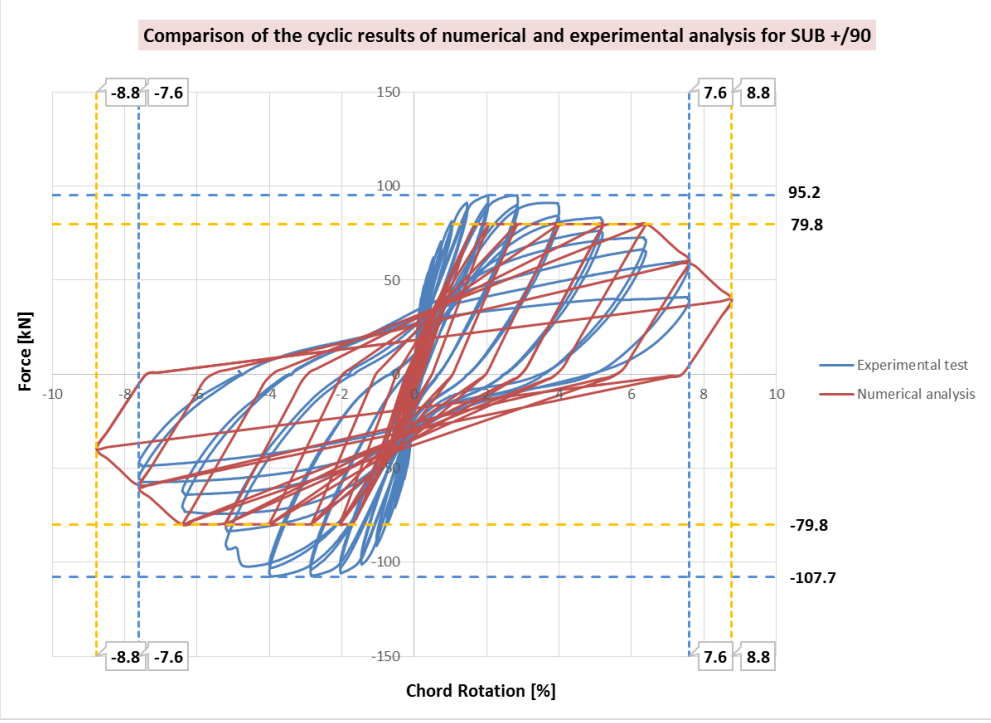

Fig 1-21. *Comparison between numerical and experimental results of cyclic behaviour for SUB+/90 RC section*

According to Fig 1-21, following results can be achieved:

1- The ultimate force of numerical analysis is lower than the one from experimental. It can be concluded that, this differences are due to following reasons:

- In experimental test, the homogeneity of materials is not ideal as used in numerical part.
- The properties of materials such as reinforcing, confining bars and concrete could be different in experimental test in comparison with what it can be assumed in numerical part such as utilization of Mander's model or effectiveness of confined core of RC section.
- According to the sensor setup which can be seen in Fig 1-22, the location of sensors and strain gauges have crucial role to detect deformations more precisely than numerical computations.

2- Larger values for displacement in numerical calculations can be due to the overestimation of numerical assumptions such as Mander's equations in EC8/2 and near collapse rotation in EC8/3.
3- Geometrical properties in experimental test can differ from dimensions defined for numerical analysis.

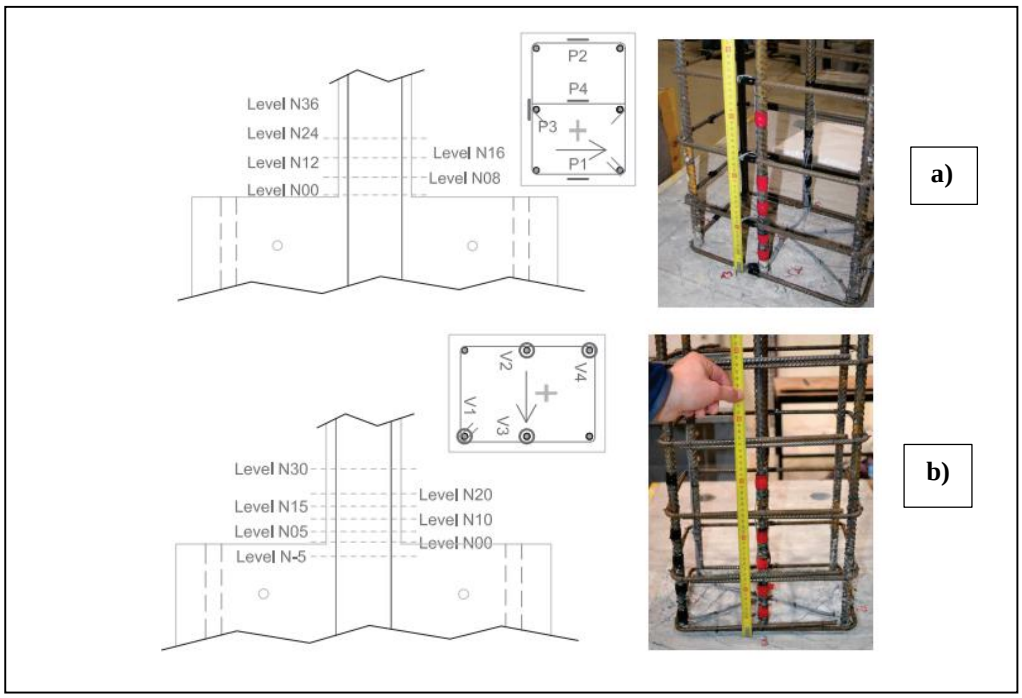

Fig 1-22. *Locations of the strain gauges mounted on the lateral and longitudinal reinforcement* [3]

5 Conclusions

In this project, the assigned RC column section as SUB+/90 is introduced based on its material properties, loading protocols and numerical calculations for moment-curvature and moment-rotation curves of column are computed according to Takeda rules with manual and OpenSees software methods. Then the achieved results for SUB+/90 RC section is compared with STD/135 ones which have just differences in f_{cm} and distances between lateral reinforcements. Consideration of results showed that force-displacement curve of STD/135 have smoother and wider range of rotation / drift ratio in comparison with SUB+/90 mainly due to the shorter distance between stirrups. Despite of the fact that there is difference between the angles of hooks, but this parameter cannot be defined directly via Mander's model or EC8/3 equations, also computation of effective area in the section can show the differences.

In next part, the influence of different parameters on ductility level of SUB+/90 section are examined and following results are achieved:

- Increasing axial force leads to the reduction of ductility
- Decreasing of concrete compressive strength causes the decreasing of ductility
- Reducing the amount of longitudinal reinforcements has direct impact on the level ductility. Having same values of tensile and compression reinforcement cannot make significant changes in ductility, but increasing the compression reinforcement can increase the ductility.
- Reducing the amount of lateral reinforcements causes the reducing of ductility level
- Standard details of RC sections leads to higher values of confined concrete properties such as confined compressive strength.
- Mainly due to the numerical computations which are based on some assumptions for ideal section , the cyclic behaviour of section shows some differences in values of displacement and forces between experimental and numerical analysis.
- Influences of different parameters on global and local buckling was not considered in the process of OpenSees calculations and modeling.

5.1 Future work

According to the considered parameters and utilized methodologies for calculation of moment-rotation envelope of column section and achieved results, following points can be assumed as interesting topics for more numerical investigation:

1- Finding suitable equations and methods to show the effects of hook-angles in the behaviour of column section directly in EC8/2 and EC8/3 for numerical calculations e.g. in OpenSees.

2- Checking the type and the formation of buckling by application of new defined and examined equations in OpenSees.

List of Figures

List of Tables

Bibliography

[1] Isakovi´c. T, Anzlin. A (2018). Lecture note of Erasmus course: “Nonlinear analysis of structures: Seismic response of RC Bridges-Blind prediction”. Ljubljana, UL, FGG.

[2] NIST, 2010d. Nonlinear Structural Analysis for Seismic Design, A Guide for Practicing Engineers, GCR 10-917-5, prepared by the NEHRP Consultants Joint Venture, a partnership of the Applied Technology Council and the Consortium of Universities for Research in Earthquake Engineering, for the National Institute of Standards and Technology, Gaithersburg, Maryland.

[3] Anzlin. A (2017). Doctoral Dissertation, “Influence of buckling of longitudinal reinforcement in columns on seismic response of existing reinforced concrete bridges”.

Project report

‘Task 2
PUSHOVER ANALYSIS OF A MULTI-SPAN BRIDGE IN THE TRANSVERSE DIRECTION’

Submitted by

‘Nooshin Hadidian Moghaddam’
‘Denis Berbić’
‘Gregor Udovč’
‘Zsombor Illés’

Group-5

M.Sc. Erasmus course

University of Ljubljana, faculty of Civil and Geodetic Engineering

Prof. Dr.Tatjana Isakovic´
Prof. Dr.Marjeta Kramar
Dr. Andrej Anžlin

Table of Contents

Declaration

Hereby, we declare that we worked on this Report independently and using only the specified sources and programs which are referred.

Ljubljana, 03.09.2018

Nooshin Hadidian.M
Denis Berbić
Gregor Udovč
Zsombor Illés

1 Abstract

Seismic analysis of bridges require completely different approaches from buildings mainly due to their dimensions, structural system, functions, seismic responses and distinguished types of damages. One of the reliable and effective standards which can be used for process of bridge design is EC8/2 which applies the concept of reduction of seismic force level for the equal displacement dominantly in design procedures. One of the most appropriate method for designing bridge is the combination of nonlinear static (pushover) analysis and the response spectrum approach utilized in ATC 40,FEMA 273 and N2 (where N stand for nonlinear method and 2 shows two mathematical models) method.

This project report describes the utilization of N2 method for seismic analysis of assigned bridge (Group-5) with 6 spans and defining peak ground acceleration according to the ultimate displacement of selected monitor point of bridge in both transverse and longitudinal directions. The details of considered dimensions and related parameters are described throughout the next chapters. OpenSees software is used to get the results of pushover analysis for this project.

1 Introduction

The N2 method can be defined as new form of capacity spectrum method based on inelastic spectra which its related demand can be determined from elastic design spectrum and the reduction factors are defined in consistency with the elastic spectrum. Displacements in each direction are calculated based on pushover analysis to get capacity curve of MDOF system and then by non-linear dynamic analysis of defined equivalent SDOF system, static nonlinear analysis of MDOF system is performed to obtain the seismic demand of bridge in each direction. This method is developed by university of Ljubljana.

1.1 Description of method and steps

STEP -1: PUSHOVER ANALYSIS

Calculation of displacement for both transverse and longitudinal directions, based on determined material properties and dimensions of MDOF system, is performed using OpenSees software to get force-displacement curve. Here mainly bridge components are divided into piers and deck and the failure deformation of first pier is deterministic factor. This

deformation/ultimate displacement can be computed according to the dimensional and material properties of piers, their reinforcing details such as standard and substandard sections, functionality of hooks and consideration of $\mathbf{s/d_{bl}}$ values via manual calculations using EC8/2 and EC8/3 related equations or appropriate softwares such as OpenSees. Ultimate /near collapse displacement value is used to obtain related force from capacity curve resulted from pushover analysis.

STEP-2: DEFINITION OF EQUIVALENT SDOF SYSTEM

Using concept of equation of motion for SDOF model, the total mass of system can be defined as $\mathbf{m^*}$ and the constant parameter of $\mathbf{\Gamma}$, can be defined to control the transformation procedure from MDOF to SDOF according to following process shown in Fig 1-1.

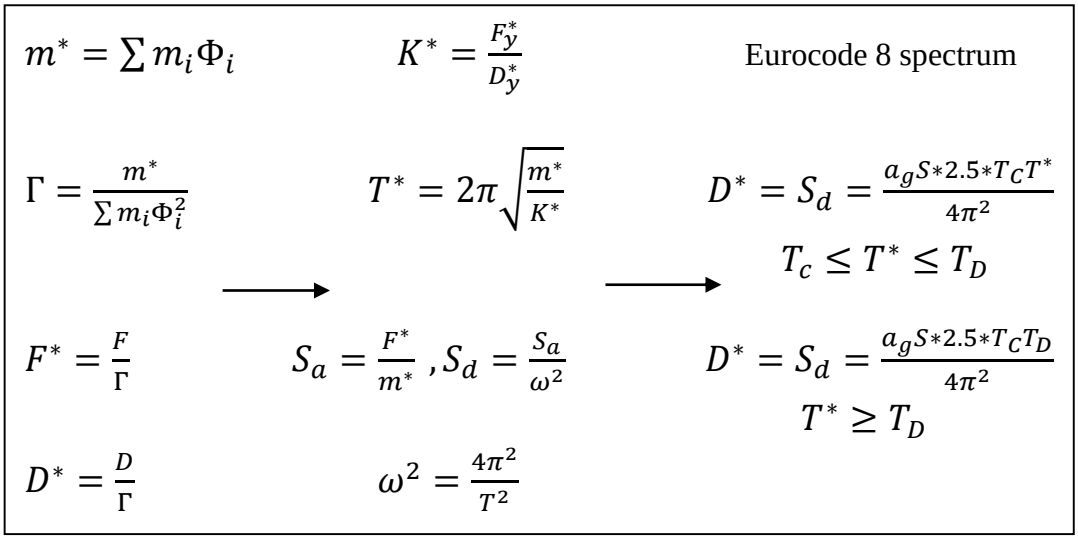

Fig 1-1. *Required equations for nonlinear dynamic analysis of SDOF [1] & [2]*

According to equations shown in Fig 1-1, peak ground acceleration can be obtained based on maximum displacement in each direction. Also in the case of assuming PGA, seismic demand of bridge components as maximum displacement can be calculated.

2 Tasks

This chapter describes about the dimension and material properties of assigned bridge and their specifications for **group-5**. The scheme of a six-span bridge (26+4x32+26=180 m) supported by five I-shaped bridge columns, the cross-section of an I-shape column and the flexural reinforcement , the detailing of the lateral reinforcement for standard - EC 8/2 design - considering $\mathbf{s/d_{bl} = 8}$, for **group-5** are shown in Fig 1-2.

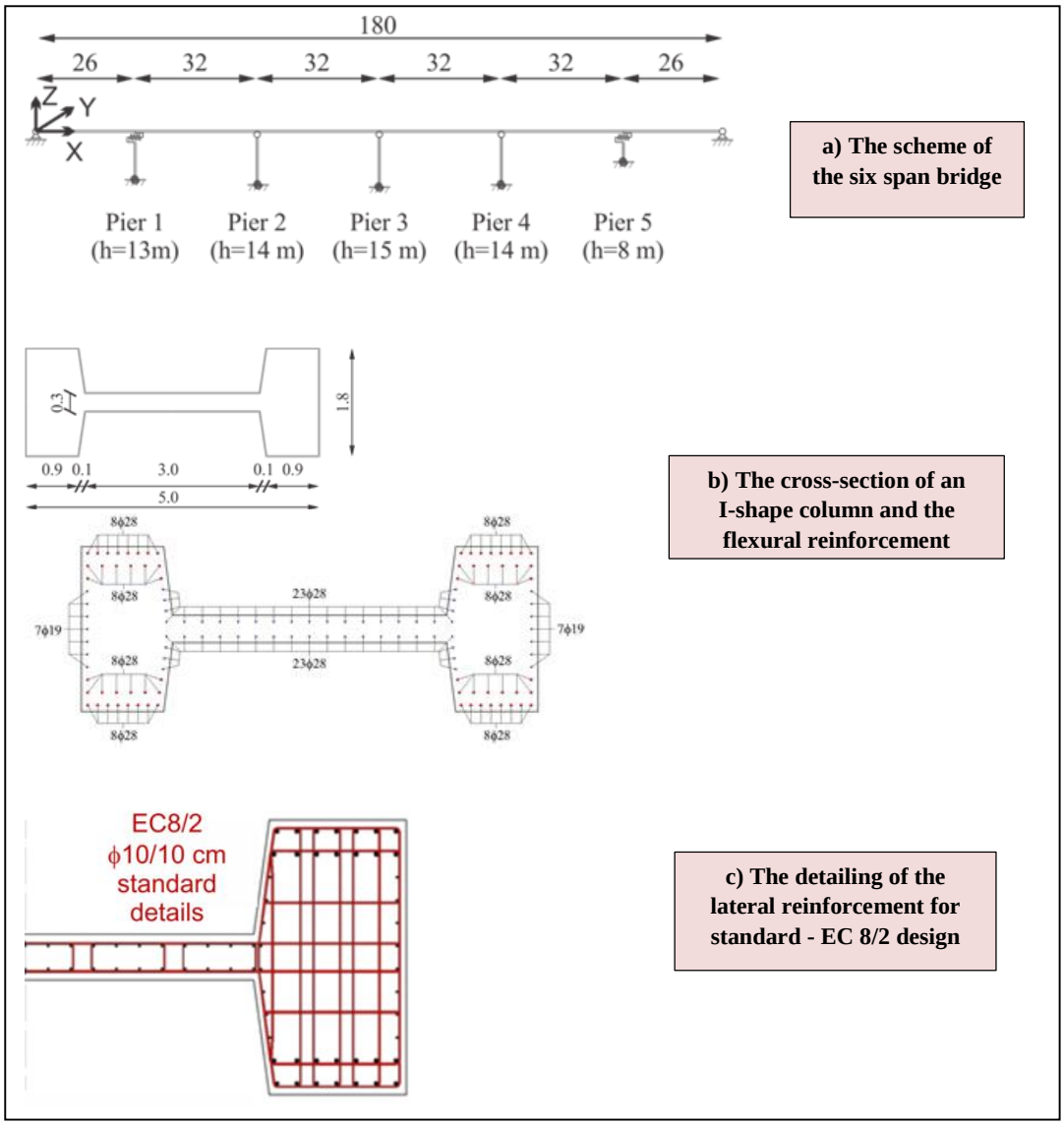

Fig 1-2. *Assigned properties of bridge for group-5*

According to the specified tasks for this work as task-2, lumped plasticity numerical model using Takeda's hysteretic rules (considering unloading stiffness degradation parameter α=0.5). are used for calculation procedure. The sub-tasks are mentioned as follows:

- Define the peak ground acceleration (PGA) corresponding to the failure of the first pier for longitudinal and transverse direction separately.
- How would the doubled mass of a bridge deck (double deck bridge) impact on the seismic behaviour of a structure?

2.1 Define the peak ground acceleration (PGA) corresponding to the failure of the first pier for transverse direction .

As mentioned in chapter 2.1, after running pushover analysis using OpenSees software and obtained matrixes, the value of $\mathbf{m}^*$ and $\mathbf{r}$ can be calculated according to Table 1-1.

Table 1-1. *Calculation of parameters for MDOF system by OpenSees/one-deck bridge*

Node	1	2	3	4	5	6	7	8	9	10
X-coordination	0	2.6	5.2	7.8	10.4	13	15.6	18.2	20.8	23.4
Phi	0	0.057	0.112	0.166	0.218	0.268	0.317	0.364	0.409	0.452
$\mathbf{m_i}$	39	78	78	78	78	78	78	78	78	78
Node	11	12	13	14	15	16	17	18	19	20
X-coordination	26	29.2	32.4	35.6	38.8	42	45.2	48.4	51.6	54.8
Phi	0.494	0.544	0.590	0.635	0.676	0.716	0.752	0.786	0.818	0.847
$\mathbf{m_i}$	140.4	78	78	78	78	78	78	78	78	78
Node	21	22	23	24	25	26	27	28	29	30
X-coordination	58	61.2	64.4	67.6	70.8	74	77.2	80.4	83.6	86.8
Phi	0.874	0.898	0.919	0.938	0.954	0.968	0.980	0.989	0.995	0.999
$\mathbf{m_i}$	145.2	78	78	78	78	78	78	78	78	78
Node	31	32	33	34	35	35	37	38	39	40
X-coordination	90	93.2	96.4	99.6	102.8	106	109.2	112.4	115.6	118.8
Phi	1.000	0.999	0.995	0.989	0.980	0.968	0.954	0.938	0.919	0.898
$\mathbf{m_i}$	150	78	78	78	78	78	78	78	78	78
Node	41	42	43	44	45	46	47	48	49	50
X-coordination	122	125.2	128.4	131.6	134.8	138	141.2	144.4	147.6	150.8
Phi	0.874	0.847	0.818	0.786	0.752	0.716	0.676	0.635	0.590	0.544
$\mathbf{m_i}$	145.2	78	78	78	78	78	78	78	78	78
Node	51	52	53	54	55	56	57	58	59	60
X-coordination	154	156.6	159.2	161.8	164.4	167	169.6	172.2	174.8	177.4
Phi	0.494	0.452	0.409	0.364	0.317	0.268	0.218	0.166	0.112	0.057
$\mathbf{m_i}$	116.4	78	78	78	78	78	78	78	78	78
Node	61									
X-coordination	180									
Phi	0.000									
$\mathbf{m_i}$	39									

It should be mentioned that the important parameters which are defined in TCL files for OpenSees software such as pier_material.tcl, pier_section.tcl and nonlinear_pushover_analysis.tcl based on determined properties such as dimension and material for deck and pier sections which are shown in Fig 1-3.

Pier section properties		
E	33000000	kN/m2
A	4.335	m2
Iz	0.93015	m4
Iy	15.02	m4
Asy	3.42	m2
Asz	0.9	m2
Mass-p	11.05	t/m
G	13800000	kN/m2

Deck cross section		
E	34000000	kN/m2
A	9.65	m2
Iz	21.5	m4
Iy	96	m4
Asy	3.82	m2
Asz	6.93	m2
It	18.25	m4
Mass-d	30	t/m

total Mass-p	709.6	ton
total Mass-d	5400	ton
ratio	0.131	
total Mass	5767.6	ton

Fig 1-3. *Assigned properties for deck and piers of bridge for group-5*

For defining PGA in transverse direction based on first failure of pier, ultimate rotation of each pier in transverse direction is obtained by getting moment-rotation envelope using EC8/2 equations and its results compared with near collapse rotation using EC8/3. Table 1-2 and 1-3, describe about the considered parameters and related results to get ultimate displacement of piers in both strong and weak axes.

Table 1-2. *Calculation of ultimate rotation for each pier based on* ***EC8/2*** *by OpenSees and getting ultimate displacement*

	height(m)	**UL_rotation**	**N-axial force (top)**	**N-axial force (bot)**	**Ultimate Displacement**
pier 1	13	0.0670	9239.1	9943.6	0.871
pier 2	14	0.0745	10176.2	10934.9	1.043
pier 3	15	0.0711	10230.4	11043.2	1.066
pier 4	14	0.0745	10176.2	10934.9	1.043
pier 5	8	0.0422	8968.2	9401.7	0.338

Table 1-3. *Calculation of ultimate rotation for each pier in based on* ***EC8/3*** *and getting ultimate displacement*

	height(m)	UL_rotation	N-axial force(bot)	Ultimate_Displacement
pier 1	13	0.029	9943.6	0.380
pier 2	14	0.030	10934.9	0.420
pier 3	15	0.031	11043.2	0.461
pier 4	14	0.030	10934.9	0.420
pier 5	8	0.025	9401.7	0.197

Using ultimate displacement results and equations for nonlinear dynamic analysis of SDOF based on N2-method, PGA values are calculated in both directions and final results are shown in Fig 1-4.

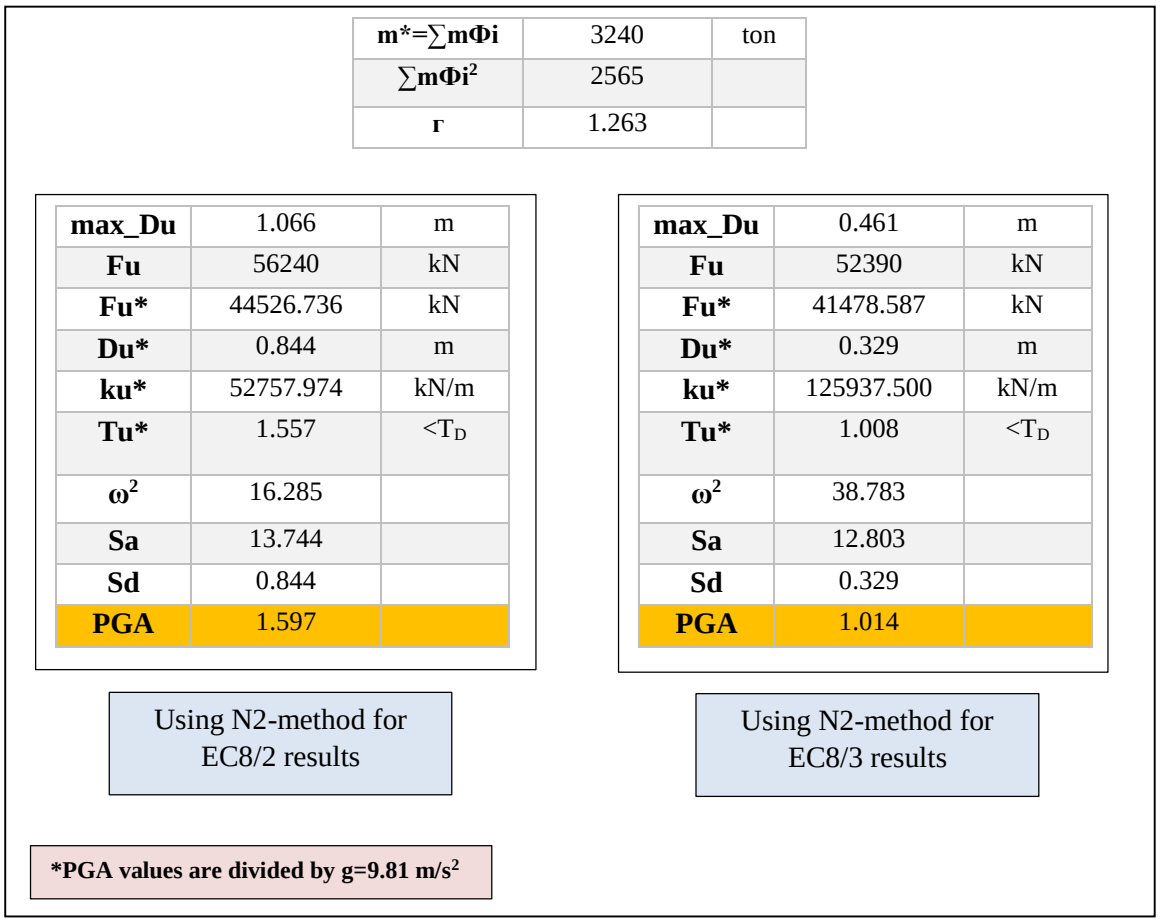

Fig 1-4. *Calculation of PGA values in EC8/2 & EC8/3 for one-deck bridge based on N2-method*

2.2 How would the doubled mass of a bridge deck (double deck bridge) impact on the seismic behaviour of a structure?

This chapter considers the effect of doubled mass of bridge deck on seismic behaviour of structure and how it can impact on PGA values in transverse and longitudinal directions. For this purpose, defined mass for deck cross section in nonlinear_lumped_pushover.tcl file is changed to obtain capacity curve based on this change after running pushover analysis. Fig 1-5, shows the example of changing mass parameter in mentioned file before running pushover analysis.

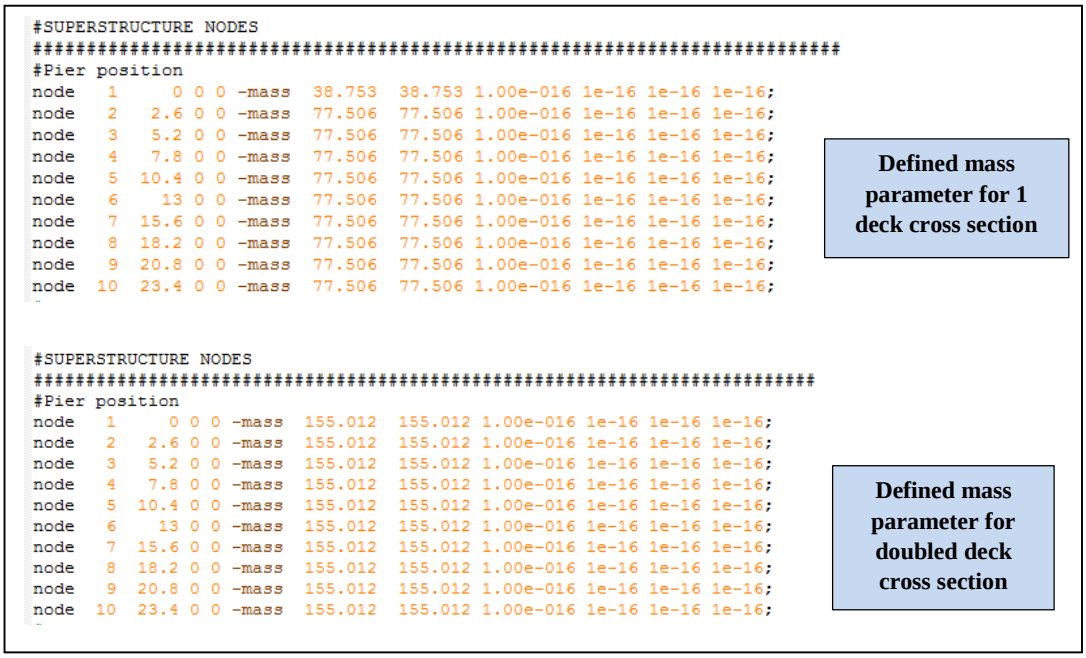

Fig 1-5. *Example of defining mass parameters of deck in TCL file for 1-deck and doubled deck before running pushover analysis in OpenSees*

Similar to steps described in chapter 3.1, the same procedures are followed and after calculation of $\mathbf{m}^*$ and **r,** and new axial forces for each pier based on doubled mass deck definition , all new parameters are calculated and related results are demonstrated in Table 1-4,1-5 and 1-6 and Fig 1-5.

Table 1-4. *Calculation of parameters for doubled deck for MDOF system by OpenSees*

Node	1	2	3	4	5	6	7	8	9	10
X-coordination	0	2.6	5.2	7.8	10.4	13	15.6	18.2	20.8	23.4
Phi	0	0.057	0.112	0.166	0.218	0.268	0.317	0.364	0.409	0.452
m_i	78	156	156	156	156	156	156	156	156	156
Node	11	12	13	14	15	16	17	18	19	20
X-coordination	26	29.2	32.4	35.6	38.8	42	45.2	48.4	51.6	54.8
Phi	0.494	0.544	0.590	0.635	0.676	0.716	0.752	0.786	0.818	0.847
m_i	218.4	156	156	156	156	156	156	156	156	156
Node	21	22	23	24	25	26	27	28	29	30
X-coordination	58	61.2	64.4	67.6	70.8	74	77.2	80.4	83.6	86.8
Phi	0.874	0.898	0.919	0.938	0.954	0.968	0.980	0.989	0.995	0.999
m_i	223.2	156	156	156	156	156	156	156	156	156
Node	31	32	33	34	35	35	37	38	39	40
X-coordination	90	93.2	96.4	99.6	102.8	106	109.2	112.4	115.6	118.8
Phi	1.000	0.999	0.995	0.989	0.980	0.968	0.954	0.938	0.919	0.898
m_i	228	156	156	156	156	156	156	156	156	156
Node	41	42	43	44	45	46	47	48	49	50
X-coordination	122	125.2	128.4	131.6	134.8	138	141.2	144.4	147.6	150.8
Phi	0.874	0.847	0.818	0.786	0.752	0.716	0.676	0.635	0.590	0.544
m_i	223.2	156	156	156	156	156	156	156	156	156
Node	51	52	53	54	55	56	57	58	59	60
X-coordination	154	156.6	159.2	161.8	164.4	167	169.6	172.2	174.8	177.4
Phi	0.494	0.452	0.409	0.364	0.317	0.268	0.218	0.166	0.112	0.057
m_i	194.4	156	156	156	156	156	156	156	156	156
Node	61									
X-coordination	180									
Phi	0.000									
m_i	78									

Table 1-5. *Calculation of ultimate rotation for each pier based on* ***EC8/2*** *considering* ***doubled mass deck*** *by OpenSees and getting ultimate displacement*

	height(m)	**UL_rotation**	**N-axial force (top)**	**N-axial force (bot)**	**Ultimate Displacement**
pier 1	13	0.0472	17773.8	18478.3	0.614
pier 2	14	0.0481	19593.8	20352.5	0.673
pier 3	15	0.0513	19648.0	20460.8	0.770
pier 4	14	0.0481	19593.8	20352.5	0.673
pier 5	8	0.0299	17502.9	17936.4	0.239

Table 1-6. *Calculation of ultimate rotation for each pier* ***based on EC8/3*** *considering* ***doubled mass deck*** *and getting ultimate displacement*

	height(m)	UL_rotation	N-axial force(bot)	Ultimate_Displacement
pier 1	13	0.027	18478.3	0.346
pier 2	14	0.027	20352.5	0.382
pier 3	15	0.028	20460.8	0.420
pier 4	14	0.027	20352.5	0.382
pier 5	8	0.022	17936.4	0.180

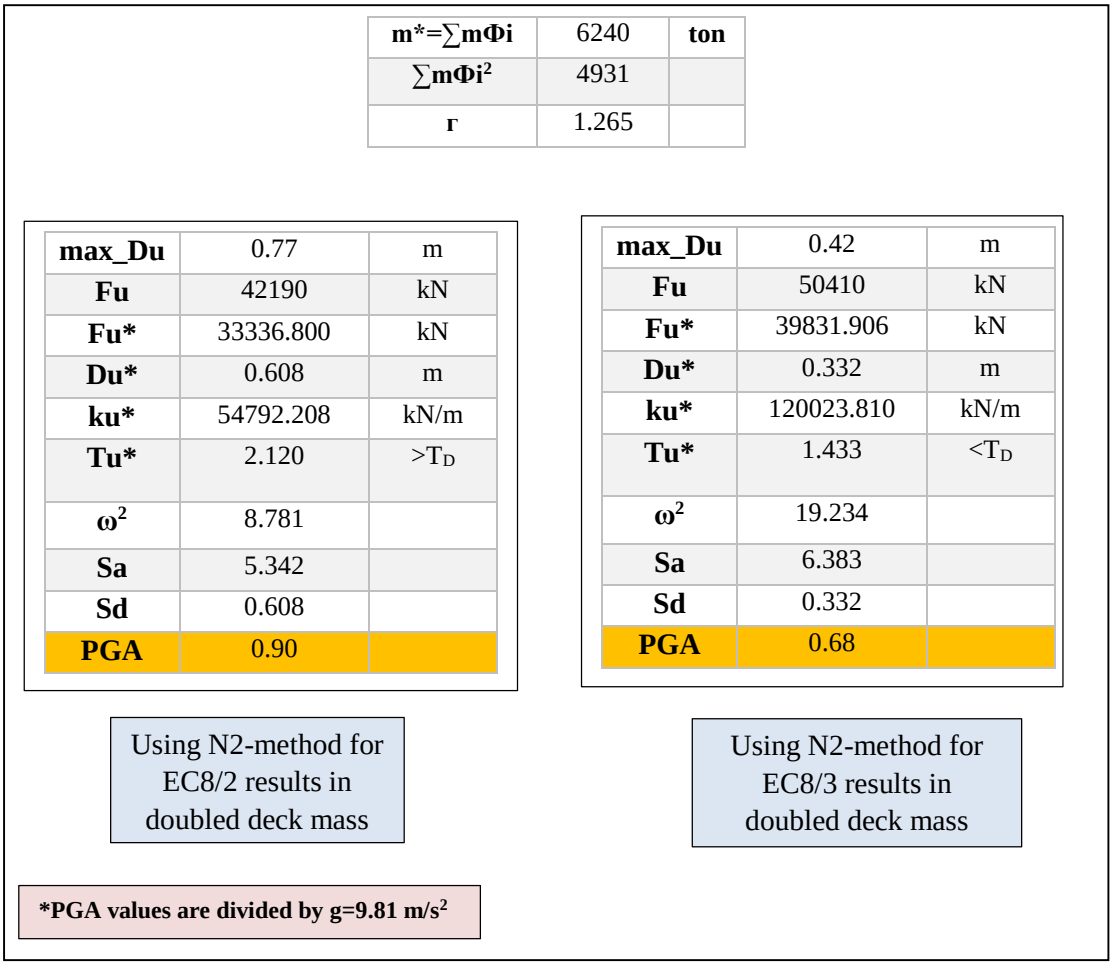

Fig 1-6. *Calculation of PGA values in EC8/2 & EC8/3 for doubled-deck bridge based on N2-method*

Fig 1-7, shows the force-displacement curve for MDOF model of bridge obtained using OpenSees software for both one-deck and doubled-deck bridge.

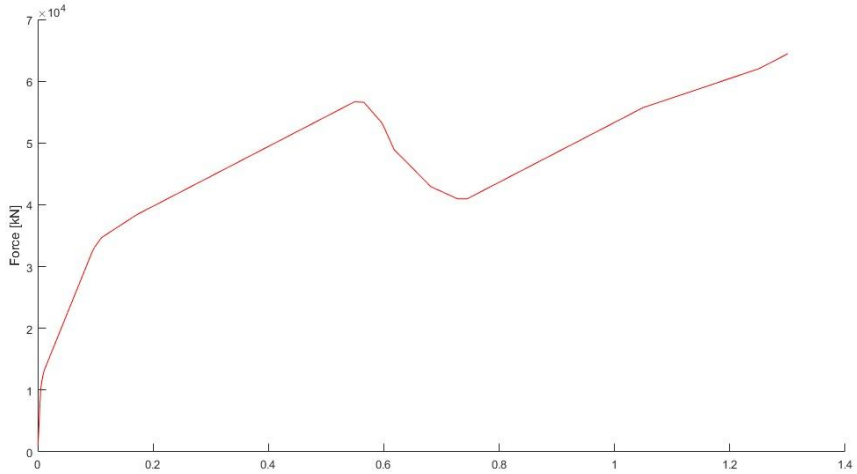

Fig 1-7. *Force-displacement curve for MDOF model of one-deck and doubled deck bridge using OpenSees*

2.3 Comparison of results

This part deals with the consideration of achieved results in chapter 3.1 and 3.2 and detailed comparison between them. Table 1-7, explains about the comparison of final defined PGA for one-deck bridge which obtained in chapter 1.3 and doubled-deck bridge in chapter 3.2 in both EC8/2 and EC8/3 methods.

Table 1-7. *Comparison of obtained PGA values for one-deck and doubled deck bridge in EC8/2 and EC8/3 methods*

One-deck bridge	PGA	Difference ratio
EC8/2	1.597 g	36.5%
EC8/3	1.014 g	
Doubled-deck bridge	PGA	Difference ratio
EC8/2	0.90 g	24 %
EC8/3	0.68 g	

Fig 1-8 shows the displacement of bridge when pushover analysis are performed for one-deck and doubled-deck bridges using both EC8/2 and EC8/3 methods.

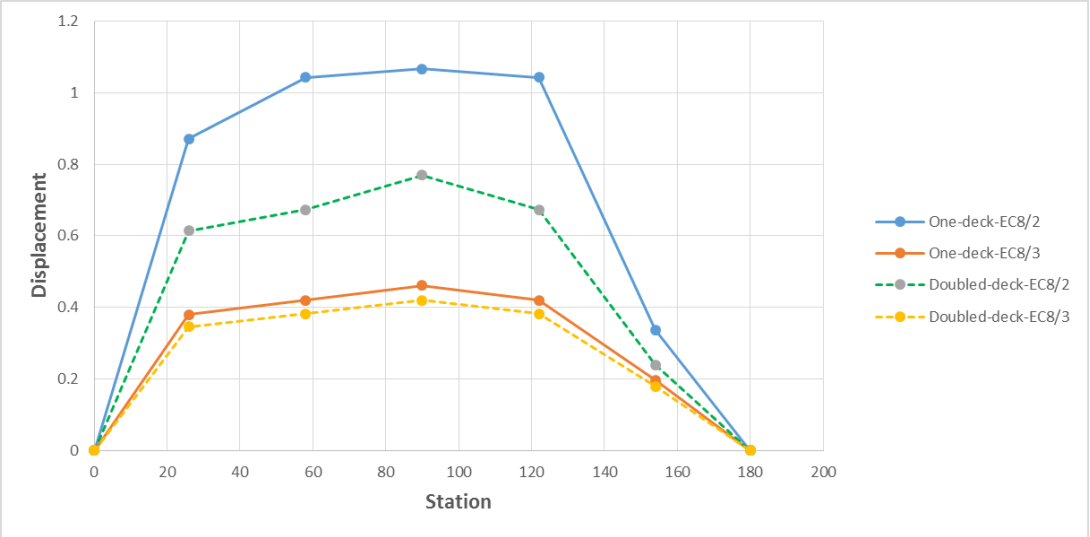

Fig 1-8. *Schematic comparison of bridge displacement in 4 different status*

3 Conclusions

In this project, according to the determined properties of deck and pier sections for group-5, such as assigning standard reinforcing detail for section with s/d_{bl} =8, calculation of moment-rotation envelope parameters such as ultimate/near collapse rotation of each pier computed regarding to calculated axial forces and mass properties of deck and pier using OpenSees software based on EC8/2 specifications and also near collapse rotation obtained from EC8/3 equation for columns.

In next step, pushover analysis is performed for both one-deck and doubled-deck bridge considering transverse direction of pier sections. After calculation of first ultimate displacement or failure mode in MDOF model, equivalent SDOF model is defined using N2 method equations. Finally PGA is obtained for four defined status (for one-deck and doubled-deck bridges with two EC8/2 and EC8/3 methods). Based on final results it can be concluded briefly as follows:

1- As expected, ultimate rotation of middle pier which caused first near collapse displacement is the largest one which results in largest obtained PGA in weak direction.
2- Doubling the deck mass caused differences in deck displacement in comparison with one-deck bridge for both EC8/2 and EC8/3 methods as shown in Fig 1-8.
3- Totally, computed PGA values for one-deck bridge in both methods are larger than ones obtained for doubled-deck bridge about 49% and 77 %.

4- Despite of the fact that, the detailed analysis of longitudinal buckling of piers are not considered here, but assigning the $\mathbf{s/d_{bl}=8}$ which is more than 6 as buckling threshold value, can play important role in moment-rotation parameters, especially when they are considered in nonlinear response of confined RC section and Mander's model .
5- The main assumptions for analysis process for this bridge were using the rigid deck model with ignoring small distance between the center of mass and stiffness.

3.1 Future work

According to the considered parameters and utilized methodologies for calculation of PGA for assigned properties of bridge and achieving results, following points can be assumed as interesting topics for more numerical investigation:

1- Consideration of bridge seismic behaviour with the dominancy of higher modes
2- Consideration of bridge seismic behaviour with short column/piers located in several points of bridge

List of Figures

List of Tables

page

Bibliography

[1] Isakovi´c. T, Anzlin. A (2018). Lecture note of Erasmus course: “Nonlinear analysis of structures: Seismic response of RC Bridges-Blind prediction”. Ljubljana, UL, FGG.

[2] Isakovi´c. T, Fischinger. M (2014).” Seismic Analysis and Design of Bridges with an Emphasis to Eurocode Standards”. Perspectives on European Earthquake Engineering and Seismology, Geotechnical, Geological and Earthquake Engineering 34, DOI 10.1007/978-3-319-07118-3_6.

Project report

Nonlinear Analysis of Structures
Seismic Response of RC Bridges – Blind Prediction

Submitted by

Benjamin Cerar

Gledson Rodrigo Tondo

Walter Castillo Vega

Robert Degiacinto

Péter Pozsgai

UNIVERSITY OF LJUBLJANA

Faculty of Civil and Geodetic Engineering

Institute of Structural and Earthquake Engineering

Table of Contents

1 Introduction

This project report is divided in two different tasks. In the first task, a cyclic analysis of a reinforced concrete column was prepared using the OpenSees software [1]. The numerical analysis was prepared based on an experiment-based cyclic test, which was performed in advance.

For this column, a set of values corresponding to the material parameters of longitudinal and lateral steel reinforcement, as well as for the concrete which was used, were adopted from earlier research [2]. A loading protocol was adopted from the same research. In addition, the considered stirrup detailing was assumed to be slightly different than the standard one, where the cross-sections differed by the shape of stirrup hooks. The results of the numerical analysis of both cross-sections were compared. Lastly, an analysis of several parameters that define the behaviour of the column was performed.

The second part of the project was also based on [2].The task required a performance of the pushover analysis of a multi-span bridge pier. The barbell-shaped column was assessed considering the standard design, in accordance to Eurocode 8/2, but with improper shape of the hooks of the lateral reinforcement.

In addition, the peak ground acceleration (PGA) corresponding to the failure of the pier was defined for both the longitudinal and transverse directions. A parametric test was also performed by doubling the mass of the structure.

2 BLIND PREDICTION OF THE STATIC CYCLIC RESPONSE OF A RECTANGULAR RC CANTILEVER COLUMN

In this task, the cyclic response of a cantilever column was assessed using the software OpenSees, the result of which are later on compared to the experimentally-obtained results, and to the standardized column.

2.1 Material and Section Properties

The column in consideration has a height of 1.8 m, with a cross-sectional dimension of 40cm x 30cm. The column has six longitudinal bars of diameter 16 mm, spaced evenly within the cross-section.

The steel properties for both longitudinal and lateral reinforcement bars are shown below, in Table 1.

Table 1 Steel properties

Bar Type	f_y	f_t	e_y	e_u	E
	[MPa]	[MPa]	[%]	[%]	[GPa]
Longitudinal	600	709	0.30	7.56	198
Lateral	554	668	0.30	10.12	186

In the same manner, Table 2 displays the properties of mean compressive cylindrical strength and the level of axial load of the concrete column N.

Table 2 Concrete properties

f_{cm}	N
[MPa]	[kN]
36.3	577

The analysed column has a substandard detailing, named STD/90 in [2], its lateral reinforcement consists of 3 bars of 8 mm in diameter, spaced at the distance of 8 cm along the length of the column. The stirrups are fixed with a 90º angle at its main bar, while the hooks of the middle bar are of 90º and 135º angles, as shown below in Figure 1.

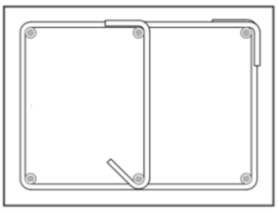

Figure 1: Cross-section design

The values were then estimated for three different material models: reinforcement steel, the concrete used in the column cover, and the concrete core of the column, confined by the stirrups.

The unconfined concrete followed the uniaxial Kent-Scott-Park theory, with no tensile strength, according to OpenSees Wiki [3]. The compressive strength at 28 days was obtained from Table 2, the strain at maximum strength was obtained from an interpolation using Eurocode 2 [4]. The concrete crushing strength for the unconfined concrete was estimated to be 0, and the spalling strain at crushing strength was calculated to be 0.8046%, according to Equation 1, shown below:

$$\varepsilon_{sp} = \frac{2^{(1+r)}\,\varepsilon_{c1}\,r}{(2^r - 1)(r - 1)} \quad \text{(Eq. 1)}$$

Where the formulation of r was derived from [2], and ε_{c1} is the strain, corresponding to compressive strength of the unconfined concrete.

The longitudinal steel bars followed the values presented in Table 1. The uniaxial material fibre followed the theory presented in the OpenSees Wiki [5], where the strain hardening of steel was taken into account. The fatigue was taken into account with coefficients C_d and C_f, which were set to 0.26 and 0.3, respectively, while the coefficient α was set to 0.5. Regarding the buckling characteristics, the slenderness ratio was set to 5 and the α coefficient was set, as default, to 1. The Menegotto and Pinto Curve Parameters, R_1, R_2 and $R3$ were set to 0.333, 13.0 and 4.0, respectively.

Confined concrete parameters were calculated using EC 8/2 [6], which is based on Mander's model of concrete confinement. The estimation for α, which represents the confinement effectiveness factor, was made. This was accomplished with Equation 2, shown below.

$$\alpha = \left(1 - \frac{s_h}{2b_0}\right)\left(1 - \frac{s_h}{2h_0}\right)\left(1 - \frac{\sum b_i^2}{6h_0 b_0}\right) \quad \text{(Eq. 2)}$$

Where b_0 and h_0 are the dimensions of the confined core measured to the centreline of the hoop, b_i is the centreline of longitudinal bars that are laterally restrained by a stirrup, and s_h is the centreline stirrup spacing.

Considering a concrete cover of 2.6 cm, the diameter of the stirrup bars of 8 mm, and the diameter of the longitudinal bars of 16 mm, the calculated value for the confinement effectiveness is equal to 0.4452.

With this parameter, the calculated mean confined concrete compressive strength at 28 days $f_{cm,c}$ is equal to 4.475kN/cm² and calculated according to the provisions of EC 8/2 [6], using Equation 3:

$$f_{cm.c} = f_{cm}\left(2.254\left(\sqrt{1 + 7.94\frac{\sigma_e}{f_{cm}}} - 1\right) - 2\frac{\sigma_e}{f_{cm}}\right) \quad \text{(Eq. 3)}$$

Where σ_e is the effective confining stress and is given in EC 8/3 [7], shown below in Equation 4:

$$\sigma_e = \alpha\ \rho_w\ f_{yw} \qquad \text{(Eq. 3)}$$

And ρ_w is the level of transverse reinforcement ratio.

The strains corresponding to the maximum and crushing strength of the confined concrete $\varepsilon_{c,c}$ and $\varepsilon_{cu,c}$, were calculated to be, respectively, 0.432% and 2.277% using Equations 5 and 6 according to EC8/2 [6], as follows:

$$\varepsilon_{c,c} = 0.002\ (1 + 5\left(\frac{f_{cm}}{f_{cm,c}} - 1\right)) \qquad \text{(Eq. 5)}$$

$$\varepsilon_{cu,c} = 0.004 + 1.4\ \rho_w\ \varepsilon_{swu}\ \frac{f_{yw}}{fcm,c} \qquad \text{(Eq. 6)}$$

Where ρ_w is the level of transverse reinforcement ratio to the cross-section, ε_{swu} is the ultimate deformation of the lateral steel reinforcement, given in Table 1, f_{cm} and f_{ym} are the mean compressive strength of the unconfined concrete and the yield strength of lateral reinforcement steel, respectively, given in Tables 1 and 2.

The initial stiffness E_c was calculated to conform to Mander et al. [8], via Equation 7, with the value of 3166,24kN/cm²:

$$E_c = 57000\ \sqrt{|f_{cm,c}|} \qquad f_{cm,c} \text{ in [psi]} \qquad \text{(Eq. 7)}$$

The maximum tensile strength and strain of concrete were estimated to be 0.332kN/cm² and 0.010%, respectively, and were determined according to EC2/1 [4]. The behaviour of the confined concrete in the analysis was based on Popovic's material model [9].

Figure 2, shown below, displays the different materials and their positions in the cross-section of the column. The darker grey colour represents the confined concrete core, while the light grey is the considered concrete cover. The black, numbered circles are the longitudinal reinforcement bars within the section.

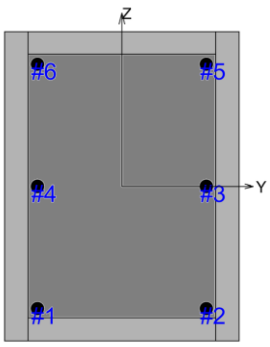

Figure 2: Model of the cross-Section, as used in OpenSees analysis [2]

On Figure 3 we present the concrete material models that were calculated with the above-listed equations and used in the analysis. On Figure 4 we show the constitutive models for the longitudinal reinforcement steel in tension and compression that were used for the preparation of the analysis. Note that both models are shown in their respective absolute form.

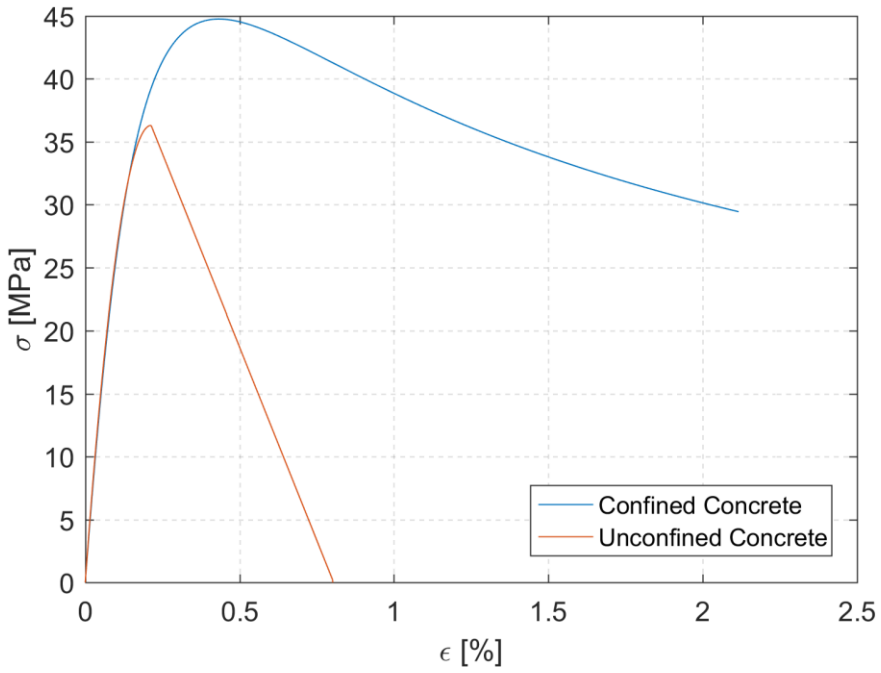

Figure 3: Used concrete material models

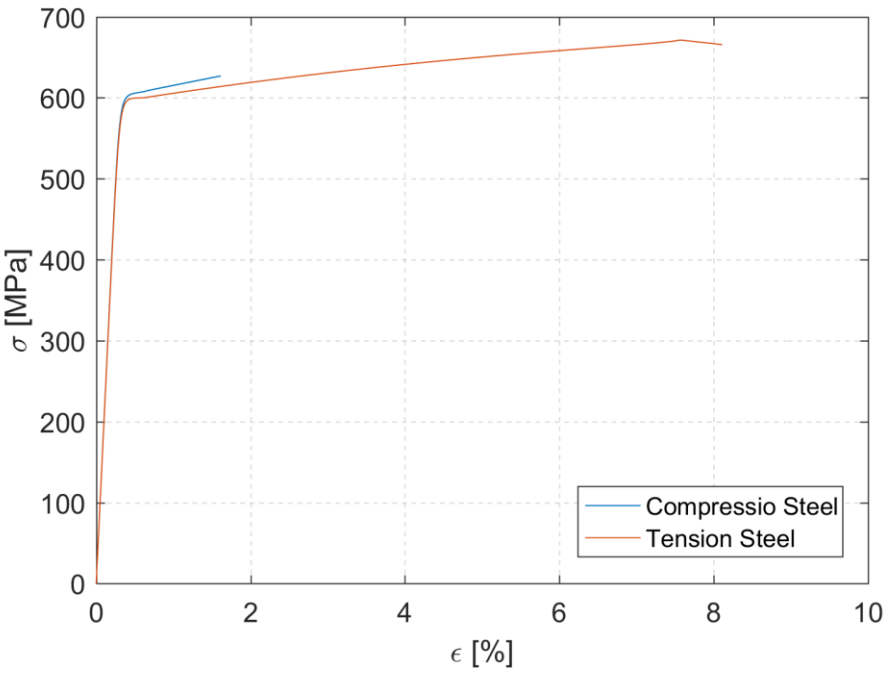

Figure 4: Used reinforcement steel material models

2.2 Cyclic Load Definition

The load applied to the real column had a cyclic behaviour, and therefore the simulated load used with the OpenSees analysis follows the same pattern. The protocol has a total of 30 cycles, and the maximum displacement is 150mm, while the load is applied at the height of 150 cm from the base of the column, which corresponds to a rotation of about 10%. Using the assumption that the distribution of displacements along the height of the column is linear, the displacements for the loading procedure at the top of the column were calculated for the use in the pushover analysis. Figure 5 displays the given cyclic load pattern.

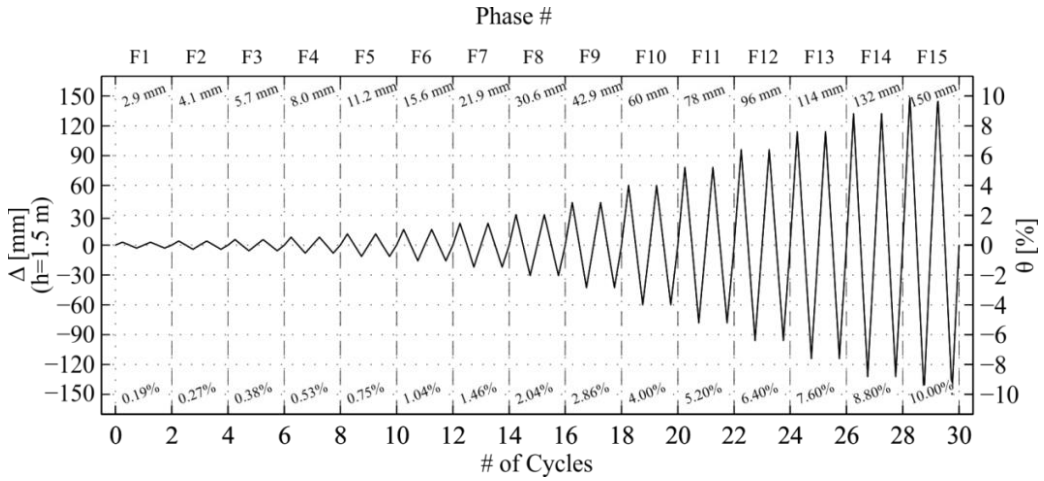

Figure 5: Cyclic load pattern

The analysis was conducted considering the external axial load of 577kN, summed up with the column's self-weight, resulting in a total of 582.4kN. The maximum curvature reached during the analysis was set to 0.45, while the total number of steps to reach this curvature was set to 500.

During the analysis, the stress-strain relationships of confined and unconfined concrete were recorded, as well as one of the reinforcement bars in tension and one in compression. A node in the column was also observed in order to record its displacement.

2.3 Nonlinear Static Analysis of the RC Column

Using the material input parameters, described in Chapter 2.1, a nonlinear static analysis of the given column cross-section was performed, using a BWH micro numerical model, with the procedure described at [1].

Following the analysis of the cross-section, the idealisation of the produced moment-curvature envelope was established in order evaluate the cross-section and compare it with the reference cross-section STD/135. Consequently, a bi-linear idealisation of the moment-curvature envelope was performed, based on yield and ultimate limit states.

On Figure 6, both calculated (red) and idealised moment-curve relationship envelopes (cyan) are presented. Furthermore, the black cross represents the cracking moment of the cross-section M_{cr}, which was calculated to be 29.18 kNm, using a semi-empirical conservative equation, shown in Equation 8:

$$M_{cr} = \left(f_{ctm} + \frac{N}{A}\right)\frac{I_z}{b/2} \quad \text{(Eq. 8)}$$

Where f_{ctm} is the calculated median value of the concrete tension strength, and I_z is the second area moment of inertia about the z-axis of the cross-section (see Figure 2 above).

Yield, ultimate steel moment and ultimate section moment, denoted on Figure 6 as red, black and green stars, respectively, were calculated based on the deformation constraints of the steel reinforcement and concrete. The values of these moments are, respectively, 147.50 kNm, 142.64 kNm and 141.72 kNm. It can also be observed, that the rupture of steel reinforcement occurs before the failure of the cross-section, which can be interpreted as an indication of the quality of the concrete confinement.

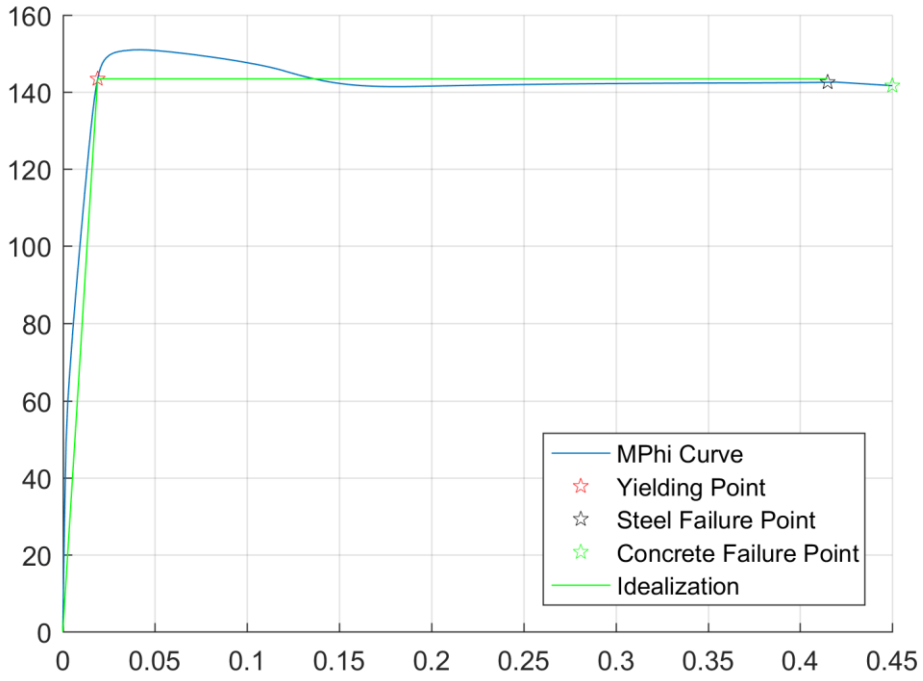

Figure 6: Idealised moment-curvature envelope compared to calculated

2.4 Seismic analysis of the RC column

In order to study the seismic response of the column, a Giberson macro numerical model [10] was prepared, where nonlinear response of the column was modelled with a nonlinear spring at the location of plasticity. The behaviour of the nonlinear spring was described according to Takeda's hysteretic rules [11].

For the analysis, the degradation parameter of unloading stiffness $\alpha = 0.5$ was considered. The quadri-linear envelope of the hysteretic envelope, corresponding to cracking, yielding, ultimate and total damage state, was established. The cracking state was determined with Equation 8, above, and Equation 9, below:

$$\theta_{cr} = \frac{M_{cr}}{L_V} 3EI \quad \text{(Eq. 9)}$$

Where θ_{cr} is the crack rotation, and L_V is the shear-span of the member, roughly estimated to be the same at the length of the member.

Yield and ultimate moments were established based on the bi-linear idealisation of the moment-curvature response, described in Chapter 2.3, while the corresponding yield and ultimate rotations were calculated according to EC8/3 [7]. The method of calculating yield rotation, considering flexural, shear, and slip rotation, is presented in Equation 10:

$$\theta_y = \phi_y \frac{L_V + \alpha z}{3} + 0.0013\left(1 + 1.5\frac{h}{L_V}\right) + 0{,}13\,\phi_y \frac{d_{bL} f_{sy}}{\sqrt{fc}} \qquad \text{(Eq. 10)}$$

The $\alpha_z$factor in the above equation was considered to be 0, while f_{sy} was taken into account as median yield strength of longitudal steel bars.

The ultimate rotation, considered to define the near collapse limit state of the column under cycling loading, was calculated with Equation 11, independently from the curvature response of the member:

$$\theta_u = K \cdot\ 0.016\ 0.3^{\nu}\left(\frac{\max(0.01;\omega')}{\max(0.01;\omega)} f_c\right)^{0.225}\left(\frac{L_V}{h}\right)^{0.35} 25^{\left(\frac{\alpha \rho_{sx} f_{yw}}{f_c}\right)} 1.25^{100\,\rho_d} \qquad \text{(Eq. 11)}$$

In the above equation, the factor *K* of $0{,}825$ was used, as demanded by [3] for members without detailing for earthquake resistance. ω and ω' represent the ratio of longitudal reinforcement in tension and compression, respectively. In our calculations, both were estimated to be equal to half of the total longitudinal reinforcement ratio of the cross-section. ρ_{sx} represent the ratio of lateral reinforcement parallel to the direction of loading, while ρ_d is the ratio of diagonal reinforcement of the cross-section, which was not included in this analysis. α represent the confinement effectiveness ratio, described in Equation 2, above.

Furthermore, post-capping stiffness was considered in the model, as described in [2], with the ratio between total and near collapse rotations $k_{pl,TC/NC} = 2$ in order to consider the influence of buckling of longitudinal reinforcement steel and to estimate the total collapse limit state..

In Table 3 below, we summarise the calculated input parameters for the hysteretic analysis.

Table 3 Input parameters for the Giberson model

$\theta_{cr}[\%]$	$\theta_y[\%]$	$\theta_u[\%]$	$M_{cr}[kNm]$	$M_y, M_u[kNm]$	$\alpha[-]$	$k_{pl,TC/NC}$
0,009	1,69	5,3	29,12	147,50	0,5	2

2.4.1 Results and Comparison with Experimental Data

On Figures 7 and 8 we present the comparison between the experimentally obtained data, and the results of the numerical analysis of the given cross-section. A slightly more conservative response can be seen from the results of the numerical analysis, exhibited by a lower maximum lateral load and a smaller post-cracking stiffness of the member, compared to the experimental results. On Figure 8 we compare the results on a normalised scale of force, where a good comparison of the total hysteretic response can be interpreted.

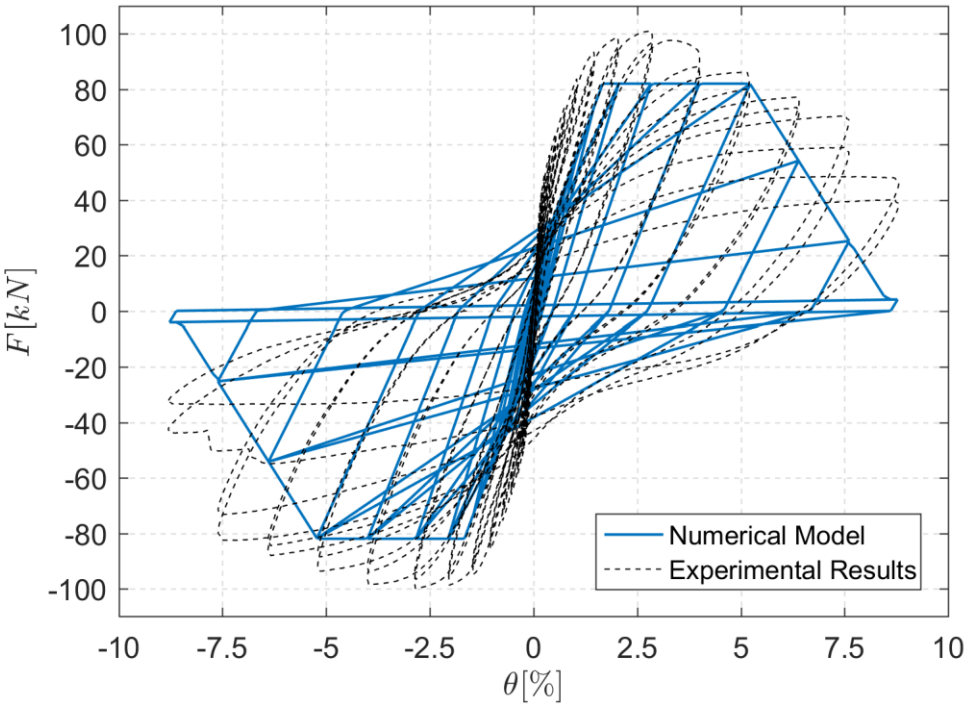

Figure 7: Comparison between results of experimental and numerical analysis

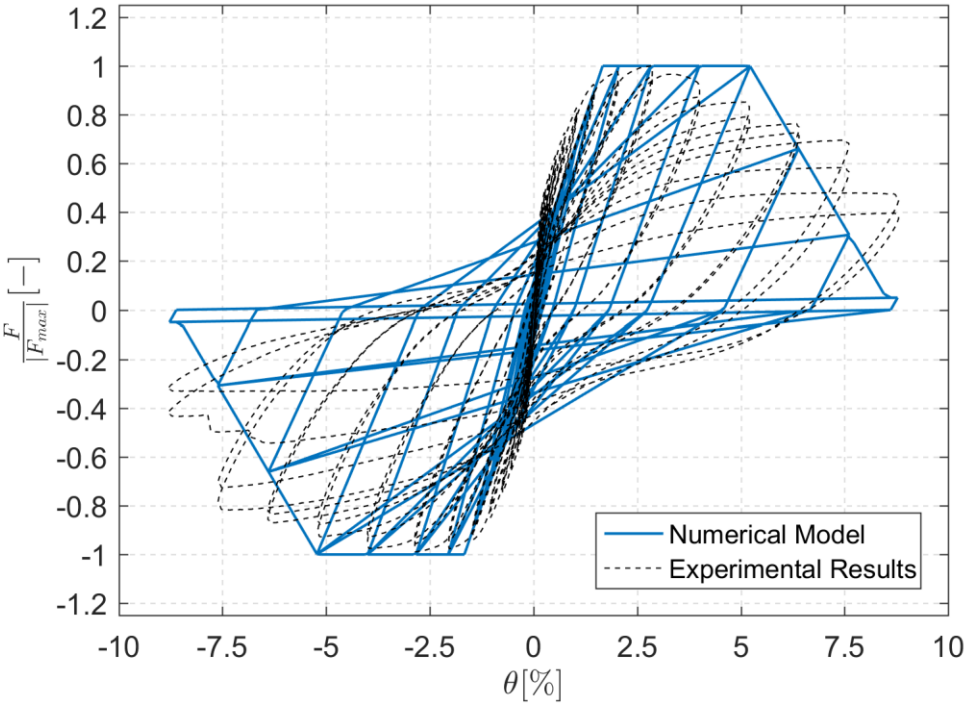

Figure 8: Comparison between results of experimental and numerical analysis – normalised

2.4.2 Results and Comparison with STD/135

Following the numerical analysis, the relationship between the calculated horizontal force F and rotation of the column θ was graphically established in order to obtain the hysteretic capacity curve of the member. Finally, the results of a previously performed hysteretic analysis of a similar cross-section, based on the same numerical model, and denoted as STD/135, were imported and compared with the given cross-section.

On Figure 9 we compare the force-rotation hysteric envelopes for the given cross-section (blue), and the reference cross-section STD/135 (dotted black). A slight distinction between the two can be noted, but a generally good fit between the responses can be established due to the similarity between the cross-sections.

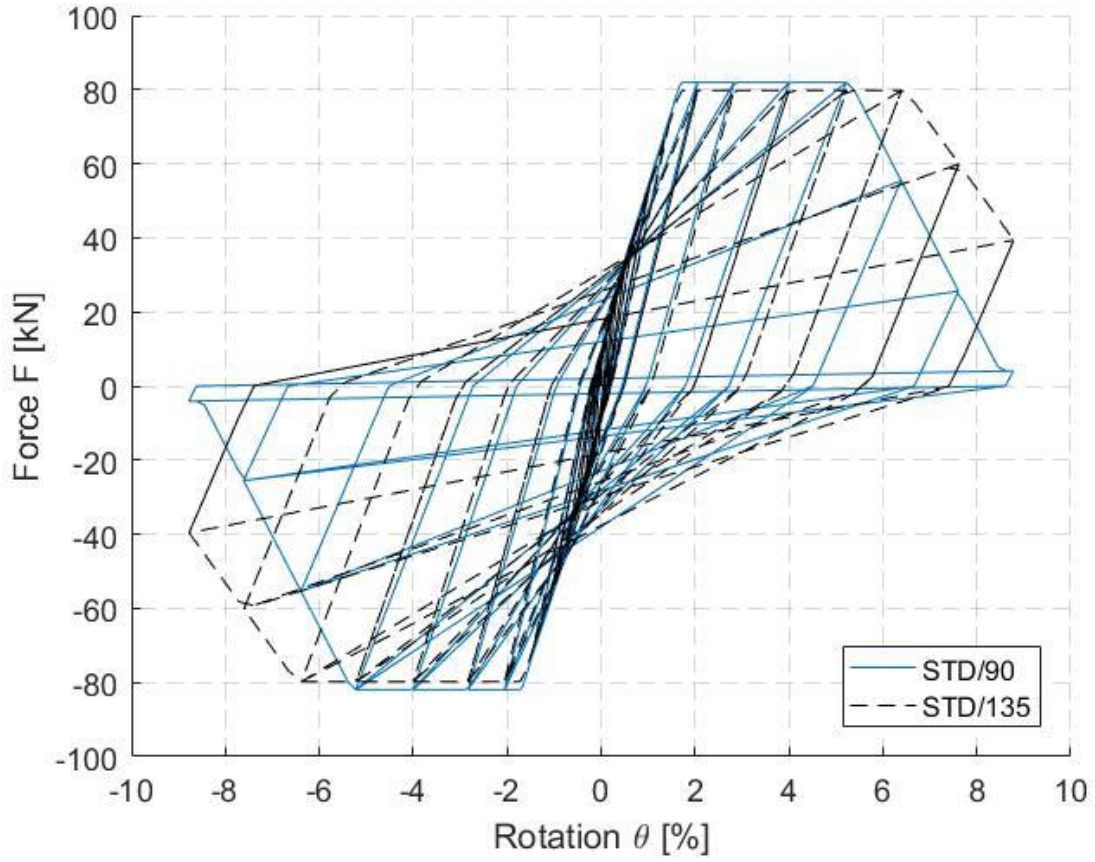

Figure 9: Comparison of results of the performed numerical analysis for the given and reference cross-section

2.5 Analysis of influences on the ductility of the column

All these parameters represent an important role in the ductility of the cross-section. The most important consideration to ensure ductility in the column is an adequate provision of transverse reinforcement to confine the compressed concrete core and prevent buckling of the longitudinal bars, as well as prevent shear failure. It can be noticed that the confinement provides a higher capacity and ductility compared to unconfined concrete.

On Figures 10 and 11 we show the impact of different concrete qualities on the moment-curvature and the hysteretic response of the column, respectively. It can be seen that the weaker the concrete is; the less ductile response it exhibits.

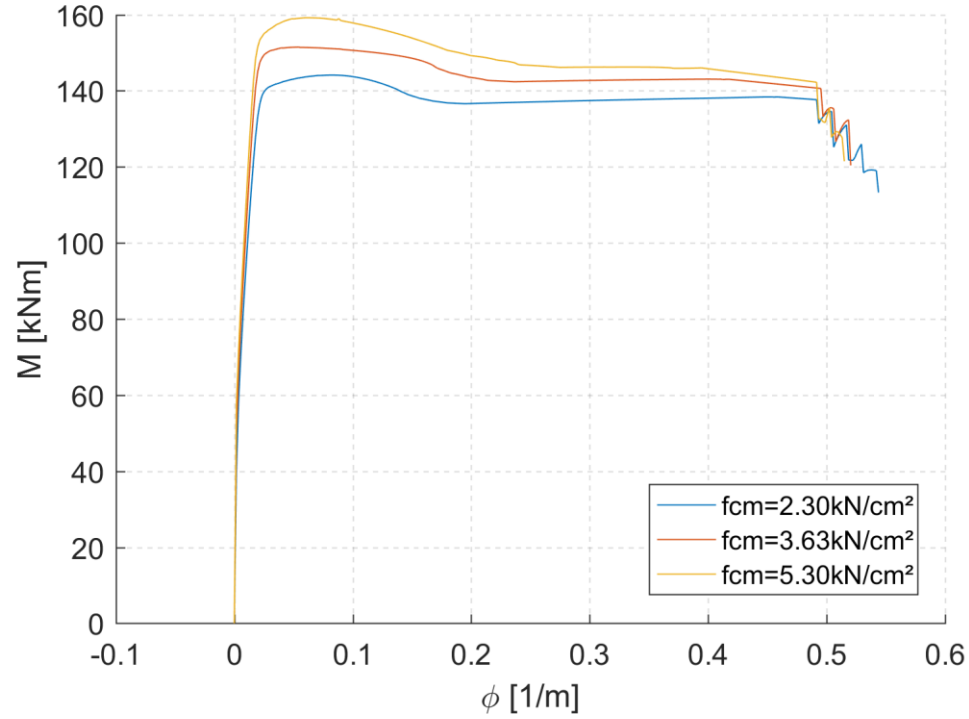

Figure 10: Comparison of different concrete qualities on the moment-curvature response

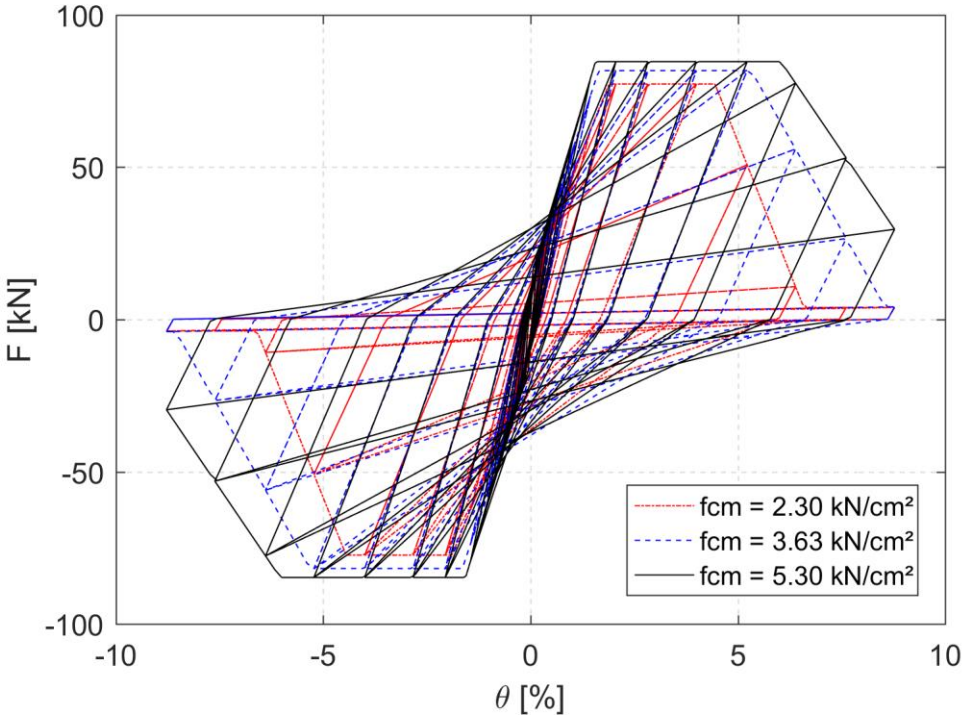

Figure 11: Comparison of different concrete qualities on the hysteretic response

With a higher axial load acting on the column, a greater amount of transverse reinforcement will be necessary to ensure ductility of the cross-section because the neutral axis depth will be larger. The yield curvature will increase, and the ultimate curvature will decrease, and therefore the cross-section ductility will be reduced.

On Figures 12 and 13 we show the influence of different levels of axial force on the moment-curvature relationship of the column, and on the hysteretic response of the column, respectively. On moment-curvature relationship, an increase of axial load appears to have a significant influence only on the yield moment of the section. The limit curvatures in this regard appear to change only slightly. On Figure 12, this is not intuitive to be seen, but by monitoring the steel strains, it could be observed that all the cases failed with a curvature of around 0.35, which is shown by the grey line below.

A significant difference in the hysteretic response with changing levels of axial force can be noted, however. With increasing axial load, the hysteretic energy, which corresponds to the area under the hysteretic curve, also increases, which ensures a more favourable performance of the column.

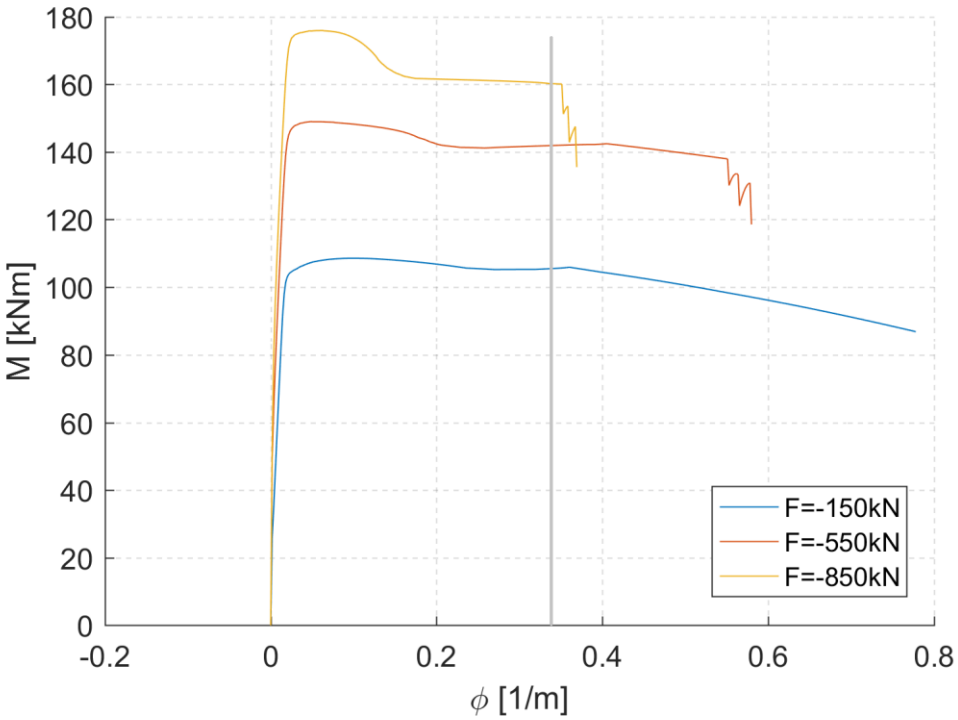

Figure 12: Comparison of different levels of axial force on the moment-curvature response

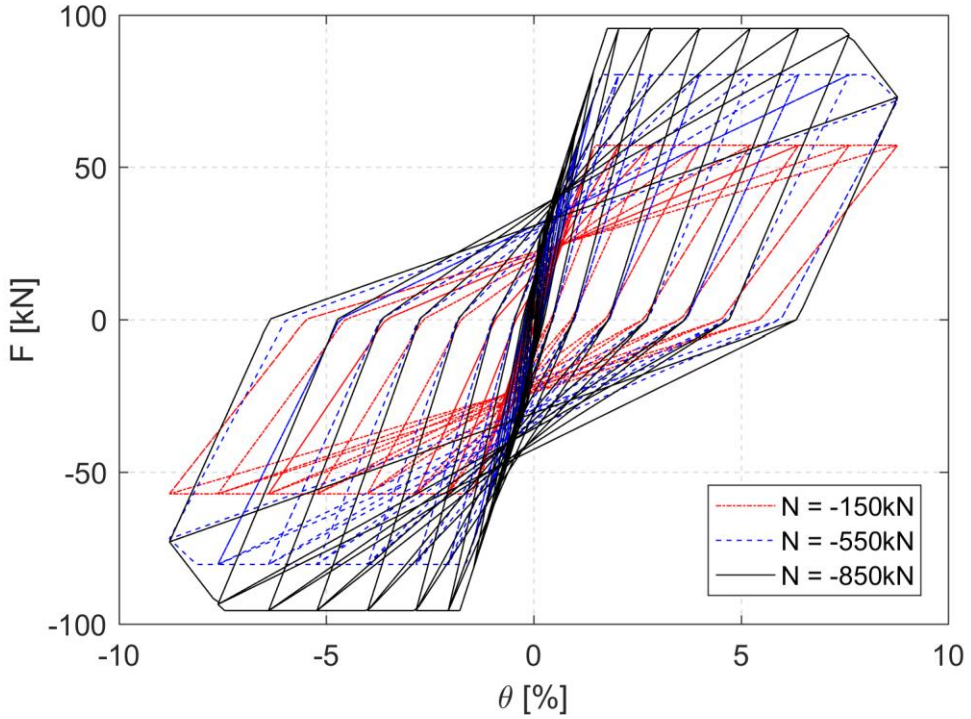

Figure 13: Comparison of different levels of axial force on the hysteretic response

On Figures 14 and 15 we show the influence of spacing of lateral reinforcement on the moment-curvature response of the column, and on the hysteretic response of the column, respectively. In terms of moment-curvature relationship, the distance between the stirrups appears to have a noticeable effect on the ductility of the member, while the change in ultimate moment is not significant. Regarding the hysteretic response, a difference between the responses can be observed with the reduction of spacing between the stirrups.

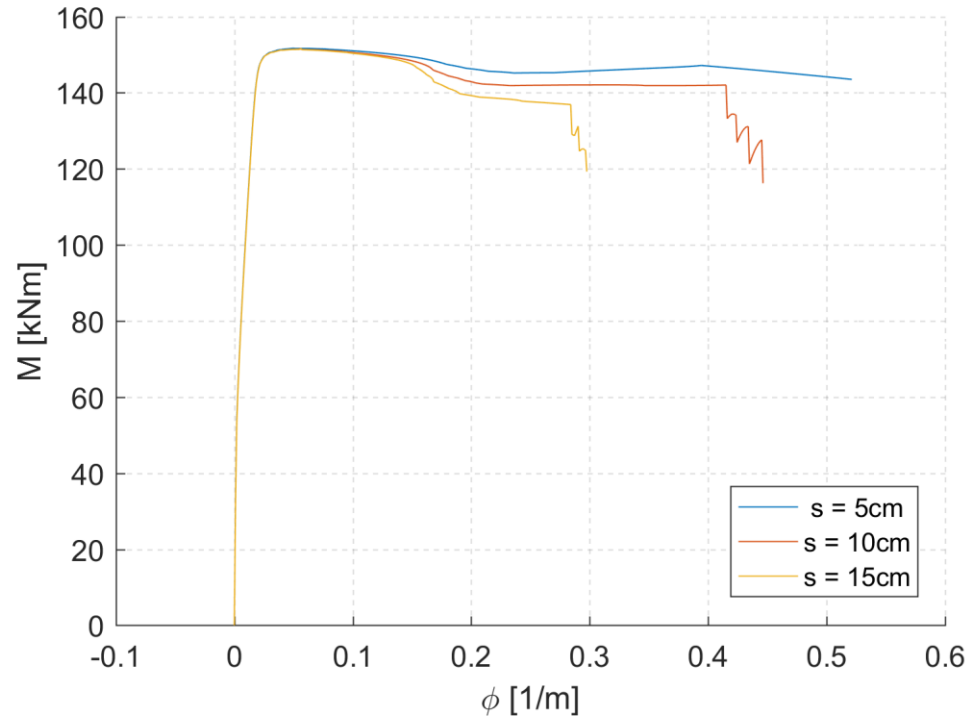

Figure 14: Comparison of different amounts of lateral reinforcement spacing on the moment-curvature response

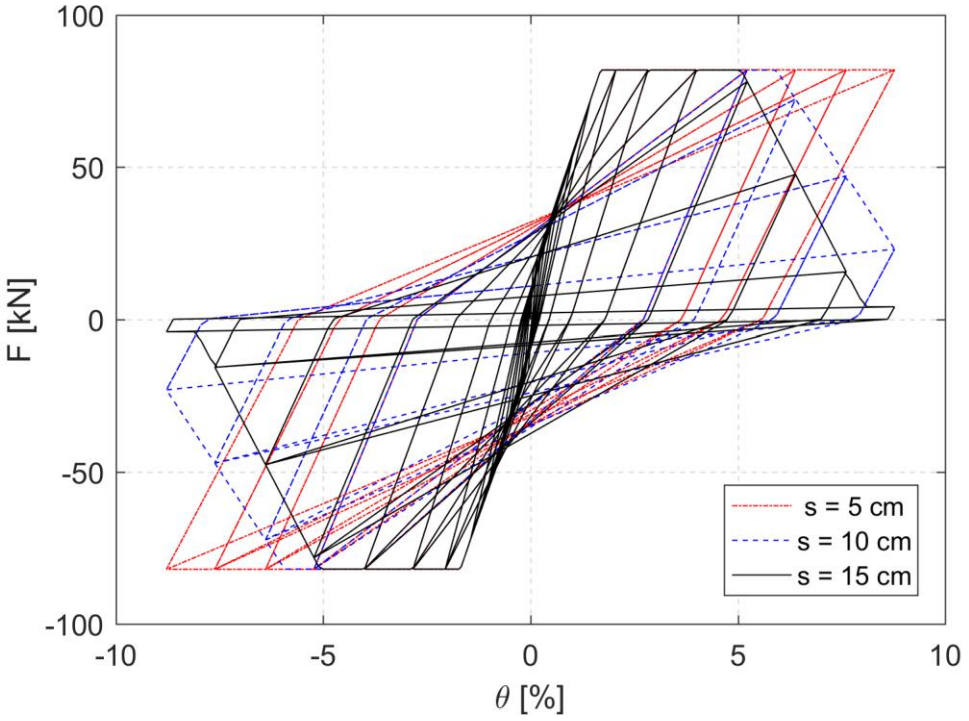

Figure 15: Comparison of different amounts of lateral reinforcement spacing on the hysteretic response

The influence of increasing the longitudinal bar diameter was also analysed. The results are displayed below in Figures 16 and 17. Because of the well-confinement of the section, all of

the bar diameters displayed similar ultimate curvature values, although the moment values change in a great manner in the post-yielding phase. This difference in the moment values is seen again in the hysteretic curve, which display a greater absorption of hysteretic energy with an increase of bar diameter.

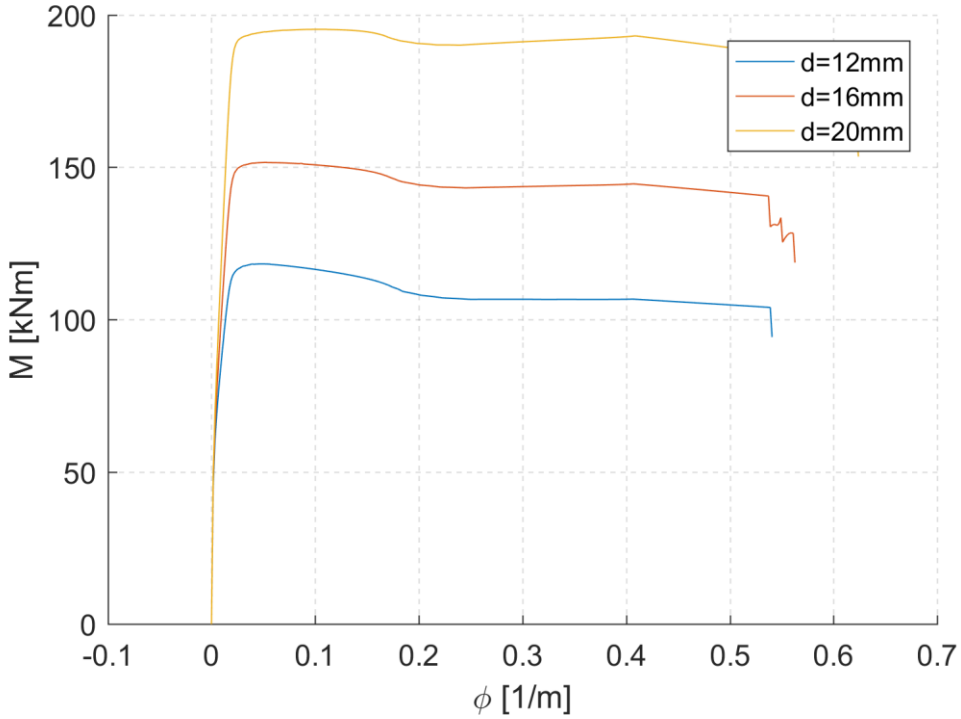

Figure 16: Comparison of different diameters of longitudinal reinforcement on the moment-curvature response

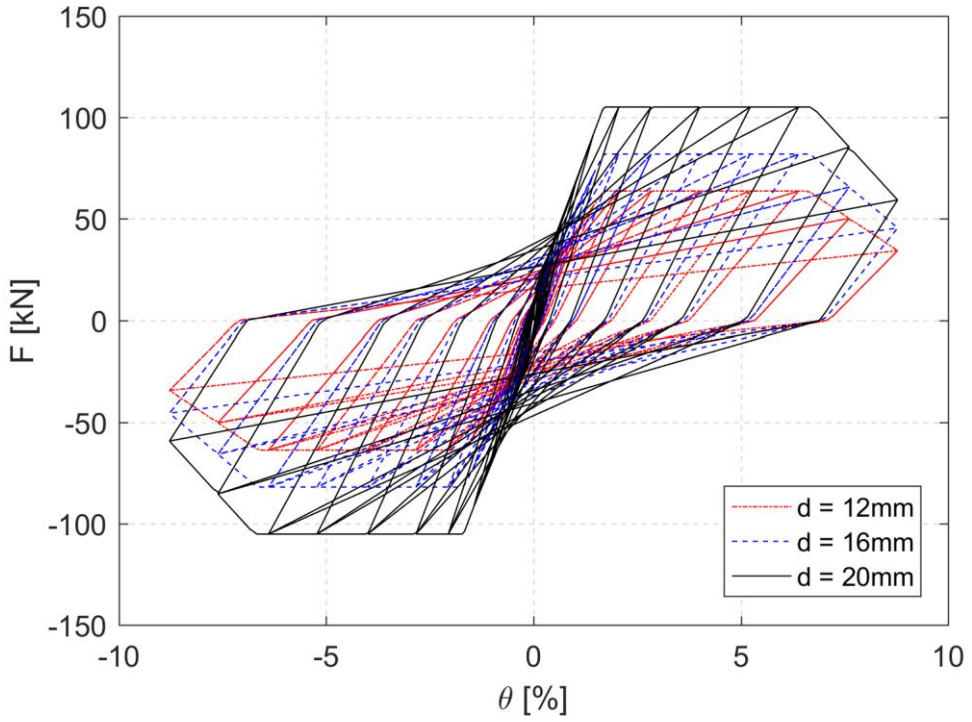

Figure 17: Comparison of different diameters of longitudinal reinforcement on the hysteretic response

3 PUSHOVER ANALYSIS OF A MULTI-SPAN BRIDGE

3.1 Material and Geometric Properties of the Bridge Structure

In the second task, a pushover analysis of a six-span bridge was performed. The two end spans are 26 m in length, while the rest span distances are 32 m. The bridge structure is shown in Figure 18. The deck is supported by five barbell-shaped columns, the dimensions of which are shown in Figure 19.

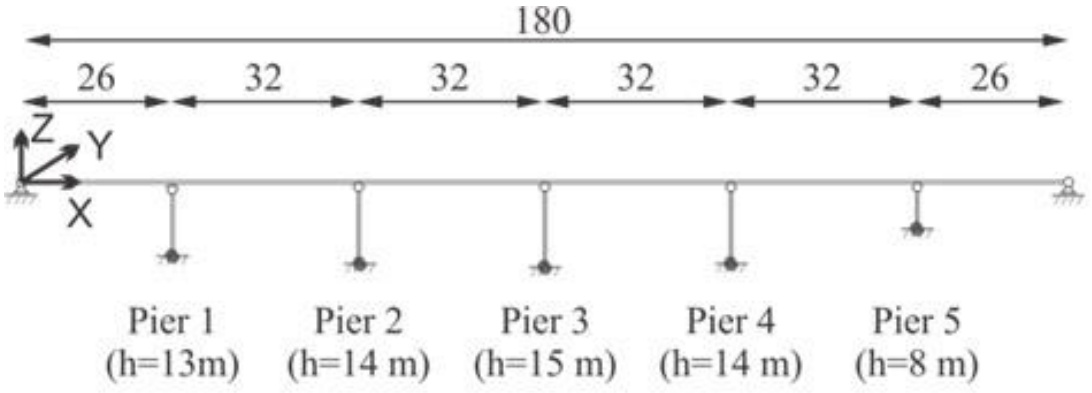

Figure 18: Considered structure of the bridge

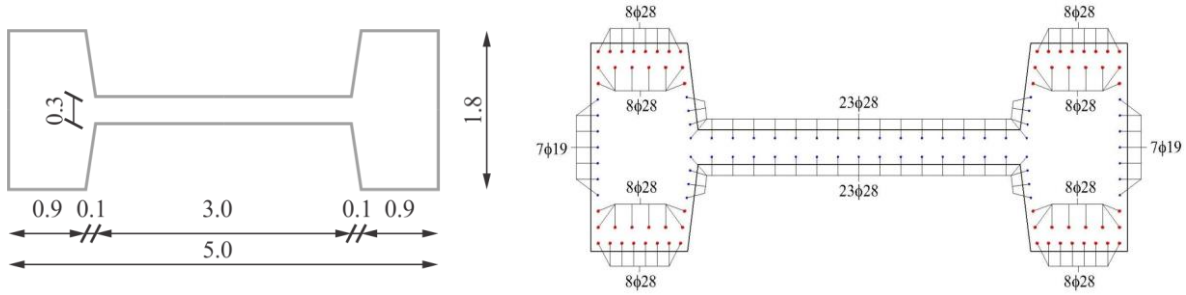

Figure 19: Cross-section of the barbell-shaped column piers (left) and the size and position of flexural reinforcement in the cross-section (right)

The cross-section of the deck is given in Figure 20. The mass of the deck was assumed to be 29.81 t/m, which was calculated using load model LM1 from [6], while mass of the cap beam was considered to be 38.3 t.

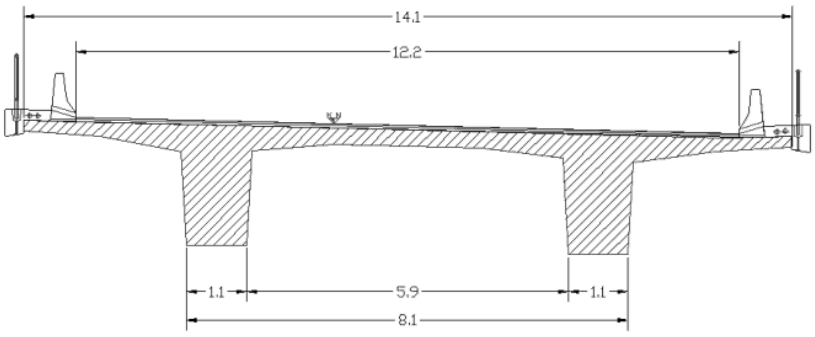

Figure 20: Cross-section of the bridge deck

The transverse reinforcement was considered as standard, with the bars of 10 mm diameter, spaced evenly at 10 cm. However, the detailing of the transverse rebars was taken as improper due to the shape of the hooks.

The material properties of the confined concrete were established according to the provisions of EC 8/2, which are based on Mander's model. The protocol for this calculation is explained in detail in subsection 2.1 of this report. For the confined concrete was used the Popovic's material model in Opensees. In order to model the behaviour of the reinforcement, the simplified bi-linear constitutive model was adopted with the use of *Steel02* material model in OpenSees.

3.2 Moment-Curvature Relationship

The moment-curvature response was prepared for each of the piers, with a procedure, similar to the one described in section 2.3. On Figures 21 and 22 we present the calculated moment-curvature relationships about Y and Z axis, respectively. The idealization of the established curves was also prepared, with the failures of steel reinforcement (black star) and concrete section (green star) of pier 3 shown on Figure 23, which represents the rotation about Y axis. It can be noticed, that for pier 3, during bending about Y axis, the reinforcement fails before the section fails. Based on the obtained results, it can also be said that physically sensible results are obtained from the numerical model only until the failure of the concrete section.

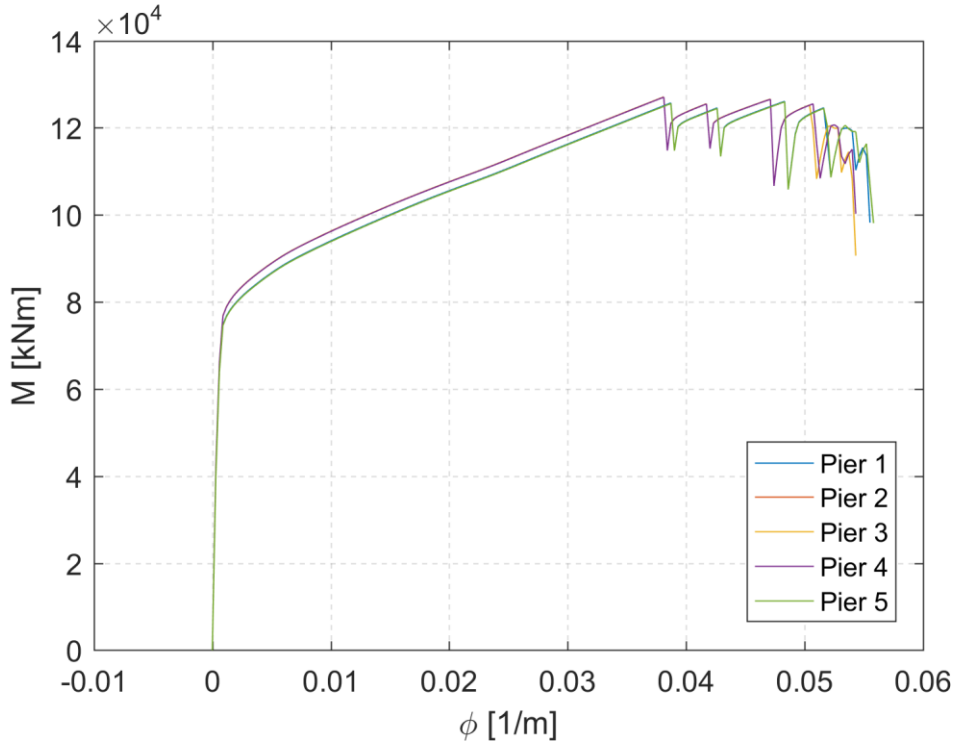

Figure 21: Moment-curvature relationship of the piers about Y axis

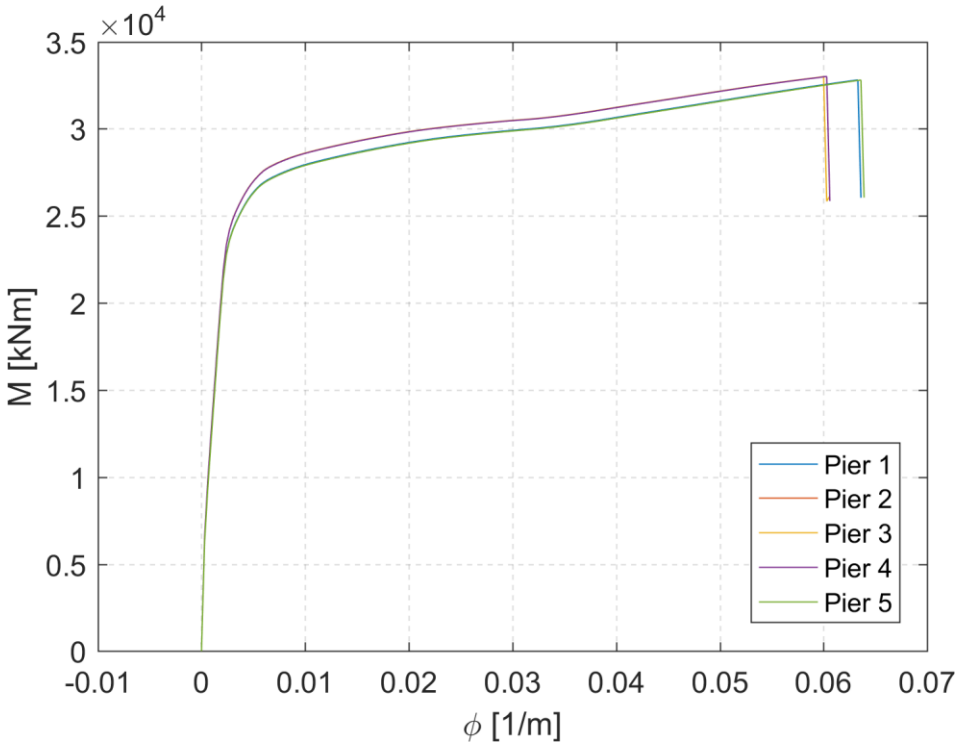

Figure 22: Moment-curvature relationship of the piers about Z axis

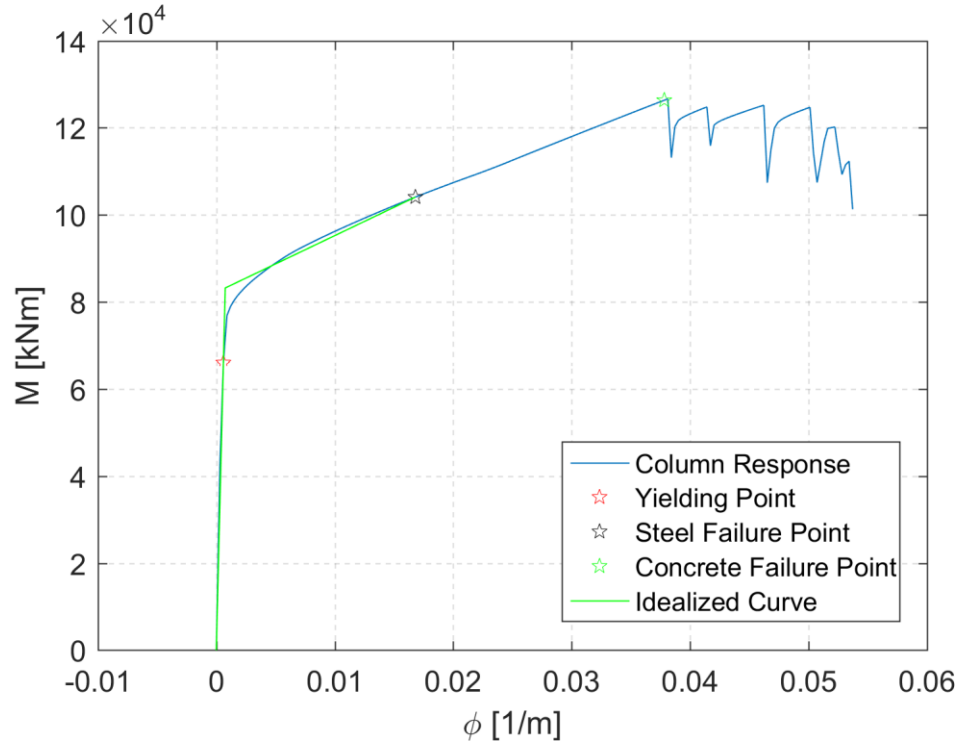

Figure 23: Idealisation of the moment-curvature relationship about Y axis for pier 3

3.3 Pushover Analysis

The pushover analysis was prepared based on the moment and curvature envelopes obtained from the moment-curvature analysis responses of the piers. Furthermore, the pushover analysis was prepared using the Giberson's lumped plasticity model, using Takeda's hysteretic rules, with the quadri-linear idealization of the piers' behaviour, as described in Chapter 2.4.

However, a key difference to Chapter 2.4. and to the hysteretic analysis in the first task, where the limit state rotations according to EC 8/3 [3] were adopted, is the definition of the rotations with the use of provisions in EC 8/2 [7].

The yield rotation was calculated with Equation 12:

$$\theta_y = \frac{\Phi_y}{3} L \quad \text{(Eq. 12)}$$

In the above equation, *L* represents the distance from the end section of the plastic hinge to the point of zero moment in the pier, in this case represents the complete length of the pier due to the rolling connection of the pier to the superstructure. Φ_y represents the yield curvature, obtained from the idealised moment-curvature relationship.

The total chord rotation θ_u was calculated as the sum between plastic rotation capacity $\theta_{p,u}$ and the yield rotation θ_y, (Equation 12). The total chord rotation calculation is shown in Equation 13:

$$\theta_u = \theta_y + \theta_{p,u} = \left(\Phi_u - \Phi_y\right) L_p \left(1 - \frac{L_p}{2\,L}\right) \quad \text{(Eq. 13)}$$

Where L_p is the plastic hinge length, calculated with Equation 14, shown below:

$$L_p = 0{,}10L + 0{,}015\, f_{yk} d_{bL} \quad \text{(Eq. 14)}$$

In the above equation f_{yk} is the characteristic yield strength in MPa, and d_{bL} is the bar diameter of the longitudinal reinforcement.

On Figure 24, we present the moment-rotation response of each pier. A distinctly similar response can be observed for piers 2 and 3, which are in essence completely identical. Pier 5 appeared to exhibit the smallest ultimate rotation. This can be attributed to its shorter height compared to other piers. Consequently, the established bending mechanism is not as effective as with other piers. However, pier 1 exhibited the smallest overall rotational capability.

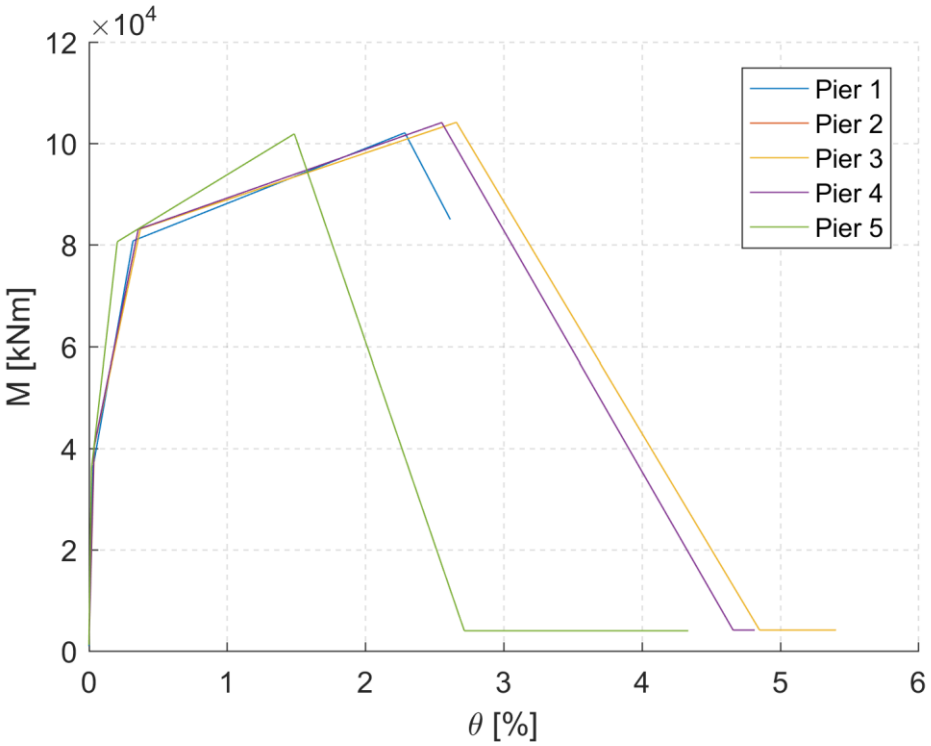

Figure 24: Calculated moment-rotation response of the piers

For the pushover analysis, each span of the bridge was divided into 10 nodes spaced evenly counting a total of 61 nodes for the total length of the deck. The control node is the 31 located at the centre of the total span (pier 3) and the control DOF direction is the translational in Y.

The forces acting on each node are calculated according to N2 method [9]. It assumes a normalized displacement shape Φ in which the displacement at the node 31 is equal to 1.

$$F_i = m_i * \Phi_i \quad \text{(Eq. 15)}$$

On Figure 25 we present the pushover curve, calculated with above-mentioned assumptions. It can be seen, that the pier 1 is the first one to yield, while pier 5 is the first one to reach failure. In order to established peak ground acceleration, an idealised version of the curve (coloured green) was also produced, where critical states were considered to be the piers that reach respective yield and ultimate states first, i.e. pier 1 and 5.

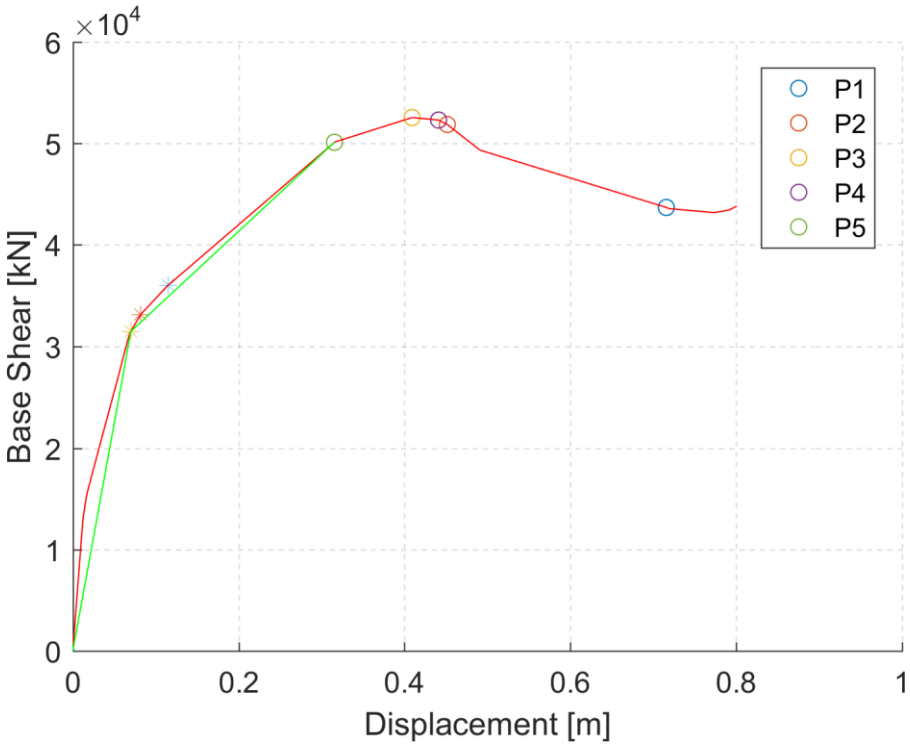

Figure 25: Calculated pushover curve of the bridge structure (red), and idealised version (green)

3.4 Calculating peak ground acceleration

The peak ground acceleration in the longitudinal direction of the structure was calculated by estimating the stiffness of the structure according to the moment-curvature relationship when the piers are subjected to loading about their weak axes. Considering the total mass of the structure, the period was calculated to be $T = 1.38$ s. By considering soil type C, the PGA was estimated to be $a_g = 0.60$ g.

The calculation of the transverse peak ground acceleration was based on the N2 method, described in [9]. This method consists in combining the pushover analysis of a multi degree of freedom model (MDOF) with the response spectra analysis of an equivalent single degree of freedom system (SDOF) in order to determine the seismic demand on the structure.

After the pushover analysis was performed, the model of the MDOF was defined into the equivalent SDOF model by first determining its mass, given in Equation 16, below:

$$m^* = \Sigma\, m_i\, \Phi_i \qquad \text{(Eq. 16)}$$

Where Φ_i represents the normalized displacements of the structure. In order to transform MDOF quantities to SDOF, the transformation factor was calculated with Equation 17:

$$\Gamma = \frac{m^*}{\Sigma m_i\, \Phi_i^2} \qquad \text{(Eq. 17)}$$

With the transformation factor, the equivalent SDOF displacement D_y^* and force F_y^*, corresponding to the point of first yielding, and V is the base shear of the MDOF model, respectively, can therefore be calculated as shown in Equations 18 and 19:

$$\mathrm{D}_{\mathrm{y}}^{*} = \frac{D_t}{\Gamma}$$
$$\mathrm{F}_{y}^{*} = \frac{\mathrm{V}}{\Gamma} \qquad \text{(Eq. 18, 19)}$$

Above D_t represents the displacement corresponding to the point of first yielding, and *V* is the base shear of the MDOF model. The deformation at the point of first yielding was established from the calculated pushover curve and amounted to 0.07 m.

Consequently, the period of the SDOF model corresponds to 0.57 s:

$$\mathrm{T}^{*} = 2\,\pi\sqrt{\frac{m^{*}\ D_y^{*}}{F_y^{*}}} \qquad \text{(Eq. 20)}$$

The displacement, which was perceived to be critical was at the point when first of the piers collapsed. This displacement corresponds to 0.31 m, where the failure occurred at pier 5. Using the perceived ultimate displacement of the structure, an equivalent ultimate displacement of the SDOF model was calculated with Equation 21:

$$\mathrm{D}_{\mathrm{u}}^{*} = \frac{0.31}{\Gamma} \qquad \text{(Eq. 21)}$$

The spectral acceleration was calculated using Equation 22, where $\mathrm{D}_{\mathrm{u}}^{*} = S_{de}$

$$\mathrm{S}_{\mathrm{ae}} = \frac{S_{de}\,4\,\pi^2}{T^{*2}} \qquad \text{(Eq. 22)}$$

Based on this, the peak ground acceleration was calculated from the definition of the elastic response spectra type 1 according to EC 8/1 [8], while also considering the type of soil C (S = 1.15):

$$\mathrm{a_g} = \frac{\mathrm{S_{ae}}}{\mathrm{S}\,\eta\,2.5} \qquad \text{(Eq. 23)}$$

The calculated peak ground acceleration was calculated to be $a_g =$ 1.08 g, corresponding to the failure of the first pier in the transverse direction.

According to N2 method, in order to visualize the seismic demand and response of the structure, it is necessary to transform the elastic spectra into acceleration-displacement (AD) format. The elastic displacement spectra was consequently calculated with Equation 22:

$$\mathrm{S_{de}} = \frac{\mathrm{T}^2}{4\,\pi^2}\mathrm{S_{ae}} \qquad \text{(Eq. 22)}$$

The reduction factor due to ductility corresponds to 2.83 calculated as follows:

$$R_{\mu} = \frac{S_{ae}(T^{*})}{S_{ay}} \qquad \text{(Eq. 23)}$$

Consequently, since $T^{*} < Tc$ the ductility demand was calculated using Equation 24 corresponding to 2.921

$$\mu = (R_{\mu} - 1)\,\frac{\mathrm{Tc}}{T^{*}} + 1 \qquad \text{(Eq. 24)}$$

In order to construct the inelastic spectra, the reduction factor is calculated for all the periods in the elastic spectra using Equations 25 and 26, which consider Tc as the characteristic transition period.

$$R_\mu = (\mu - 1) * \frac{T}{Tc} + 1 \quad \text{(Eq. 25)}$$

$$R_\mu = \mu \quad \text{(Eq. 26)}$$

Finally, the inelastic spectral acceleration and displacement are calculated to obtain the inelastic spectra.

$$S_a = \frac{S_{ae}}{R_\mu} \quad \text{(Eq. 27)}$$

$$S_d = \frac{\mu}{R_\mu} * S_{de} \quad \text{(Eq. 26)}$$

On Figure 26 is presented the elastic and inelastic demand spectra versus the idealized capacity curve of the pushover analysis. The seismic demand corresponds to the intersection of the constant period line, which is the period of the elastic period ($T^* = 0.57s$) corresponding to a displacement of 0.252 m and a spectral acceleration of 3.11g, both for the SDOF model. The values corresponds to a ground motion of $a_g = 1.08g$.

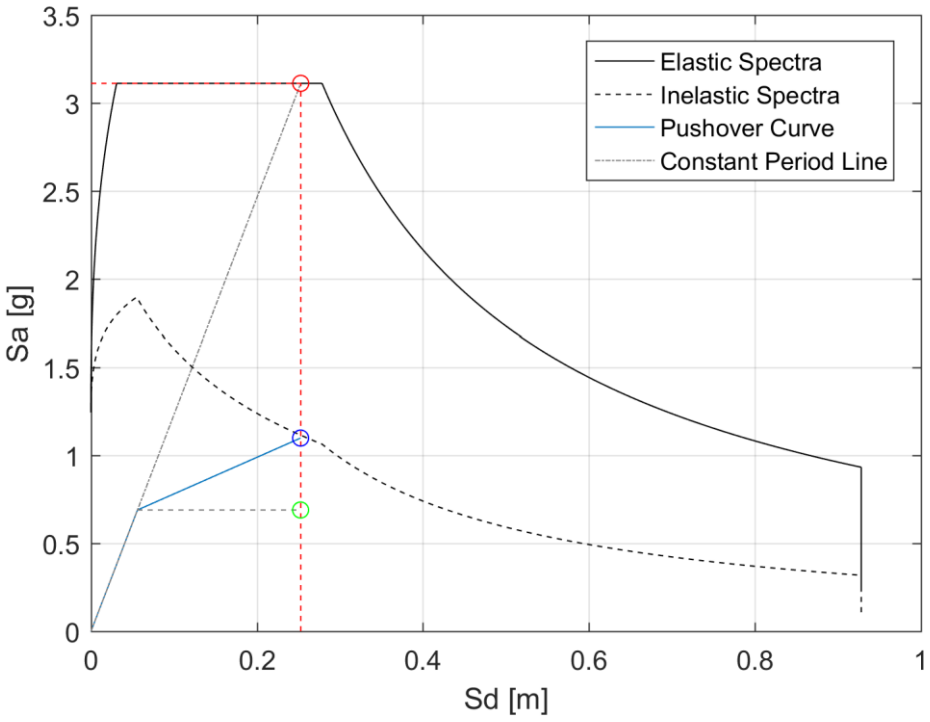

Figure 26: Elastic and inelastic demand spectra versus capacity diagram

When the mass of the bridge deck is doubled there is change in the seismic response of the response. On the Figure 27 we present the moment-rotation response of each pier and it can be noticed that the rotations are the same but since the mass is increased, the forces acting are increased as well and the moment require to get that rotations will be higher. In the comparison of both capacity curves (Figure 28) the same behaviour can be noticed. The mass of the deck is doubled and therefore there is a higher base reaction on the structure to reach the same damage states.

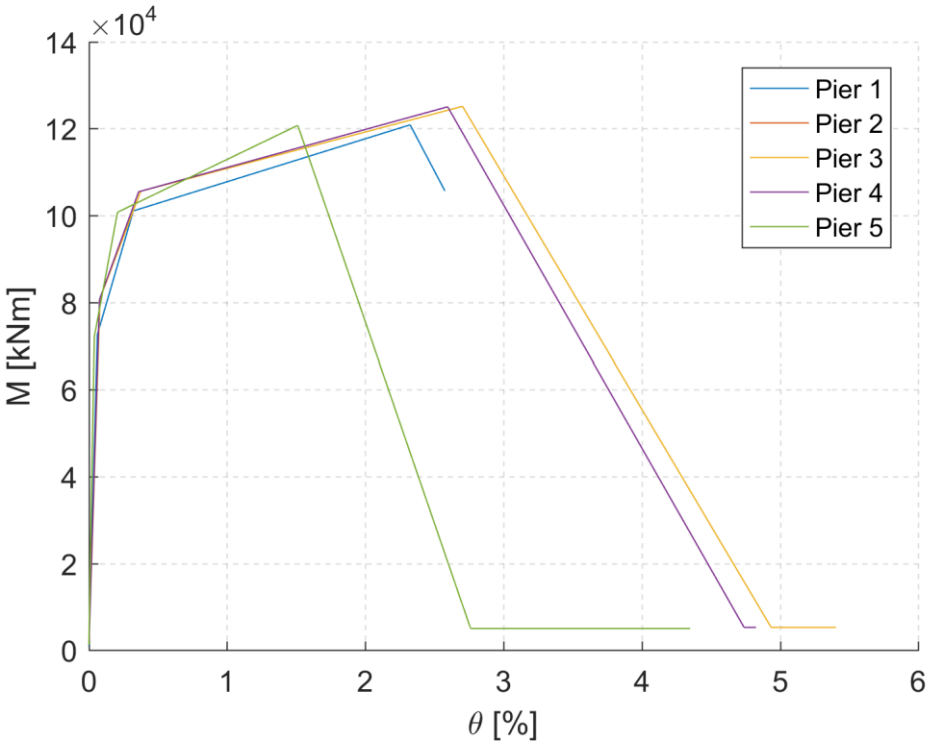

Figure 27: Calculated moment-rotation response of the piers with the doubled mass

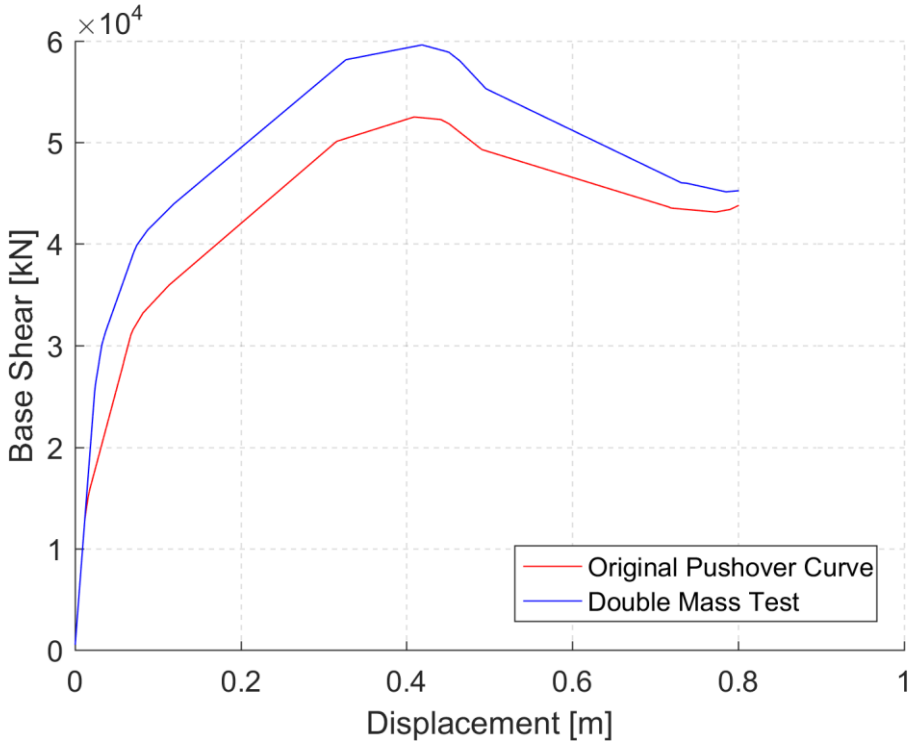

Figure 28: Calculated pushover curve of the bridge structure with the doubled mass

4 Conclusions

In conclusion, first task included the establishment of the moment-curvature relationship of the given column, and consequently an analysis of the hysteretic response of the column, while taking into account confinement of concrete.

During the preparation of the analysis, a Mander-based material model for the calculation of the confined concrete properties, was used. The model itself does not take into consideration shapes of stirrup hooks, however, since the column was given with adequate reinforcement detailing, with only minor deficiencies, the effect of hook shapes was considered as negligible. Therefore, the use of Mander's model was justified.

The moment-curvature analysis was based on the confined concrete model. It was noted, that rupture of the tensile reinforcement bars occurs before the failure of the cross-sections. This was interpreted as a measure of good quality of the confinement. In order to perform the cyclic analysis of the column, a bi-linear idealization of the moment-curvature relationship was performed, where the cracking and yield moments and rotations were calculated. It must be noted, however, that buckling of reinforcement bars in the compression zone of the cross-section was not considered directly in the numerical model.

The cyclic response was based on Giberson's numerical model, with the use of Takeda's hysteretic rules. Consequently, a quadri-linear hysteretic envelope was established according to cracking, yield, near collapse, and total collapse damage states of the column. Yield and ultimate rotations, which corresponds to near collapse limit state of the column, were calculated according to EC 8/3, where the latter was established completely independent from the moment-curvature response of the column. Cracking state was established partially analytically, while yield and near collapse moment were taken from bilinear idealization of the moment-curvature relationship. The state of total collapse was estimated in a simplified manner, using a post-capping stiffness coefficient.

The results of the prepared numerical model were compared to the experimental results. A slightly more conservative estimation of the response was noted, in comparison with the experiment. Lastly, the parametrical comparison shows that there is an influence of different factors on the hysteretic behaviour of the column.

In the second task, a pushover analysis of a multi-span reinforced concrete bridge was performed. The analysis was prepared based on the provisions included in EC 8/2, while the detailing was considered standard with improper hooks. Consequently, the hooks of the internal U-shaped stirrups were considered to be inappropriately shaped, which had an impact on the material properties of the confined concrete.

The moment-curvature relationship of each pier was calculated. It was established that the piers showed a similar response in both directions of loading. In order to calculate the pushover curve, and idealisation of the obtained moment-curvature data was performed. This considered post-yielding linear behaviour. The envelope of the idealisation procedure was then used as an input parameter for the calculation of Takeda non-linear properties.

With calculated Takeda parameters, the pushover procedure was carried out. This took into account an imposed parabolic shape of displacements in the transverse direction. Based on the pushover curve, it was established that the third pier yields first, while the fifth pier reaches failure first.

The peak ground acceleration was then determined in both directions of the structure. The calculated values were shown to be higher than the maximum peak ground acceleration corresponding to the return period of 475 years of Slovenia, $a_g = 0.25$ g. In conclusion, the bridge has satisfactory seismic behaviour.

A pushover analysis was also conducted, where the effect of increasing structure's mass was studied. An increase of moment values of the moment-curvature response of piers was observed. This resulted in a greater base shear value, observed from the pushover analysis, that is, considering the same displacement.

List of Figures

page

List of Tables

page

5 Bibliography

[1] UCLA, Berkley, "Open System for Earthquake Engineering Simulation," The Regents of the University of California, 1999. [Online]. Available: http://opensees.berkeley.edu/. [Accessed 17 August 2018].

[2] A. Anžlin, Influence of Buckling of Longitudal Reinforcement on Seismic Response of Existing Reinforced Concrete Bridges, Ljubljana: Self-published, 2017.

[3] CEN 2005, *Eurocode 8: Design of structures for earthquake resistance - Part 3: Assessment of and retrofit of buildings,* Brussels: Comité Européen de Normalisation, 1998.

[4] M. F. Giberson, "Two nonlinear beams with definitions of ductility," *Journal of the Structural Division,* vol. 95, no. 2, pp. 137-157, 1969.

[5] T. Takeda, M. Avni Sozen and N. Norby Nielsen, "Reinforced concrete response to simulated earthquakes," *Journal of Structural Divison,* vol. 96, no. 12, pp. 2557-2573, 1970.

[6] CEN 2003, *Eurocode 1: Actions on structures - Part 2: Traffic loads on bridges,* Brussels, 2003.

[7] CEN 2005, *Eurocode 8: Design of structures for earthquake resistance - Part 2: Bridges,* Brussels, 2005.

[8] P. Fajfar, "A Nonlinear Analysis Methodd for Performance Based Seismic Design," *Earthquake Spectra,* vol. 16, no. 3, pp. 573-592, 2000.

[9] CEN 2005, *Eurocode 8: Design of structures for earthquake resistance - Part 1: General rules, seismic actions and rules for buildings,* Brussels, 2005.

Project report

Nonlinear Analysis of Structures: Seismic Response of RC Bridges – Blind Prediction

Group 1

PUSHOVER ANALYSIS OF A MULTI-SPAN BRIDGE IN THE TRANSVERSE DIRECTION

Submitted by:

Alexander López Henao, Bauhaus University Weimar, Germany

Doron Hekič, University of Ljubljana, Slovenia

Tena Ilijov, Josip Juraj Strossmayer University of Osijek, Croatia

Gabór Németh, Budapest University of Technology and Economics, Hungary

University of Ljubljana

Faculty of Civil and Geodetic Engineering

Prof. Dr. Tatjana Isaković

Dr. Andrej Anžlin

Ljubljana, September 2018

CONTENTS

1 INTRODUCTION

In this report a pushover analysis of a multi-span bridge in the transverse direction is presented. The analysis was performed using both, Opensees platform (MacKenna et al. 2018) and MATLAB Software. In the beginning of the report the considered bridge and material constitutive laws are described. In order to obtain the pushover curve the moment-rotation envelope for each pier was defined based on the bilinear idealisation of the moment-curvature diagrams and using the equations presented in EC8/2 for ultimate and yield rotation. Pushover analysis was then performed in the transverse direction applying a parabolic-shaped displacement vector which is valid for bridges whose response is dominated by its first vibration mode. The obtained capacity curve was then idealised according to the equal energy principle and taking the first yielding and failure of the piers as reference. The results were then transformed into a SDOF system by applying appropriate factors, for later being presented into ADRS format. Eurocode spectra type 1 was then used to apply the N2-Method and determine the PGA value that would cause the failure of the first pier. In the second part, the analysis on the influence of the bridge deck mass on the response is presented considering that this mass is doubled. Finally, the analysis in the longitudinal direction for the normal case scenario is presented.

1.1 Considered bridge

Figure 1 presents the geometry of the considered bridge. It is a six-span bridge. The two outer spans have a length of 26 m and the inner spans have a length of 32 m for a total length of 180 m. It considered pinned supports on the abutments which allows the translation in the longitudinal direction (rollers).

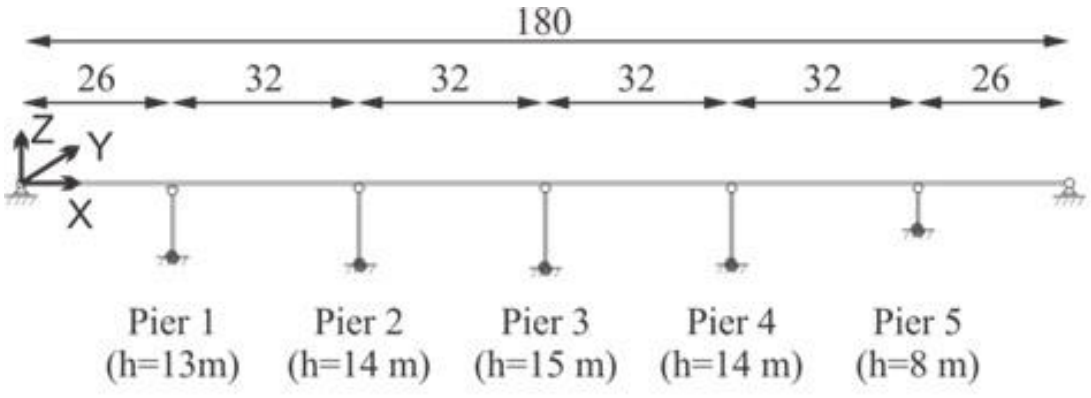

Figure 1: Considered bridge structure

The bridge deck is supported by five barbell-shaped piers of variable height which are assumed to be fixed at the base. In the connection of the bridge deck and the piers, it is assumed that elastomeric devices are provided, so that, rotations in the plane are allowed and displacements are restricted. The cross-section of the bridge piers and their longitudinal reinforcement are shown in Figure 2.

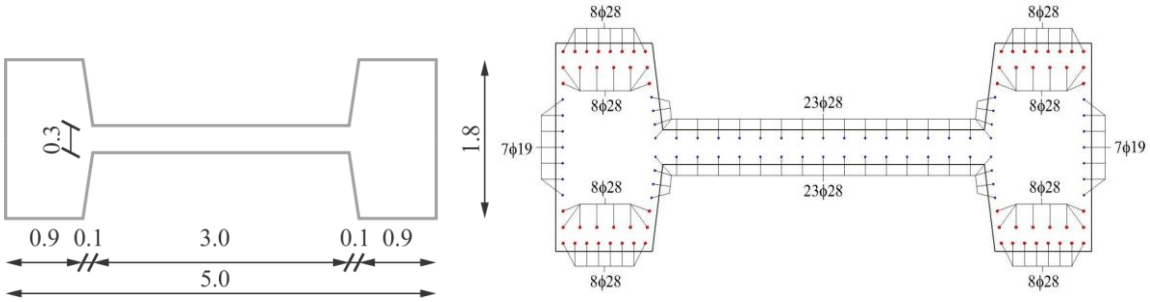

Figure 2:Cross-section of the bridge piers (left) and longitudinal reinforcement definition (right)

The cross-section of the bridge deck is presented in Figure 3. It has a mass of 29.81 t/m, additionally the cap beam at the top of the piers was considered to have a mass of 38.3 t. This values were later used to define nodal loads in the OpenSees model.

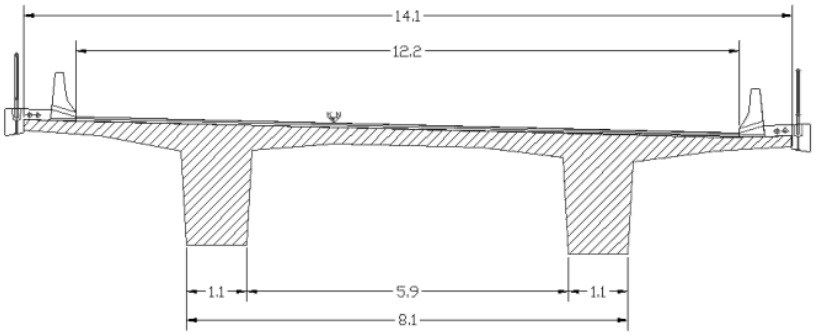

Figure 3: Cross section of the bridge deck

Basic geometrical properties for the structural elements are presented below.

Bridge Piers:

- Area = 4.35 m^2
- Inertia around strong axis, I_y= 15.022 m^4
- Inertia arounf weak axis, I_z= 0.91 m^4
- Polar moment of inertia, J_o= 0.1 m^4 (it was neglected)
-

Bridge Deck:

- Area = 9.21 m^2
- Inertia around weak axis, I_y= 3.98 m^4
- Inertia around strong axis, I_z= 129.5 m^4
- Polar moment of inertia, J_o= 0.001 m^4 (it was neglected)

The transverse reinforcement of the piers was considered as standard with stirrups of 10 mm diameter and evenly spaced in height at 10 cm.

2 MATERIAL CONSTITUTIVE LAWS

In order to perform moment-curvature analysis of the cross section of considered column, material characteristics were defined considering *Eurocodes* (CEN 2005c; CEN 2005d) and other recommendations (MacKenna et al. 2018). In *Opensees* platform (MacKenna et al. 2018) *Concrete01* and *Concrete04* models were used for unconfined and confined concrete, respectively. For the response of longitudinal reinforcement steel material model *Steel02* was used.

Material models of concrete and steel material were prescribed in *Opensees* platform (MacKenna et al. 2018) through defining steel, unconfined and confined concrete fibers.

2.1 Concrete

The characteristics of concrete were defined considering the procedure described in EC8/2 (CEN 2005d) and Mander (Mander et al. 1988). *Concrete01* material model was used for unconfined concrete and *Concrete04* material model was used for confined concrete.

2.1.1 Unconfined concrete

Characteristics of unconfined concrete were contrary to EC8/2 (CEN 2005d) recommendations defined according to Mander (Mander et al. 1988) with some modifications after $2\varepsilon_{c1}$, as shown in Figure 4. Since it is not possible in *Concrete04* model to define spalling strain i.e. point where the straight line of the falling branch in the unconfined concrete reaches zero stress as defined in Mander et al. (1988b), *Concrete01* model was used instead.

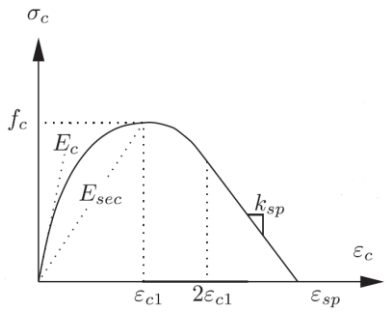

Figure 4: The σ-ε diagram of unconfined concrete presented by Popovics (1973) with some modifications after $2\varepsilon_{c1}$, which is based on the same formulation as concrete model presented by Mander et al. (1988b),. Adapted from Anžlin (2017).

Due to the fact that in *Concrete01* model, the descending part of the σ-ε curve is assumed to be linear, straight line from the peak stress to the zero stress at spalling strain ε_{sp} is considered in the definition of unconfined concrete. Calculation of unconfined concrete characteristics is shown below. The value of

mean concrete strength f_{cm} = 38 MPa was assumed for all structural elements. Strain at the peak stress ε_{c1}, initial tangent modulus of elasticity E_c, parameter r and spalling strain ε_{sp} were defined according to Mander et al. (1988b):

$$\varepsilon_{c1} = 0{,}002 \tag{1}$$

$$E_c = 5\sqrt{f_{cm}[\text{MPa}]} = 32837\ MPa \tag{2}$$

$$\varepsilon_{sp} = \frac{2^{1+r}\ \varepsilon_{c1}\ r}{(2^r - 1)\ (r - 1)} = 1{,}042\% \tag{3}$$

2.1.2 Confined concrete

Characteristics of confined concrete were defined considering procedure described by Mander et al (1998b)). For the representation of confined concrete the *OpenSees - Concrete04* model was used.

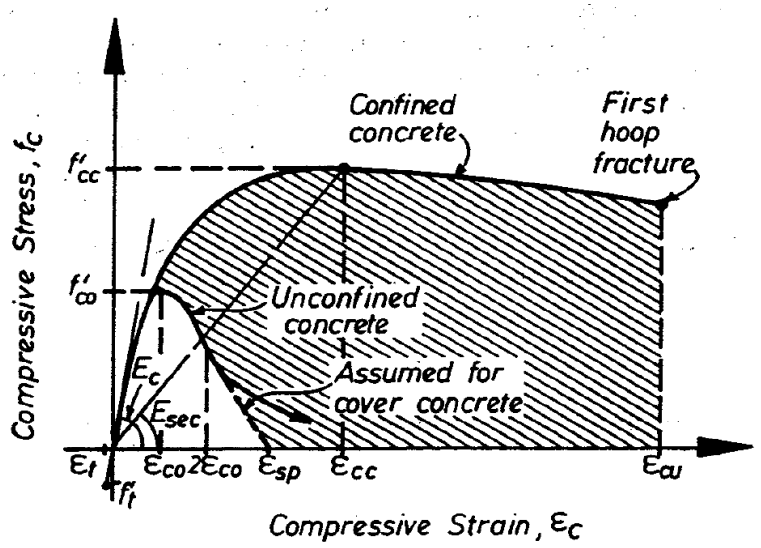

Figure 5:The σ-ε diagram of confined concrete model presented by Mander et al. (1988b)

Confined concrete characteristic values were defined according to the following expressions

$$f_{cc} = f_c(2.254\sqrt{1 + 7.94f'_l/f_c} - 2f'_l/f_c - 1.254) \tag{4}$$

$$\varepsilon_{cc} = 0.002(1 + 5(f_{cc}/f_c - 1)) \tag{5}$$

$$\varepsilon_{ccu} = 0.004 + 1.4\rho_w\varepsilon_{swu}\frac{f_{yw}}{f_{cc}} \tag{6}$$

For the calculation of the confined concrete properties a 90x180cm rectangular section was assumed. Transverse reinforcement detailing is shown in Figure 5, as well as an example of the section fiber definitions in *OpenSees*.

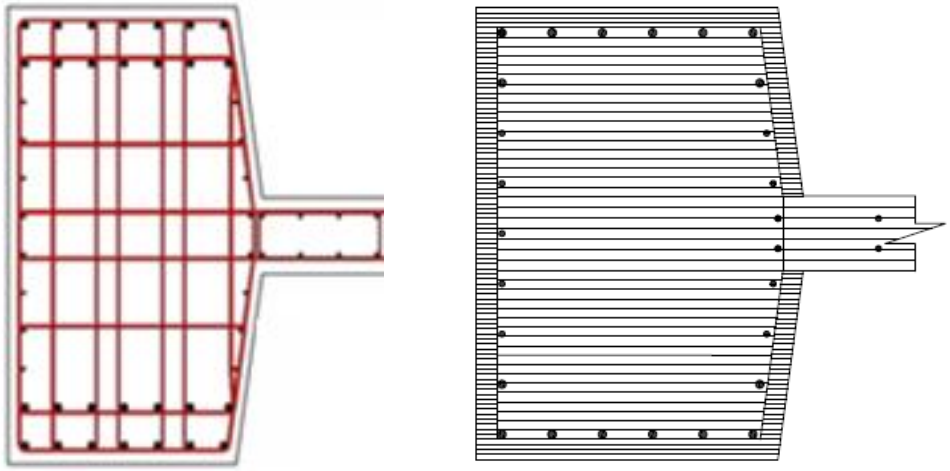

Figure 6: Transverse reinforcement detailing (left) Section fiber model (right) taken from Anžlin (2017).

The obtained results are presented below.

- Confined concrete strength: f_{cc} = 52.6 MPa
- Ratio between confined and unconfined concrete strength: f_{cc}/ f_{cm} = 1.39
- Strain at the confined concrete strength, ε_{cc} = 0.6325%
- Ultimate confined concrete strain, $\varepsilon_{cc,u}$ = 1.61%

2.2 Reinforcement

For the response of the longitudinal reinforcement the steel material model *Steel02* was used in *Opensees* platform (MacKenna et al. 2018). The mean material properties of longitudinal reinforcement were taken according to steel grade S500C standard properties.

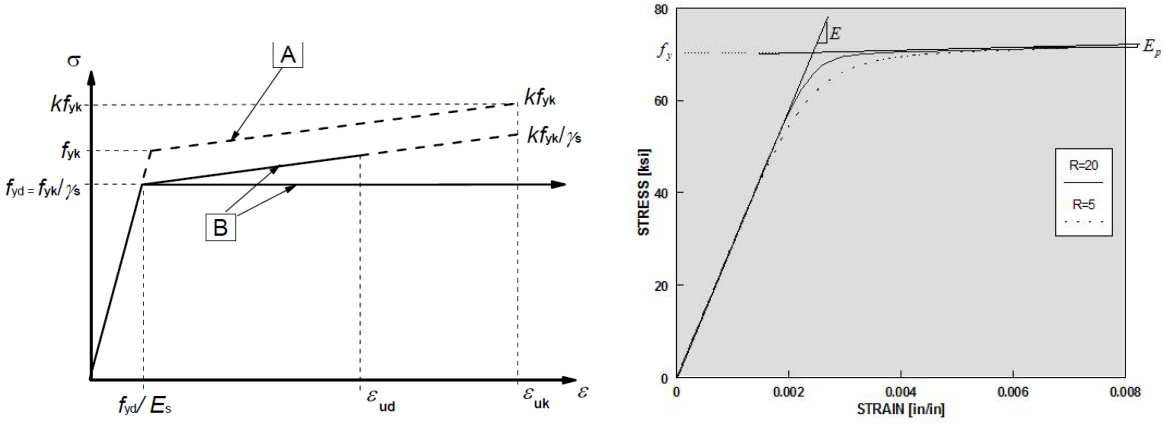

Figure 7: Steel model according to EC2/1 (left) Steel model in *OpenSees* (right).

Both longitudinal and transverse reinforcement are assumed to have the properties described below.

- Steel yield strength: f_{yk} = 500 MPa
- Steel tensile strength: f_t = 575 MPa
- Modulus of elasticity: E_s = 200.000 MPa
- Steel yield strain, ε_{sy} = 0.25%
- Steel ultimate strain, ε_{su} = 7.5%

3 MOMENT-CURVATURE ANALYSIS AND IDEALISATION

Full moment-curvature analysis of considered pier was performed in *Opensees* platform, using *MomentCurvature* script (MacKenna et al. 2018). Furthermore, yield and ultimate moment, as well as corresponding curvatures were obtained from bi-linear idealisation with strain hardening of the full moment-curvature analysis. Equal energy approach was considered for the idealisation taking into account the first yield and ultimate curvature ϕ_u was derived from the condition that either reinforcement or confined concrete strains have reached ultimate values.

Table 1: Axial load for each pier.

Pier	Height	Selfweight	Width	Axial Load	
	[m]	[kN]	[m]	[kN]	σ_c/f_{cm}
1	13	1414	29	10270.1	6.2%
2	14	1523	32	11256.2	6.8%
3	15	1631	32	11364.9	6.9%
4	14	1523	32	11256.2	6.8%
5	8	870	29	9726.4	5.9%

Table 1 presents the considered axial force for each pier to perform the moment curvature analysis.

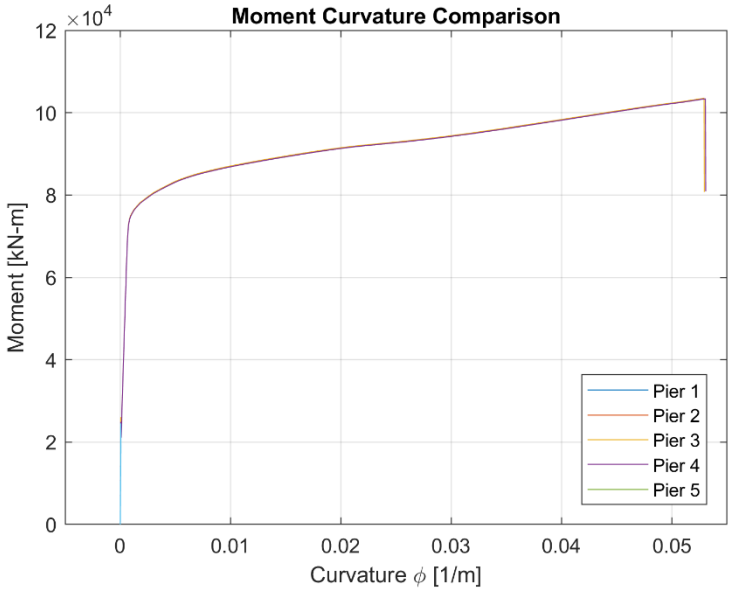

Figure 8: Moment curvature analysis around the strong axis

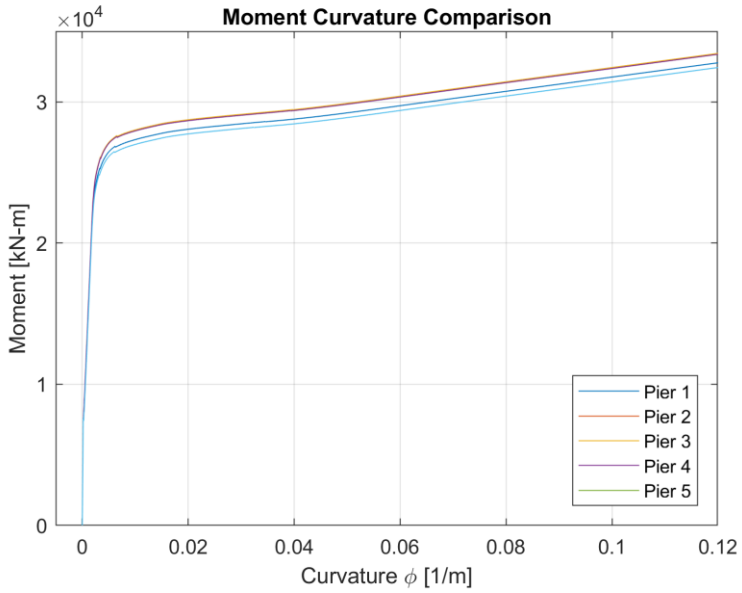

Figure 9: Moment curvature analysis around the weak axis

According to Figures 8 and 9 it can be seen that the different levels of axial force in the piers do not significantly affect the results, therefore it was decided to use the moment-curvature diagram for Pier 3 to carry out the idealisation. Figures 10 and 11 show the obtained results.

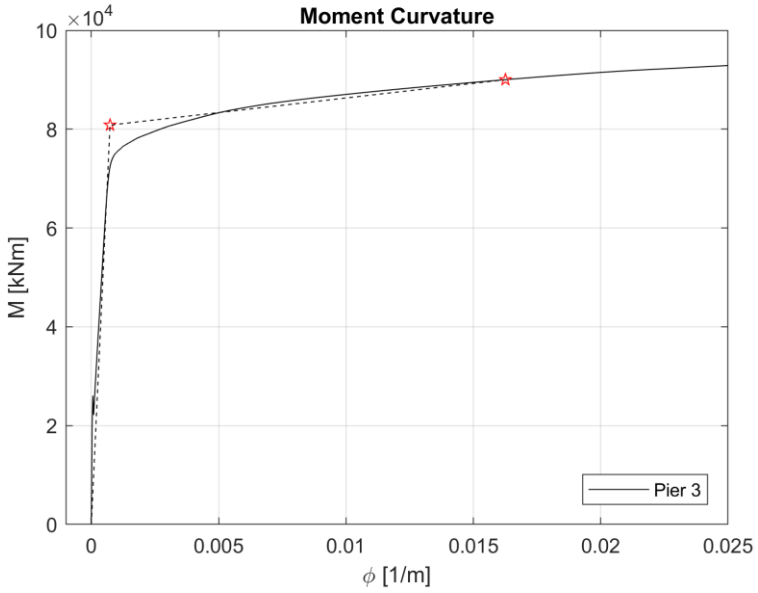

Figure 10: Moment curvature idealisation around the strong axis

Ultimate moment, yield moment and corresponded curvatures that were obtained from the idealisation of moment-curvature diagram for Pier 3 around the strong axis are presented below.

Yielding moment: M_y= 80831 kNm Yielding curvature: φ_y= 7.35e-4 1/m

Ultimate moment: M_u= 90015 kNm Ultimate curvature: φ_u= 0.0163 1/m

Figure 11 show the idealisation of the moment-curvature diagram for Pier 3 around the weak axis.

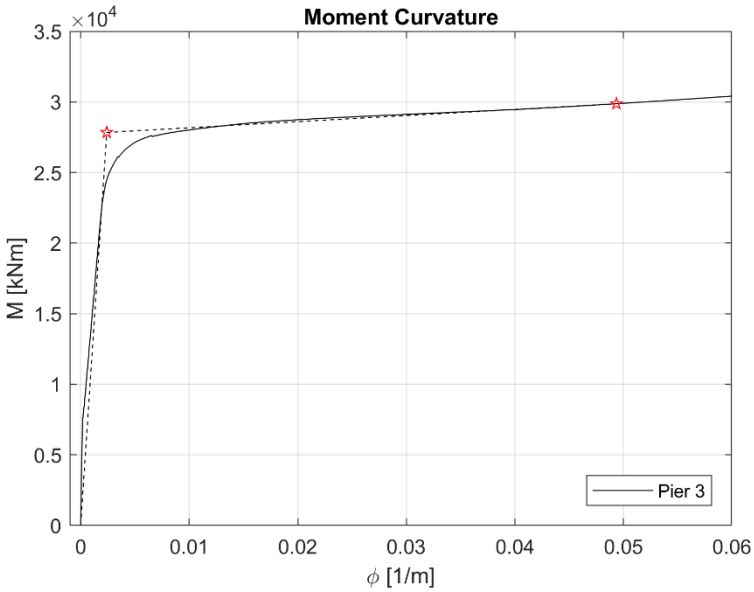

Figure 11: Moment Curvature idealisation around the weak axis

Ultimate moment, yield moment and corresponded curvatures that were obtained from the idealisation of moment-curvature diagram for Pier 3 around the weak axis are presented below.

Yielding moment: M_y= 27841 kNm Yielding curvature: φ_y= 0.0024 1/m
Ultimate moment: M_u= 29874 kNm Ultimate curvature: φ_u= 0.04936 1/m

It is important to notice that for both cases the ultimate curvature was governed by the failure of the steel rebars.

4 MOMENT-ROTATION ENVELOPE

The yield and ultimate rotations were defined according to Equations 7 to 9, as defined in EC8/2 (CEN 2005d).

$$\theta_{cr} = \Phi_{cr} \cdot \frac{L}{3} \tag{7}$$

$$\theta_y = \frac{\Phi_y}{3} L \tag{8}$$

$$\theta_u = \theta_y + \theta_{p,u} = \left(\Phi_u - \Phi_y\right) L_p \left(1 - \frac{L_p}{2\,L}\right) \tag{9}$$

The value of the plastic hinge length is given by the following equation:

$$L_p = 0{,}10L + 0{,}015\, f_{yk} d_{bL}$$

ϕ_{cr} is the cracked curvature of the section

ϕ_y is the yield curvature of the section

ϕ_u is the ultimate curvature of the section

L is the height of the column

d_{bL} is the longitudinal bar diameter

f_{yk} is the characteristic value of the steel yield stress [MPa]

The obtained results for the moment - rotation envelope are shown in Figures 12 and 13

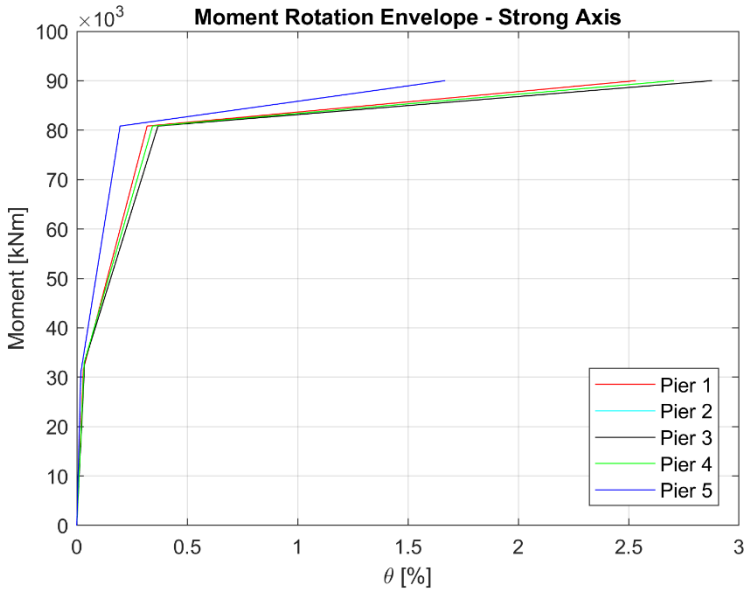

Figure 12: Moment rotation envelope around the strong axis

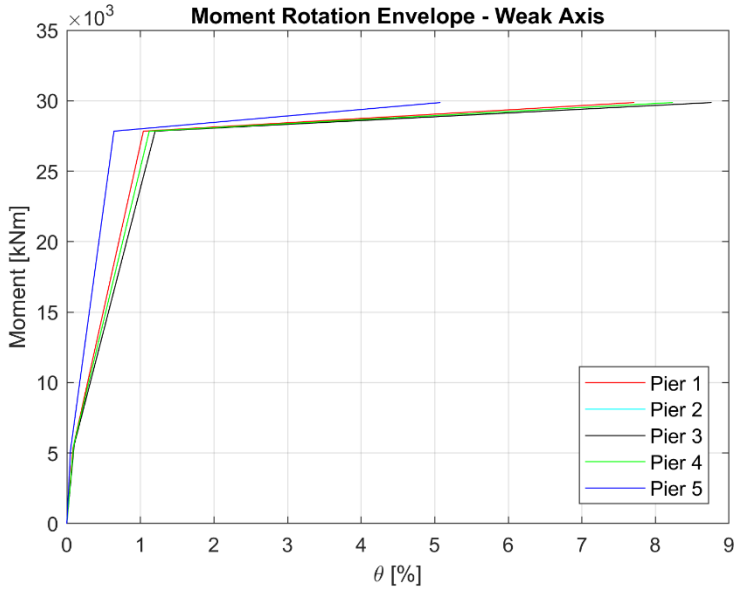

Figure 13: Moment rotation envelope around the weak axis

5 LUMPED PLASTICITY NUMERICAL MODEL

The Giberson's model where the behaviour of the assumed non-linear spring was defined using Takeda's hysteretic rules (Takeda et al. 1970) was used in the analysis. Stiffness degradation parameter α = 0,5 was considered. The quadri-linear envelope corresponded to cracking, yielding, ultimate and total damage state. The cracking damage state was defined as follows:

$$\theta_{cr} = \frac{M_{cr}}{3EI} L_V \tag{16}$$

$$M_{cr} = \left(f_{ctm} + \frac{N}{A}\right) W_c \tag{17}$$

The yield and ultimate moment as well as yielding strain were obtained from the bi-linear idealisation of the full moment-curvature response of the considered cross-section.

- Post-capping stiffness: $K_{pl,TC/NC}$ = 2
- Stiffness modifier factor (Ibarra,2005) n = 0 All the plasticity is concentrated in the non-linear spring.

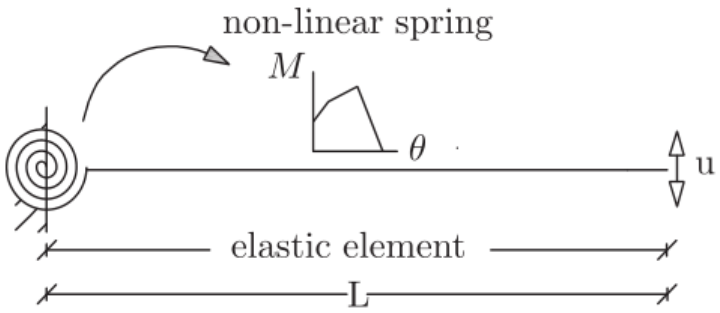

Figure 14: Lumped plasticity model taken from taken from Anžlin (2017).

6 PUSHOVER ANALYSIS IN THE TRANSVERSE DIRECTION

Figure 15 shows the displacement vector that was applied to the super-structure, a parabolic shape was considered because it was assumed that the bridge response was controlled by the first vibration mode.

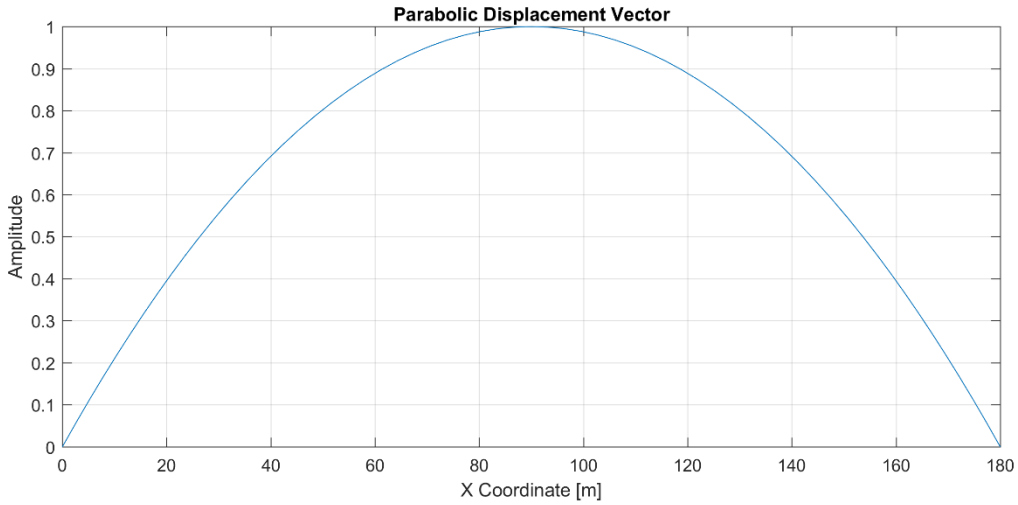

Figure 15: Parabolic-shaped displacement vector for pushover analysis

Figure 16 shows the obtained pushover curve from the analysis in the transverse direction. The analysis was performed until the displacement in the monitored point, which was defined at the top of the middle pier, reached 0,80 m.

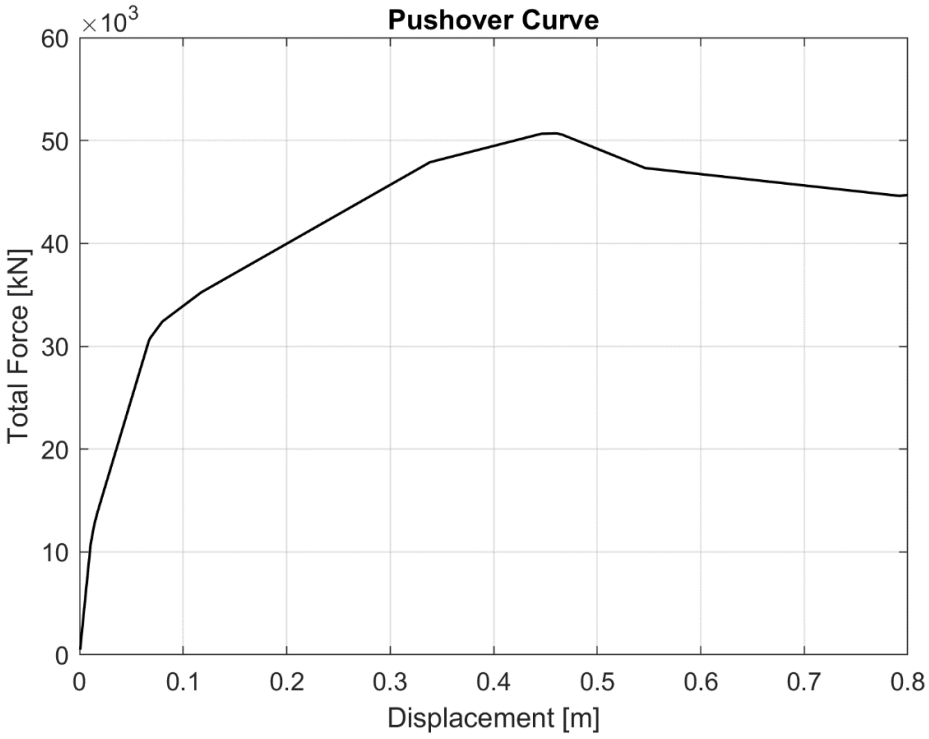

Figure 16: Pushover curve

Moreover, figure 17 shows the moment rotation response of each individual pier.

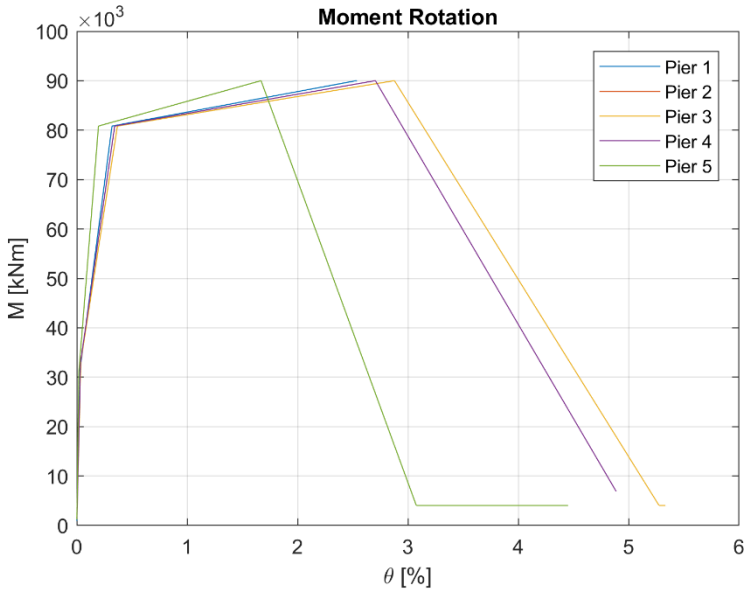

Figure 17: Moment rotation response of individual piers

The idealisation of the pushover curve was carried out considering the displacement-force pair of point for which each individual pier reach yield and failure. This is presented in figure 18, where the blue and black squares represented the yielding points and the failure points for each pier, respectively. The criteria for the idealisation of the pushover curve was then defined by the first yielding (Pier 2) and the first failure (Pier 5) points and considering the equal energy approach.

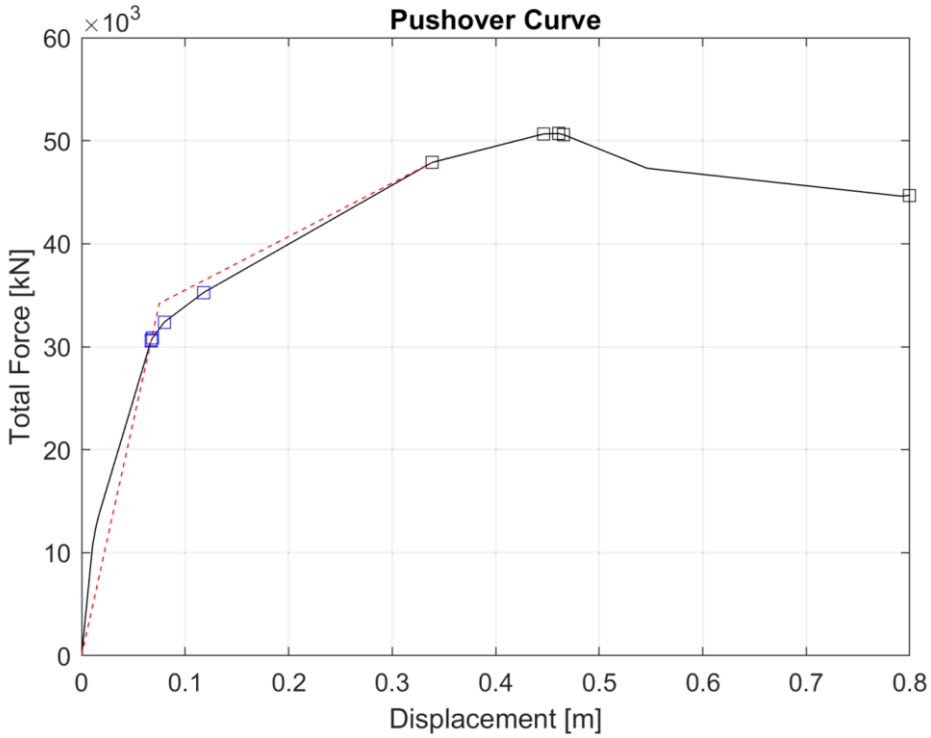

Figure 18: Idealisation of the pushover curve

The obtained results are shown below:

Yield force: $F_y = 34207$ kN
Yield displacement: $D_y = 0.0751$ m
Ultimate force: $F_u = 47891$ kN
Ultimate displacement: $D_u = 0.3385$ m

In order to represent the MDOF system as a SDOF system it is necessary to apply a transformation coefficient given by the following equation

$$\Gamma = \frac{\sum m_i \Phi_i}{\sum m_i \Phi_i^2} = 1.2459$$

where

m_i = mass vector containing nodal masses of the MDOF system

Φ_i= displacement vector containing all the displacements for each node of the MDOF system

The characteristic values of the pushover curve for the SDOF are then calculated as:

Forces: $F^* = F / \Gamma;$
Displacements: $D^* = D / \Gamma$

Yield force: $F_y^* = 27456$ kN Yield displacement: $D_y^* = 0.0602$ m
Ultimate force: $F_u^* = 38439$ kN Ultimate displacement: $D_u^* = 0.2717$ m

The characteristics properties of the SDOF are then defined according to the previous values as shown below

Mass of the SDOF system: $m^* = \sum m_i \Phi_i = 3995$ ton
Stiffness of the SDOF system: $k^* = \frac{F_y^*}{D_y^*} = 457579$ kPa
Period of the SDOF system: $T^* = 2\pi\sqrt{\frac{m^*}{k^*}} = 0.588$ s

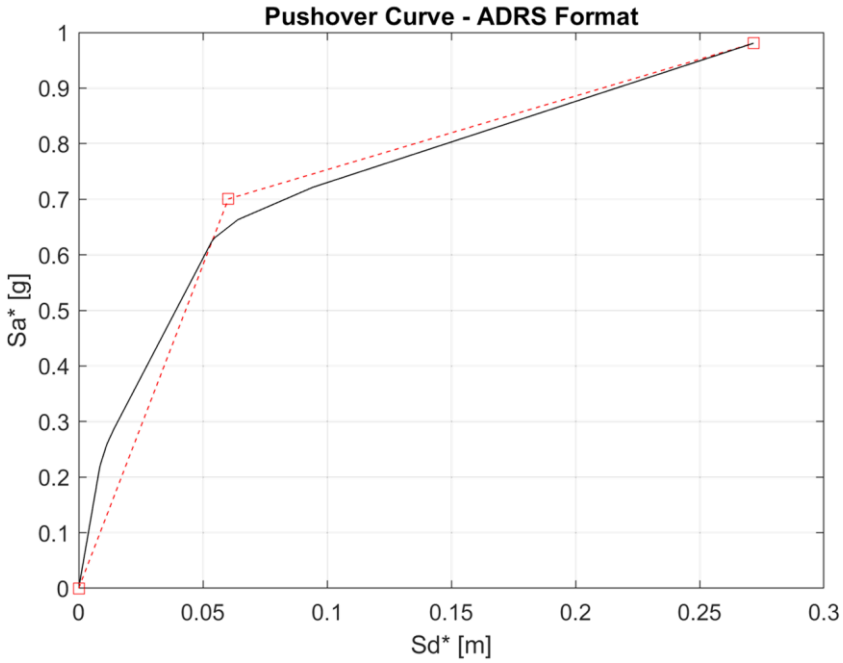

Figure 19: Pushover curve of the SDOF in the ADRS-Format

The next step in the process is to define the demand which was given by Eurocode spectra Type 1 considering a type C soil profile

Table 2: Eurocode spectral parameters

Ground Profile type	S	TB [s]	TC [s]	TD [s]
C	1.15	0.20	0.60	2.00

Eurocode acceleration spectra is defined by the following equations.

$$0 \le T \le T_B\colon\ S_a = a_g\, S \left[1 + \frac{T}{T_B}(2.5\eta - 1)\right]$$
$$T_B \le T \le T_C\colon\ S_a = 2.5\, a_g\, S\, \eta$$
$$T_C \le T \le T_D\colon\ S_a = 2.5\, a_g\, S\, \eta \left[\frac{T_C}{T}\right]$$
$$T_D \le T \le 4s\colon\ S_a = 2.5\, a_g\, S\, \eta \left[\frac{T_C T_D}{T^2}\right]$$

And displacement spectra follows the following relationship.

$$S_d = S_a \left[\frac{T}{2\pi}\right]^2$$

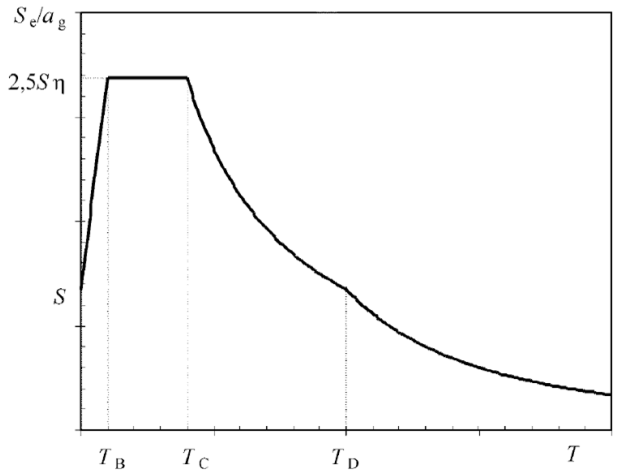

Figure 20: Eurocode acceleration spectra

In order to calculate the PGA that produces the failure of the first pier, the displacement demand should be assumed to be equal to the ultimate displacement of the idealized pushover curve.

$$S_d^* = D_u^* = 0.2717 \text{ m}$$

And since $T^* = 0.588\ s < T_c$, the displacement demand equation is given by

$$S_d^* = 2.5\ \mathrm{a_g}\ \mathrm{S}\ \eta \left[\frac{T^*}{2\pi}\right]^2$$

therefore, the PGA that produces the first failure of the pier is now calculated as

$$a_g = 0.2717 * 4 * \pi^2 \left(2.5 * 1.15 * 1.0 * 0.588^{\,2}\right)^{\,-1}$$

$$a_g = \frac{10.8\, m}{s^2} = 1.10\ \text{g}$$

In order to graphically see the results the estimated value for the PGA = 1,10 g was used as input value for applying the N2-Method. Figure 21 presents the obtained results.

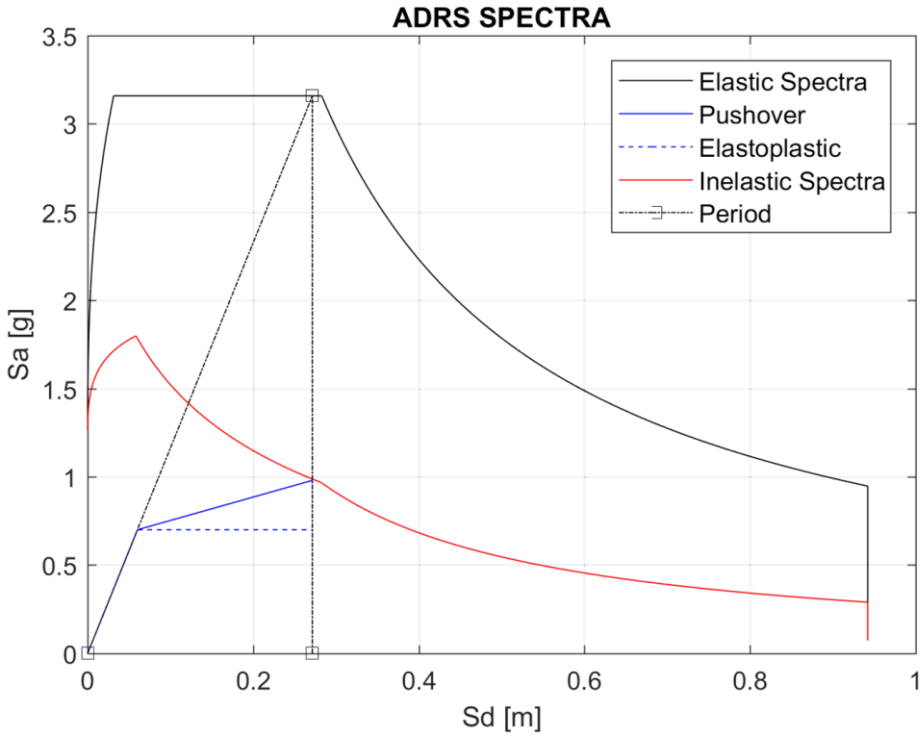

Figure 21: ADRS Spectra for PGA=1,10g (N2-Method)

7 INFLUENCE OF BRIDGE DECK MASS

In this chapter the influence of the double bridge deck mass is presented. The same analysis procedure was followed from the beginning, starting by obtaining new moment curvature relations, moment-rotation envelopes, pushover curve and estimated PGA.

Figure 22 shows the influence in the moment curvature diagram for Pier 3. It can be seen that the increment of the mass has only effect on the strength but there are not significant changes in the deformation capacity. This is explained because of the low axial load levels in the piers which vary form an average of 6% of fcm for the initial case to an average of 12% of fcm in the second case.

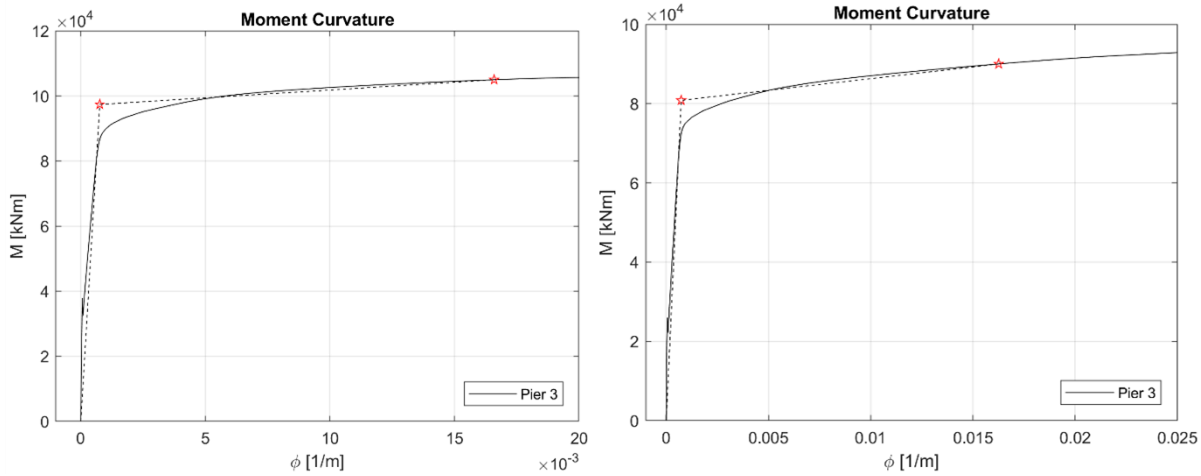

Figure 22: Influence on moment curvature diagram. Double mass (left) and normal mass (right)

Figure 23 shows the influence in the moment rotation envelope for all piers. The same behaviour described for the moment curvature case is presented due to the fact that the curvature is the main input for the rotations calculations.

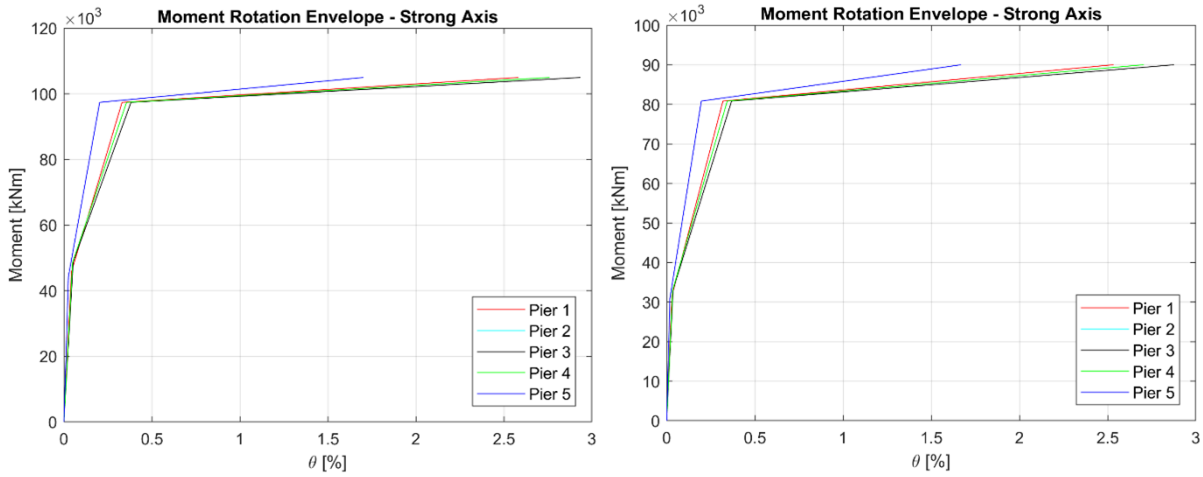

Figure 23: Influence on moment rotation envelopes. Double mass (left) and normal mass (right)

Figure 24 shows the influence in the pushover curve. The increment in the strength leads to an increment in the initial stiffness of the system, but it was already mentioned the displacement capacity doesn't suffer significant changes.

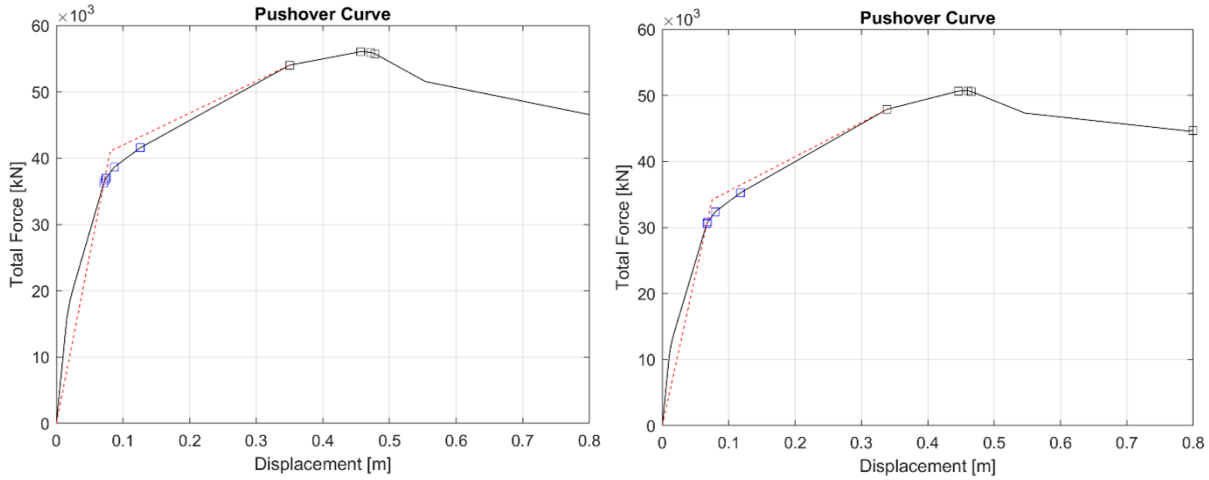

Figure 24: Influence on pushover curve. Double mass (left) and normal mass (right)

Figure 25 shows the influence in the idealised pushover curve in the ADRS format.

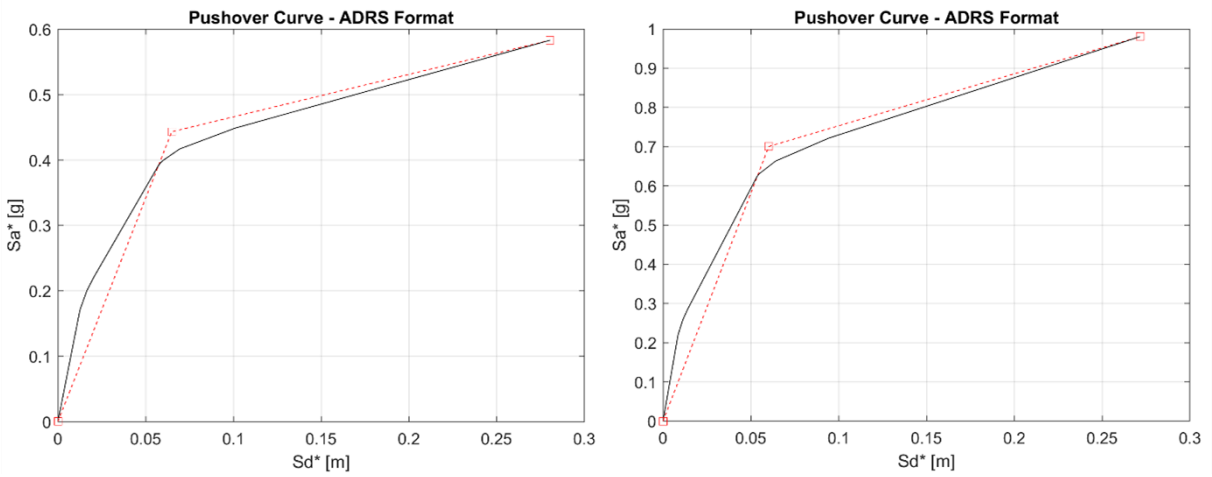

Figure 25: Influence in idealised pushover curve ADRS format. Double mass (left) and normal mass (right)

The influence on the SDOF parameters is shown below

Double Mass	*Normal mass*
Mass = 11278 ton	Mass = 6266 ton
Γ= 1.2477	Γ= 1.2459
$m^* = 7572$ ton	$m^* = 3995\ ton$
$F_y^* = 32900$ kN	$F_y^* = 27456\ kN$
$D_y^* = 0.0649$ m	$D_y^* = 0.0602\ m$
$F_u^* = 43295$ kN	$F_u^* = 38439\ kN$
$D_u^* = 0.2805$ m	$D_u^* = 0.2717\ m$
$k^* = 507180$ kPa	$k^* = 457579\ kPa$
$T^* = 0.7677$ s	$T^* = 0.588\ s$
PGA= 0.85 g	PGA=1,10 g

It can be seen from the results that the period of the SDOF for the doubled mass case increases from 0,588s to 0,767 s due to the change in stiffness and mass. Therefore the difference in the required PGA for reaching failure of the first pier is also calculated, in the case of double mass this value decreases to 0,85 g instead of 1,10 g for the normal mass case.

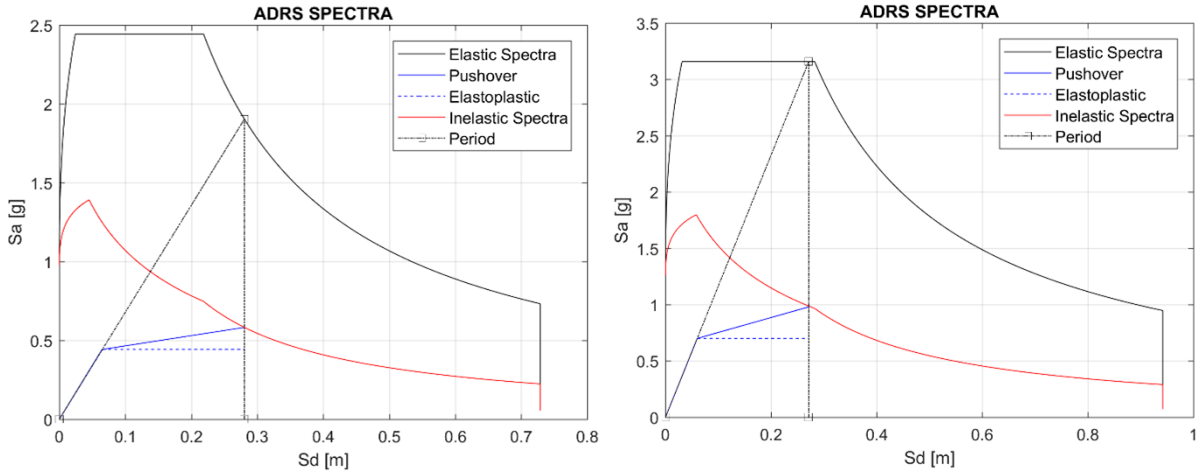

Figure 26: Influence on the estimated PGA by N2-Method. Double mass (left) and normal mass (right)

8 ANALYSIS IN THE LONGITUDINAL DIRECTION

In this chapter the analysis in the longitudinal direction is presented.

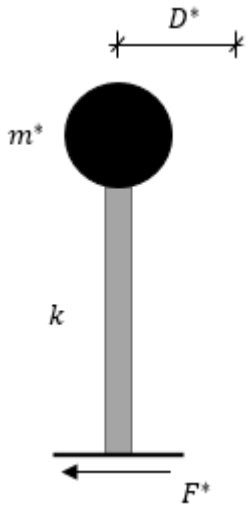

Figure 27: SDOF system model

In the longitudinal direction a SDOF model is used for the analysis because the axial stiffness of the bridge deck guarantees equal displacement in all piers. The characteristic parameters of the SDOF model in the longitudinal direction are calculated as follows.

mass $= 5912$ ton

The cracked stiffness is calculated as the sum of individual pier cracked stiffnesses which are calculated according to the yielding moment-rotation values.

$$K_{Cracked} = \sum k_{cr,i} = 119490\ kPa \qquad k_{cr,i} = \frac{M_{yi}}{\theta_{yi} H_i^2}$$

Then the period is estimated in 1,40 s in the longitudinal direction.

$$T = 2\pi \sqrt{\frac{mass}{K_{Cracked}}} = 1.40\ s$$

For defining the displacement demand of the first failure pier the concept of chord rotation is used. Since Pier 5 is the shortest one and it has also the lowest rotation capacity, it will control the displacement.

Pier 5

$\theta_u = 5.05\%$

$H = 8\ m$

$\Delta = S_d = 0.404\ m$

Then the displacement demand is 0,40 m

The last step is to apply Eurocode acceleration spectra equation in the adequate period range.

Since $T^* = 1{,}40\ s < T_D$, then:

$$T_C \leq T \leq T_D\colon\ S_a = 2.5\ a_g\ S\ \eta \left[\frac{T_C}{T}\right]$$

$$S_d = S_a \left[\frac{T}{2\pi}\right]^2$$

$$\mathrm{a_g} = 0.404 * 4\pi^2 (2.5 * 1.15 * 1.0 * 0.60 * 1.40)^{-1}$$

$$\mathrm{a_g} == \frac{6.6\ m}{s^2} = 0.67\ g$$

This value is used as an input for the graphical solution using N2 Method and the results are shown in figure 28

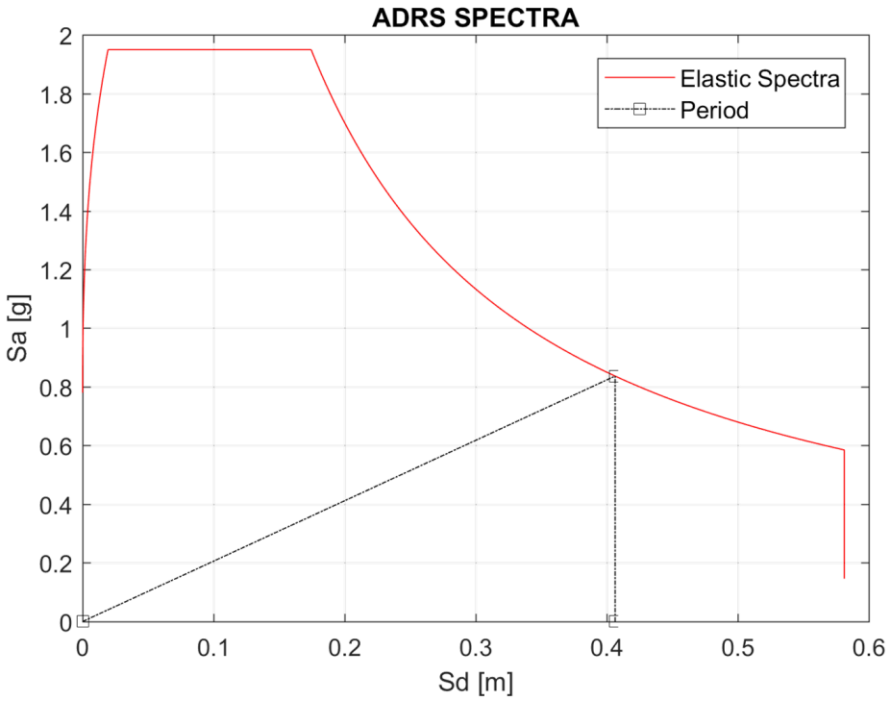

Figure 28: ADRS Spectra for PGA=0,67 g (N2-Method)

9 CONCLUSIONS

- The estimated period of the SDOF system for the bridge is around 0.60 s
- The pushover analysis in the transverse direction showed that Pier 2 is the first to reach yield and Pier 5 is the the first in reaching failure.
- The estimated PGA that corresponds to the failure of Pier 5 for transverse direction is 1.10 g
- The influence of the doubled bridge mass deck showed an increase in the strength capacity of about 20% without significant variations displacement capacity of the bridge due to low levels of axial force in the piers.
- The period for the doubled deck mass increase from around 0.60 s to 0.75 s, the PGA that would lead to the failure of the first pier decreased to 0.85g
- The analysis in the longitudinal direction was performed for a SDOF system, and showed that the PGA that would lead to the failure is 0.67g
- The obtained results greatly depend on the criteria of the engineer to define the non-linear characteristics of the materials, as well as the definition of failure and yielding points used for the idealization of the pushover curve.

BIBLIOGRAPHY

Anžlin, Andrej. 2017. Influence of buckling of longitudinal reinforcement in columns on seismic response of existing reinforced concrete bridges. PhD thesis. Univerza v Ljubljani.

CEN. 2005a. Eurocode 2: Design of concrete structures - Part 1-1: General rules and rules for buildings, Brussels, Belgium.

CEN. 2005b. Eurocode 8: Design of structures for earthquake resistance - Part 1: General rules, seismic actions and rules for buildings (EN 1998-1:2005), Brussels, Belgium.

CEN. 2005c. Eurocode 8: Design of structures for earthquake resistance - Part 2: Bridges, Comit_e Europ_een de Normalisation (EN 1998-2:2005), Brussels, Belgium.

CEN. 2005d. Eurocode 8: Design of structures for earthquake resistance - Part 3: Assessment and retro_t of buildings, Comit_e Europ_een de Normalisation (EN 1998-3:2005), Brussels, Belgium.

Coffin Jr, L Fo. 1953. *A study of the e_ects of cyclic thermal stresses on a ductile metal*. tech. rep. Knolls Atomic Power Lab.

MacKenna, F., GL. Fenves, and MH. Scott. 2016. *Open system for earthquake engineering simulation. Univ. of California, Berkeley*. url: http://opensees.berkeley.edu/ (visited on Jul. 18, 2018).

Maekawa, Koichi, JI Takemura, Paulus Irawan, and MA Irie. 1993. Triaxial elasto-plastic and fracture model for concrete. *Proceedings - Japan Society of Civil Engineers*. DOTOKU GAKKAI, pp. 131-131.

Mander, JB, MJN Priestley, and P Park. 1988. Theoretical stress-strain model for confined concrete. *ASCE J Struct Eng* 114, 8: 1804-1826. DOI: /10.1061/(ASCE)0733-9445(1988) 114:8(1804).

Manson, Samuel S. 1954. *Behavior of materials under conditions of thermal stress, Report 1170*. tech. rep. Lewis Flight Propulsion Laboratory, Cleveland, Ohio.

Popovics, S. 1973. A numerical approach to the complete stress-strain curves for concrete. Cement and Concrete Research 3, 5: 583-599. DOI: 10.1016/0008-8846(73)90096-3.Takeda, Toshikazu, Mete Avni Sozen, and N Norby Nielsen. 1970. Reinforced concrete response to simulated earthquakes. *Journal of the Structural Division* 96, 12: 2557-2573